UNIVERSITA' DEGLI STUDI DI PADOVA

Sede Amministrativa: Università degli Studi di Padova
Dipartimento di Principi e Impianti dell'Ingegneria Chimica "I. Sorgato"

DOTTORATO DI RICERCA IN INGEGNERIA CHIMICA
CICLO XX

MODELING CATALYTIC METHANE PARTIAL OXIDATION WITH DETAILED CHEMISTRY

Direttore: Ch.mo Prof. Paolo Bariani

Coordinatore: Ch.mo Prof. Massimiliano Barolo

Supervisore: Ch.mo Prof. Paolo Canu

Correlatore: Ch.mo Prof. Lanny D. Schmidt

Dottoranda: Daniela Dalle Nogare

DATA CONSEGNA TESI
31 gennaio 2008

Contents

Abstract

Detailed mechanisms are being promising, but they are not extensively used yet. Particularly in multi-phase reactions, their interaction with the transport phenomena is often underrated.

Partial oxidation of methane in monolithic reactors (structured or foam-like) showed competitive in converting natural gas into syngas, an intermediate for the syntheses of higher hydrocarbons and methanol, or a new form of energy vector. Because of that, very many experimental data have been produced. In the present work this process is modeled, coupling transport phenomena and detailed kinetics.

Several 1D models, of increasing accuracy, are applied to the square channel monolith: from the ideal PFR to a lumped model including solid conduction and both heat and mass transfer coefficients. Results show how the apparent stoichiometry changes if diffusional resistances are taken in account, slowing down the kinetics. The same geometry is solved also with the CFD, and results are compared to pseudo-homogeneous models'. Also, the obtaining of the transfer coefficient by means of CFD is discussed.

The foam monolith is modeled both with the PFR model and with a lumped model accounting for transport resistances, gas phase axial diffusion and solid conduction and radiation. Results are validated through spatially resolved measurements of temperature and composition. Differences between the bulk and the boundary layer compositions are ascribed to mass transfer resistances, as well as to the surface production rates.

Sherwood numbers obtained from heat transfer correlations don't often agree with those calculated with the CFD, particularly if the reaction is fast: we suggest that Sh correlations should also account for the reaction order.

Riassunto

I meccanismi dettagliati si sono dimostrati promettenti, ma essi non hanno ancora un utilizzo molto diffuso. In particolare alla presenza di reazioni multi - fase, la loro interazione con i fenomeni di trasporto è spesso sottovalutata.

L'ossidazione parziale di metano in reattori monolitici (strutturati o a schiuma) si è rivelata una tecnologia competitiva nel convertire il gas naturale in gas di sintesi, il quale può essere un intermedio per le sintesi di idrocarburi superiori e metanolo, oppure una nuova forma di vettore energetico. Per tale motivo si sta producendo un gran numero di dati sperimentali. Nel presente lavoro si modella questo processo, accoppiando i fenomeni di trasporto all'uso di una cinetica dettagliata.

Diversi modelli 1D, di dettaglio crescente, sono applicati al monolito con canali a sezione quadrata: dal PFR fino a un modello a parametri concentrati che include la conduzione nel solido ed entrambi i coefficienti di trasporto di massa e calore. I risultati mostrano come la stechiometria apparente cambi qualora le resistenze alla diffusione siano incluse, rallentando la cinetica. La stessa geometria è simulata anche con la CFD, e i risultati sono confrontati con quelli del modello pseudo omogeneo. Inoltre, si affronta la questione del calcolo dei coefficienti di trasporto via CFD.

Il monolito a schiuma è modellato sia con il PFR, sia con un modello a parametri concentrati che include le resistenze al trasporto, la diffusione assiale in fase gas nonché la conduzione e l'irraggiamento nel solido. Si è potuto convalidare i risultati con grande dettaglio grazie al confronto con misure di profili spaziali di temperatura e composizione all'interno del reattore. Le differenze di concentrazione tra la massa del gas e lo strato sottile vicino alla superficie sono dovute sia alle resistenze al trasporto di massa che alle velocità di produzione superficiali.

I numeri di Sherwood ottenibili dalle correlazioni per il trasporto di calore spesso non concordano con quelli calcolati con la CFD, in particolare in presenza di reazioni veloci: si suggerisce che le correlazioni per Sh debbano anche tenere conto dell'ordine di reazione.

Summary

In Chapter 1 some papers are described to introduce the modeling approaches to the Partial Oxidation of Methane (POM).

In Chapter 2 the use of a kinetics interpreter is introduced, explaining the various advantages in using it instead of implementing all the thermo-physical properties and the kinetics. Two different softwares are compared, and hints are given for the right choice.

In Chapter 3 a study upon the traditional approach to the transport coefficient is carried out by means of the CFD. Discrepancies are highlighted, which warn against the use of the heat transfer correlations for deriving mass transport coefficients, mostly for fast reacting systems.

In Chapter 4 several 1D reactor models are described. Complexity of the physical model increases together with that of the solution techniques. To a simple PFR, many features can be added: solid conduction might be important in oxidation processes, due to the high temperature gradients; heat and/or mass transfer coefficients allow differentiating the bulk gas from the solid properties; gas phase diffusion/conduction is usually to include for Pe close to unity; radiation might be effective with a discontinuous solid structure.

In Chapter 5 some of the 1D models described in the previous chapter are solved for a square channel monolith, and results are compared with experimental data. Results are critically interpreted: to understand the importance of some physical phenomena; to decide which of the models gets closer to the data and why; to extract and apparent stoichiometry that tells us the alternating of the reactions.

In Chapter 6 the PFR model and the most complex among the models described in Chapter 4 are solved for a foam monolith. Results are compared to spatially resolved measurements of temperature and composition, so that the model validation is very definite. Analysis of the bulk and boundary layer compositions is achieved, and the corresponding differences in composition are explained.

In Chapter 7 a fluidynamic and thermal analysis of the square channel monolith is obtained using the CFD. The hypotesis that one single channel is representative of the whole monolith is justified, because of the uniform flow rate and the adiabatic behavior.

In Chapter 8 the CFD modeling of the square channel with detailed kinetics is described. Results are compared with the lumped model's, and the different profiles are explained with the inadequacy of the literature correlations in calculating the mass transfer coefficients.

Chapter 9 is dedicated to some general conclusions.

Notation

a = basis step in the mesh

c_i = molar concentration, mol $\cdot m^{-3}$

cp = bulk specific heat, J $\cdot kg^{-1} \cdot K^{-1}$

cp_S = solid specific heat, J $\cdot kg^{-1} \cdot K^{-1}$

d = characteristic dimension of the system, m
(d=l in Chapter 5 and d=S_V^{-1} in Chapter 6)

D_i = species molecular diffusivity, $m^2 \cdot s^{-1}$

dpore = pore diameter, m

f = tortuosity factor

gf = growth factor for the mesh definition

G = superficial mass flow rate, G=$\rho \cdot v$, kg $\cdot m^{-2} \cdot s^{-1}$

h_i = species enthalpy, J $\cdot kmol_i^{-1}$

ΔH_R = enthalpy of reaction, J $\cdot kmol^{-1}$

k = permeability of the porous zore, m^2

K = Extinction coefficient, m^{-1}

K_C = mass transfer coefficient, m $\cdot s^{-1}$

K_T = heat transfer coefficient, W $\cdot m^{-2} \cdot K^{-1}$

l = square channel edge, m

L = each monolith length, m

P = pressure, Pa

r = species production rate, $kmol_i \cdot m^{-3} \cdot s^{-1}$

R = reaction rate, kmol $\cdot m^{-3} \cdot s^{-1}$

$\dot{r}$ = species production rate, $kmol_i \cdot m^{-3} \cdot s^{-1}$

$\dot{s}$ = species production rate by surface reaction, $kmol_i \cdot m^{-2} \cdot s^{-1}$

S_V = catalytic surface per void volume, m^{-1}

S_V' = catalytic surface per bed volume, m^{-1}

t = time, s

T_G = bulk gas temperature, K

T_S = solid temperature, K

v = interstitial velocity, $m \cdot s^{-1}$

W = molar mass, $kg_i \cdot kmol_i^{-1}$

X_G = bulk mass fractions, kg_i/kg_{tot}

X_{BL} = BL mass fractions, kg_i/kg_{tot}

Y_G = bulk mass fractions, kg_i/kg_{tot}

Y_{BL} = BL mass fractions, kg_i/kg_{tot}

z = axial coordinate, m

Greek letters

ε = foam porosity, V_{void}/V_{bed}

ε_g = gas emissivity

η = viscosity, $kg \cdot m^{-1} \cdot s^{-1}$

λ = bulk thermal conductivity, $W \cdot m^{-1} \cdot K^{-1}$

λ_S = solid thermal conductivity, $W \cdot m^{-1} \cdot K^{-1}$

ρ = bulk density, $kg \cdot m^{-1}$

ρ_{BL} = boundary layer gas density, $kg \cdot m^{-1}$

ρ_S = solid density, $kg \cdot m^{-1}$

σ = Stefan-Boltzmann constant, $W \cdot m^{-2} \cdot K^{-4}$

Dimensionless numbers

$$\mathrm{Da} = \frac{k \cdot c_A^{0(n-1)} \cdot d}{D}$$

$$\mathrm{Nu} = \frac{K_T \cdot d}{\lambda}$$

$$\mathrm{Nu'} = \frac{K_T}{\lambda \cdot S_V'}$$

$$\mathrm{Pe_M} = \frac{d \cdot v}{D} \ (= \mathrm{Re} \cdot \mathrm{Sc})$$

$$\mathrm{Pe_T} = \frac{c_P \cdot G \cdot d}{\lambda} \ (= \mathrm{Re} \cdot \mathrm{Pr})$$

$$\mathrm{Pr} = \frac{\eta \cdot c_P}{\lambda}$$

$$\text{Re} = \frac{G \cdot d}{\eta}$$

$$\text{Re'} = \frac{G}{\eta \cdot S_V'}$$

$$\text{Sc} = \frac{\eta}{\rho \cdot D}$$

$$\text{Sh} = \frac{K_C \cdot d}{D}$$

$$\text{Sh'} = \frac{K_C}{D \cdot S_V'}$$

Chapter 1

Introduction

1.1 Reactor modeling

Partial oxidation of methane (POM) in monolithic reactors showed competitive in converting natural gas into syngas, an intermediate for the syntheses of higher hydrocarbons and methanol, or a new form of energy vector.

To deeply understand the chemistry the process has been modeled, coupling transport phenomena and detailed kinetics. The reactor model is implemented both with a dedicated 1D model and with the CFD, whilst we outsource the kinetic interpreter.

At first the widespread use of the dimensionless number approach is investigated, finding the Chilton-Colburn analogy rather limited in reacting systems. Nonetheless, a wide range of 1D reactor models are proposed, applied to a structured straight channel monolith as well as to an un-structured foam monolith, also using the boundary layer approximation. Calculations are compared with experimental data. Eventually, a most advance model, coupling the CFD with a detailed surface mechanism, is shown, applicable only to the structured geometry.

1.1.1 Noticeable state of the art of the theory

In the reactor modeling several advancements have been achieved in the last 15 years, simultaneously with the spreading of more and more powerful calculators. Often, theories used in these works are being seized from the past, when reduced computational equipments forced researchers to develop simplified models. Nowadays, many of those simplifications are dropped, and efforts are being made to renew some well-established techniques based on outdated hypotheses. This thesis tries to join this school. Furthermore, a modern approach to reactor modeling bases its fundamentals on Computational Fluid Dynamics (CFD), approaching the equipments characterization with a detailed, multi-dimensional description, as a continuum, of the whole flow field and other phenomena occurring; adjusting the new multiphase or reactive flows tools, as well as turbulence and particle description.

The catalytic combustion is under study, because of the widespread use of combustion in the industrial processes, and because of the promising advantages that a catalytic contribution can give to the efficiencies and to the environmental problems. Many research groups have been working on experimentations, for years, testing substrates – the monolith – shapes, supports – the washcoat – characteristics and metals – the catalyst – properties. It is less common, though, that a proper modeling follows those experimental campaigns. Our efforts are motivated by the firm belief that the

modeling may contribute significantly to accelerate and deepen the understanding of the process.

Let's have a brief excursus of some examples of reactor modeling, which inspired and guided us through this work, with special applications to the catalytic combustion.

A good beginning might be to talk about Pfefferle's review [34] on models used in catalytic combustion, from Yale University. It is focused on processes where a transport regime is dominant. From the relative importance of the homogeneous/ heterogeneous chemistry she outlines the correct model to be used, whether a "lumped-parameter-transport laminar boundary-layer" model in case of prevalent heterogeneous kinetics or a "full two-dimensional" model where also homogeneous kinetics is important. Also, she warns the reader against a thoughtless use of the Chilton-Colburn analogy, which should be corrected by means of the Da number to take in account for the presence of a homogeneous kinetics. Here we add: also to consider a heterogeneous kinetics which order is such that it doesn't give at the wall a constant composition or a constant mass flux (conditions at the basis of the heat tranfer theory).

I'd give prominence also to a trilogy, named here after the first author: Bizzi02 [1], Bizzi03 [2] and Bizzi04 [3], by Saracco's group from Turin Polytechnic (Italy). As an aside, you'll find that the title of Chapter 6 is a tribute to the last one. They investigate a packed bed catalytic reactor for methane partial oxidation, operated in transport regime.

In Bizzi02 a global kinetics was used, including the basic reactions occurring in the process: total oxidation, partial oxidation and water gas shift. A preliminary analysis of the kinetics by means of a PFR model is needed to calibrate the kinetic parameters. A reactor model was solved, which includes the described kinetics and both heat and mass transport coefficients. The main result is that increasing the GHSV (Gas Hourly Space Velocity) the conversion is higher, as well as the temperature and the CO and H_2 selectivities. Rising the velocity, transport takes advantage because the radial mixing is enhanced and a higher oxygen concentration is expected at the catalytic surface. This means the phenomenon dominating in the actual reactor is transport. Besides, the oxidation is exothermic, thus the enthalpy of reaction leads to a higher temperature: the process is autocatalytic.

Results from Bizzi02 were extended in Bizzi03. The authors found out that the reactor is working in transport regime for a wide range of conditions. Therefore, they decided to adopt a thermodynamic equilibrium approach, instead of solving the kinetics, which would be anyway very fast. The solid thermal model was improved, including solid conduction and radiation towards the room: they account for both with a unique effective parameter. In addition to find again that a higher GHSV increases the conversion, they draw attention to the difference between the solid and the bulk gas temperatures, due to the reaction and to the transport resistance. This, again, enhances the kinetics, which occurs on the surface, and a higher conversion and CO and H_2 selectivities are gained.

Bizzi04 is the outcome of the cooperation with Deutschmann, from University of Karlsruhe (Germany). The 1D lumped model from Bizzi03 is used here in conjunction with a detailed surface mechanism. It consists in two heat balances, for the surface and the gas temperatures, and one equation for the species balance, containing the production term as a flux comprising two resistances in series: the kinetics and the transport. For each species, an equivalent first-order kinetic constant is calculated by dividing the chemical source term given by the production rate by its bulk molar concentration. The total active catalytic area, not available experimentally, is fitted over the data: with respect to the structured monolith, where the kinetics was deduced, the packed bad has 3 times more active surface. Results confirm again the previous statements about the GHSV, at least up to a maximum, where the diminishing of the contact time with increasing feed velocity prevails. With this model a prediction is possible for the maximum flow rate at which the reactor blows out. The model can also be adopted as an optimization tool, for the temperature and the composition of the feedstock, and for the reactor scale-up.

The detailed surface mechanism just mentioned was originally developed in the Schmidt's group, at the University of Minnesota, where Deutschmann himself implemented it into a CFD code, through user-defined subroutines [10]. This work represents only the beginning of a long series of studies with CFD and detailed kinetics. Eventually, he got to refine both the mechanism [37] and the kinetics solver, which became independent assuming the name DETCHEM [11]. In that first work, the foam monolith is modeled as a straight tube, with both homogeneous and heterogeneous chemistry. Both for Rh and for Pt catalysts, they find CH_4 conversions higher than 90% and also syngas selectivity is more than 90%. This behavior is close to the experimental data. Because of the insulation and the inlet composition (CH_4/O_2=1.8, 30% N_2) the reactor is autothermal. They expect the gas phase kinetics to be negligible at low P, but elsewhere it should reduce the syngas selectivity, because it supports the formation of total oxidation species. At low P the surface mechanism [21] produces conversion and selectivity very close to those observed, even if the mechanism was deduced using a PFR model. From the results of the simulations, they infer that the products are obtained from partial oxidation (PO) more than from a total oxidation (TO) plus reforming. The gas species that trigger the gas phase kinetics (OH) are negligible, as well as the ethylene, a typical product of homogeneous chemistry. They prove this way that the gas phase reactions are so slow that they can be neglected. They analyzed the catalyst inlet: in the first millimeter huge variations occur: of velocity, temperature, properties and a great deal of conversion. In the following, the isothermal hypothesis is used: because of the conduction, the solid is at uniform temperature. Comparing Rh with Pt, the latter proved better for the TO, and not so good for the PO, giving therefore a lower CH_4 conversion. It turns out that the Pt has a lower O_2 coverage. Increasing the inlet velocity, there's a breakthrough in the O_2, because the contact time in the reactor is too short for the reaction to complete. As a consequence, the selectivity of the TO species increase, because they form more quickly. A higher temperature, which could be done with a feedstock preheating, enhances the syngas selectivity. The ratio CH_4/O_2 modifies the

temperature, as well. Moreover, it affects the coverages: for CH_4/O_2=2, the main coverage is C(s), for CH_4/O_2=1.2 the CO(s) prevails and for CH_4/O_2=0.5 O(s) dominates. High P simulations show that above 10 bars the homogeneous kinetics starts to be important, and a great influence is expected in the industrial pressure range: 20-30 bars.

Last but absolutely not least, we report a work by Groppi's group, from Milan Polytechnic [30]. It's an analysis of the steady state and transient behavior of catalytic reactor for POM, with different substrate structure: foam, honeycomb with square channels and sphere bed. The mathematical model of the reactor is particularly interesting. The model includes gas and solid, species and energy balances, as well as a momentum balance. That makes five balances, of which the species ones are vectors. Gas balances involve an accumulation term, the convection and the radial transport towards the surface. In the species solid balance, the transport equals the production. In the energy solid balance the accumulation equals the transport from the gas, the production by the reaction enthalpy and a solid effective axial conduction term, which includes the effects of radiation. The kinetic mechanism is formed by six Langmuir-Hinshelwood reactions. They found that transport phenomena has a decisive role in the POM process and affects heavily the reactor performances. The foam monolith has the best transport properties. If the O_2 conversion is controlled almost exclusively by transport, that of CH_4 is governed by a mixed chemical-transport regime (!). I only wish they used a detailed chemistry: I think this is the only flaw of this remarkable work.

Instead of addressing to a great variety of references, with general comments and fragmented quotations, I preferred to describe in detail a representative set of works. In these we find, on the side of the reactor modeling, the development of the lumped-models implementation and the application of the CFD, and, on the chemistry point of view, different degrees of detail. Experimentally, the POM's been widely investigated, and some insights have been achieved. Further new information over the process are expected from more and more sophisticated experimental techniques, but also the modeling is destined to take the lion's share in the task. Now that the reader formed an idea about the field of POM modeling, he can get through this thesis more consciously, surely finding several references to the concepts mentioned here.

Chapter 2

Justification, choice and use of a kinetic interpreter

2.1 Why use a kinetic interpreter?

A kinetic interpreter has many advantages with respect to a home-made program. It's able to handle whatever mechanism with no limitations on the reactions' number or kind. Only the geometry (and the respective mesh) should be changed to adapt our own simulator to a new problem, with no further concern with the chemistry. Last but not least, it is safe from programming bugs, which would be tough to find out in such a non-linear subject the kinetics is.

One of the most quoted kinetic interpreters is CHEMKIN [8]. It's very powerful and, in the last release, very user friendly. On the pros, it's very well-established and a big effort is put in further improvement. Also, it's got several reactor models available, that make it easy to apply to many industrial problems. Of course it's a licensed software, and it has some (other) fundamental cons for scientific applications: it's not possible to link it to a programming language to write one's own reactor model, and extracting basic chemistry details, such reaction or production rates, is very difficult. An important feature of this software is the standardized format for the mechanisms. A very common way to send out a new kinetic in literature is adopting this format. Therefore, a large amount of input files are available, for a wide range of applications, both with homogeneous and heterogeneous kinetics. Of course these files can be converted and used by other softwares, as well, as enlightened in the following paragraph.

Cantera [6] is a recently developed, free software. It was created in a scientific environment - like, many years before, was the open source of CHEMKIN – and it suits the new computational resources and the latest scientific demand. It's linkable with all the most common programming languages. Every step in the kinetics is to inspect, so that not only there are full reactor models, but also all the information helpful for writing a new model are gathered. As in the modern point of view of the object oriented programming, the simulator refers to the interpreter to gain the thermodynamic and transport properties, as well as the kinetics. Everything related to the chemistry comes from a proper function calling, to include in the differential equations system that forms the reactor model. To all those pros, we must add some cons, which are the relative youth of the code, still not refined, and the lack of a proper documentation. The expert CHEMKIN user finds Cantera rather friendly, but I expect a tenderfoot to be appalled by it.

2.2 Comparison Chemkin – Cantera

This paragraph aims to compare the behavior of the two kinetic interpreters when a detailed surface chemistry is inserted. They use the same basic equations, so we should expect the same results in output. Actually, there is a difference in the way

they handle the sticking coefficients: Cantera doesn't use the Motz-Wise correction, because Goodwin claims it's implemented in the wrong way in CHEMKIN. Since CHEMKIN allows turning off this correction, we compare them using the same settings.

Cantera database is in the same format as in CHEMKIN and in NASA. The mechanism is written in a different way, though, and a conversion is required. For a homogeneous mechanism, the program "ck2cti.m" works it out. When a surface mechanism contains specific keywords, such as sticking coefficients or coverage dependence, a manual "re-writing" of the input file is necessary, following existing examples.

As an example, we've got the Deutschmann – Pt mechanism (A. 1) which is already amid the Cantera demos (A. 2). Running the two programs, we obtain a perfect superposition of results (Fig 2.2-1).

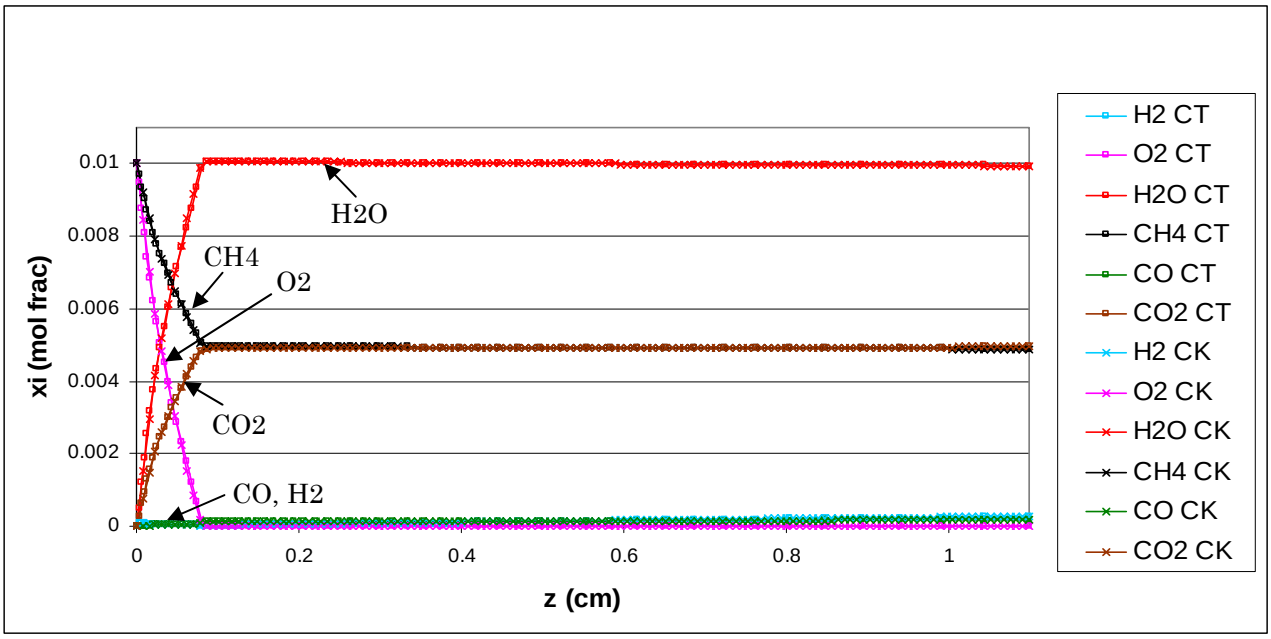

Fig 2.2-1 Comparison between the results of CHEMKIN and Cantera, with the same mechanism.

Not only a naked eye comparison, but also the absolute numerical error (defined as the difference between outlet compositions) states that the results are the same (Table 2.2-1).

	H2	O2	H2O	CH4	CO	CO2
CK	2.695E-04	7.944E-22	9.944E-03	4.891E-03	1.627E-04	4.944E-03
CT	2.658E-04	8.071E-22	9.946E-03	4.892E-03	1.632E-04	4.943E-03
err	-3.73E-06	1.27E-23	2.46E-06	5.95E-07	4.60E-07	-1.04E-06

Table 2.2-1 Errors in the output compositions by the two kinetic interpreters.

When using the different sticking coefficient formulas, though, the results can be seriously different (several percent points).

In Appendix A another mechanism is reported: the Deutschmann – Rh mechanism is converted from the CHEMKIN (A. 3) to the Cantera (A. 4) format. Here again the comparison, not reported, shows that the conversion was made correctly.

2.3 Conclusions

Two kinetic interpreters have been presented, and reasons for choosing Cantera in this background were given.

CHEMKIN and Cantera databases are the same, but in different format: only with surface chemistry the translation of the mechanisms is not trivial. The two softwares, which might work with different settings, when run in the same conditions give identical results.

Chapter 3

Sherwood number for nth order kinetics: generalized correlations vs CFD

3.1 Purpose

The actual geometry of the reactor is responsible for the changes taking place in the fluid flowing through it. The complete description of the flow field would give a very precise solution of all the phenomena occurring in the reactor. Unfortunately that requires handling a complex system of partial differential equations, which is sometimes hard to solve, particularly if the geometry is complicated.

For chemical engineering needed anyway solutions, traditionally the problem was dealt using lumped models, where all the dimensions but one were discarded and replaced by a description of what happens near the surface and in the bulk of the fluid. The farther the particles move away from the surface, the fewer it affects them. This produces a thin layer of fluid near the surface, called boundary layer, in which either the velocity or the composition or the temperature changes from zero at the surface to the free stream value (the mean bulk gas) away from the surface.

Constituent quantities describing these zones are related with a function of the driving force between them, namely a linear contribution in the constituent equations such as a transport coefficient times the difference in the balanced quantity. Transport coefficients can then be obtained either from experiments on the actual facility or from the literature correlations, given as generalized coefficient through dimensionless numbers.

In the past century this analysis was made for simplified reacting systems: a single first order kinetic. This way, it was straightforward to extend heat transport coefficients (the more easily and extensively investigated) to the mass transport ones. This 1st order kinetic assumption is very particular, and can no longer be borne. Modern techniques are now available and allow looking inside the problem in a more general and realistic way, deriving **correlations for mass transfer in reacting and developing laminar flow with arbitrary kinetics**.

3.2 Reaction and diffusion in series

In heterogeneous catalysis a real common problem is the presence of two phenomena in series that determines the production/destruction term in the species balance: the transport of the reactants from the bulk to the surface, by diffusion, and the reaction itself.

When the reaction is slow, there's plenty of time for the species to move in the section, to compensate the gradient of concentration determined by the

reaction. In this case, the radial profile of each species is almost flat, and we can neglect the transport resistance in our balance. The system is said to be in a chemical regime.

More often the catalyst on the wall speeds up the reaction, so that it can be considered instantaneous. This time, a local equilibrium exists near the surface among the species in the small portion of gas in contact with the wall (the boundary layer). Therefore the balance can be written incorporating the transport term only, with an equilibrium concentration representing the wall concentration. This is a transport controlled regime.

In general, the two regimes might be of the same order of magnitude, and both terms should be taken in account for a proper description of all the phenomena. The following simplified analysis shows a few examples where the problem of transport and reaction in series (Fig 3.2-1) was solved.

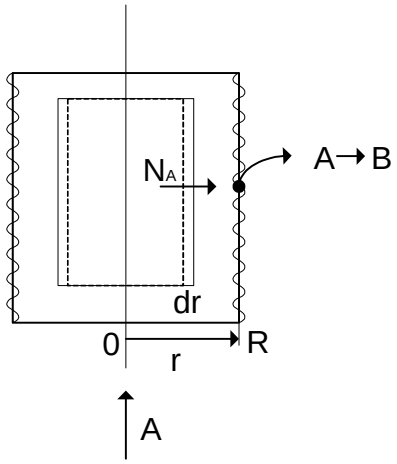

Fig 3.2-1 Section of a tube reactor, with the catalyst on the wall, and control volume for the balances.

In this simplified analysis, the reaction involves a unique reactant, A, turning into the product B after the reaction on the catalytic wall. A gradient of A exists in the radial direction, which is the driving force for a flux of A, N_A.

$$\text{3.2-1}\quad N_A = -D \cdot \frac{dC_A}{dr}$$

According to Fick's law, N_A is proportional to the diffusivity of A and to its gradient. It's not shown in the figure that there is also an opposite flux of B, since the sum of all the fluxes should give zero.

3.2.1 Instantaneous reaction

The simplest case is a very fast reaction, because the concentration is known (either the equilibrium value or the zero concentration). Boundary conditions are for example:

$$\text{3.2-2}\quad \begin{cases} r = 0, & C_A = C_{A0} \\ r = R, & C_A = 0 \end{cases}$$

After integration, the flux is:

$$3.2\text{-}3\quad N_A = -\frac{D}{R}\cdot C_{A0} = -K'_{eff}\cdot C_{A0}$$

Where, for similitude with the subsequent cases we set:

$$3.2\text{-}4\quad D/R=\beta$$

3.2.2 First order, slow reaction

When the reaction is slow, the kinetic must be included in the boundary conditions.

$$3.2\text{-}5\quad \begin{cases} r=0, & C_A = C_{A0} \\ r=R, & C_A = \dfrac{N_A}{k} \end{cases}$$

When a first order kinetic occurs, the flux is still linear in the bulk concentration of the reactant:

$$3.2\text{-}6\quad N_A = -\frac{1}{\dfrac{1}{\beta}+\dfrac{1}{k}}\cdot C_{A0} = -K''_{eff}\cdot C_{A0}$$

3.2.3 Second order, slow reaction

Suppose to further complicate the problem including a second order, not instantaneous reaction:

$$3.2\text{-}7\quad \begin{cases} r=0, & C_A = C_{A0} \\ r=R, & C_A = \sqrt{\dfrac{N_A}{k}} \end{cases}$$

The flux becomes non linear in the bulk composition, and it can no longer be written as a transport coefficient times the bulk composition.

$$3.2\text{-}8\quad N_A = \left(\frac{\beta}{2\sqrt{k}} \pm \sqrt{\frac{\beta^2}{4k} + \beta\cdot C_{A0}} \right) \neq -K'''_{eff}\cdot C_{A0}$$

Taking into account both transport and reaction, in the species balance in 1D model, needs a new approach to the problem and new studies. Otherwise, a new reactor model might be required, for describing the radial direction: a 2D or 3D model might be the best option with n^{th} order kinetics.

3.3 Introduction to Sh

The Sherwood number (Sh) is a dimensionless number used in mass-transfer problems. It represents the ratio of length-scale to the diffusive boundary layer, or, more simply, the ratio of the effective transport to diffusion.

$$\mathrm{Sh} = \frac{K_C \cdot d}{D}$$

It is the mass-transfer equivalent of the Nusselt number, and, because of that, it's been traditionally calculated in analogy with the heat-transfer problem.

3.3.1 Sh: heat transfer analogy

The heat transport problem reflects the simplest situations discussed in the previous paragraph. There are two limiting cases: when the wall is in contact with a thermal reservoir, its temperature is constant; on the other hand, it might be exposed to a constant temperature environment, so that the heat transport for conduction follows a first order dependence on the temperature. In general, a series of intermediate cases may occur, but they are bounded by those just described, and the heat correlation for them lies between those of the constant temperature or of the constant flux.

In the same way, Brauer and Fetting [4] give a linear correlation between constant (=null) wall concentration, Sh(∞), and constant wall flux (=reaction), Sh(0), for the first order kinetic.

$$\textbf{3.3-1}\quad Sh = Sh(0) - \frac{Sh(0) - Sh(\infty)}{Sh(\infty)} \cdot \frac{2DaII' \cdot Sh}{2DaII' + Sh}$$

Which can be traced back to the former definition of transport coefficient for first order kinetic (3.2-6)

$$\textbf{3.3-2}\quad \frac{1}{K_{eff}} = \frac{1}{\beta} + \frac{1}{k}$$

When plotted in a Damköler dependence, it results in a quadratic function (Fig 3.3-1).

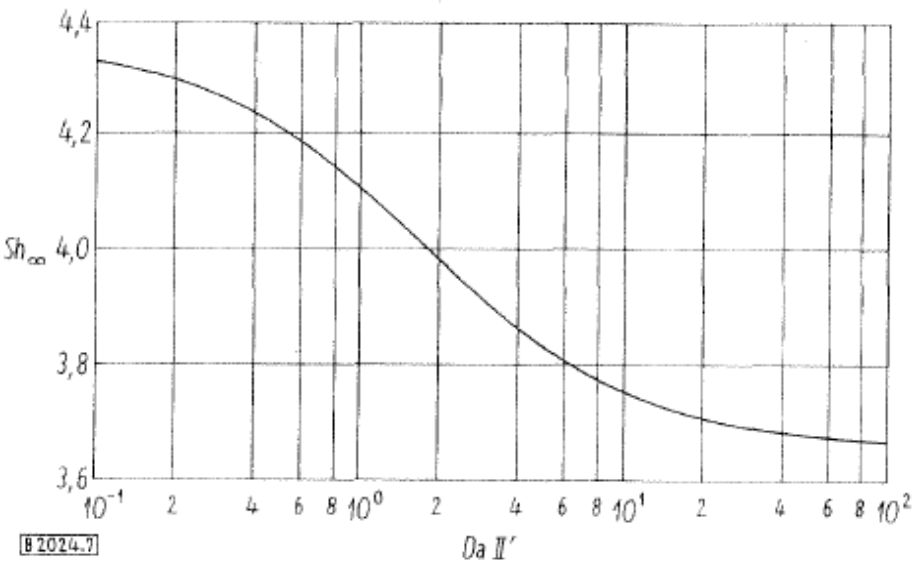

Fig 3.3-1 Asymptotic Sh number as a function of Da number, according to Brauer e Fetting.

Note that only the asymptotic value is considered here, that is the value of the transport coefficient where the flow field is fully developed.

3.4 Numerical solution of the R-D problem

When the entry region is of interest, a series of studies exists for heat transport. For circular pipes of diameter *d*, an exact solution was given by Grigull and Tratz [18], both for constant wall temperature and constant wall flux. To date, these formulas have been applied to the mass transport problem simply by replacing Nu with Sh and Pe_H with Pe_M.

$$Nu_T = 3.655 + (6.874 \cdot (10^3 \cdot Z^*)^{-0.488}) \cdot \exp(-57.2 \cdot Z^*)$$

3.4-1 $$Nu_F = 4.364 + (8.680 \cdot (10^3 \cdot Z^*)^{-0.506}) \cdot \exp(-41.0 \cdot Z^*)$$

$$Z^* = \frac{z}{d \cdot \mathrm{Pe}}$$

For the most common pipe section geometries, this study was extended by Shah and London [36]. An example is shown here, for the honeycomb monolith, written for constant wall flux and in terms of Sh:

$$Sh = 2.977 + (8.827 \cdot (10^3 \cdot Z^*)^{-0.545}) \cdot \exp(-48.2 \cdot Z^*)$$

3.4-2 $$Z^* = \frac{z}{d_{cell} \cdot \mathrm{Pe}}$$

In the following these formulas will be compared with the results of a numerical experiment, on one hand to verify whether the analogy is correct for a first order kinetic, on the other to see what happens for a second order kinetic.

If we consider a pipe of whatever geometry, with a catalytic activity on the inner surface, a concentration profile arises at the inlet.

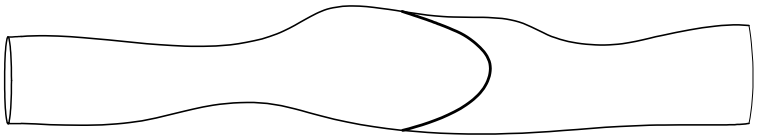

Writing a 1D model of it, we may want to relate the mean gas concentration to the concentration near the surface (which determines the production term in our balance, and that we want to include in the expression of the reaction rate).

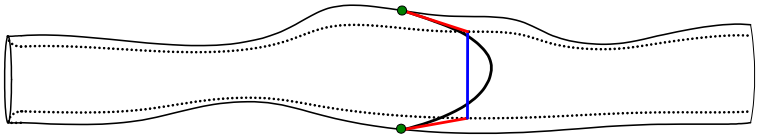

The mean Sh number can be calculated as the ratio between the slope of the concentration profile, evaluated at the surface, and the difference between the bulk mean concentration and that on the surface itself.

$$\overline{\mathrm{Sh}} = \frac{-\left(\frac{dY}{d(r/d)}\right)_S}{Y_b - Y_s} \qquad \textbf{3.4-3}$$

This way, if we can solve a full 2D or 3D model, we can evaluate $\overline{\mathrm{Sh}}$.

3.4.1 First order kinetics

The fluid-dynamic modeling is a powerful tool for "looking inside" the reactor, since it provides the complete description of the flow field and the composition of the system. If the geometry of the reactor is suitable to be drawn in an easy way in 3D (even better if it has such symmetries that it can be simulated through a 2D model!), the full fluid-dynamic description is the best choice for out modeling. There are problems, though, we can't reproduce in enough detail, such a packed bed or a foam monolith, in which simpler models must be used.

For the purposes of this chapter, we'll study a very simple circular pipe reactor, studied through a Multiphysics [32] (in the following, MP) axial symmetric 2D model. A first order reaction occurs at the wall. No heat release. The reactant enters the reactor with a hydrodynamic full developed profile.

The predictions of Grigull's (3.4-1) and Brauer's (3.3-1) are compared with the calculated Sh from MP. Constant composition Sh is referred as $\mathrm{Sh_C}$, while constant flux one is $\mathrm{Sh_W}$. Moreover, Brauer's equation can be made explicit in Sh as follows:

$$\mathrm{Sh(Da)} = \frac{1}{2\cdot \mathrm{Sh_C}}\left(\mathrm{Sh_W}\cdot\left(\mathrm{Sh_C}-\mathrm{Da}\right)+\sqrt{\left(\mathrm{Sh_C Sh_W}\right)^2+\left(\mathrm{Sh_W Da}\right)^2+2\mathrm{Sh_C Sh_W Da}\cdot\left(2\mathrm{Sh_C}-\mathrm{Sh_W}\right)}\right)$$

We must discern between slow and fast reaction.

FIRST ORDER FAST REACTION

For a first order fast reaction the concentration of the reactant close to the surface drops fast to a value close to zero (Fig 3.4-1). To recall what said before, we are in the case of transport regime, and the reaction is almost instantaneous. As in §3.2.1, the flux of the reactant towards the surface depends only on the concentration in the bulk and on the diffusion to radius ratio. Besides, the concentration in the bulk decreases through the reactor, and the flux lowers, as well as the difference between bulk and surface concentration. In Fig 3.4-2 the resulting Sh is depicted.

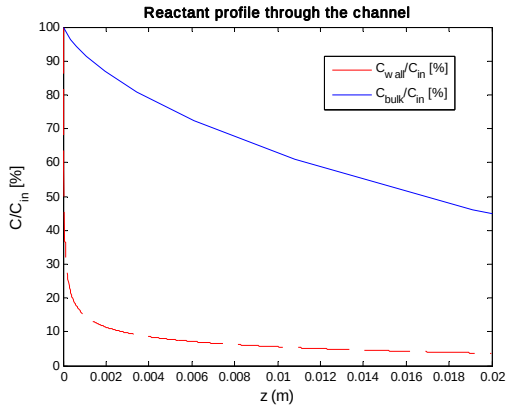

Fig 3.4-1 Profiles of the reactants in the middle of the channel and close to the surface, in terms of C/Cin, for a first order fast reaction.

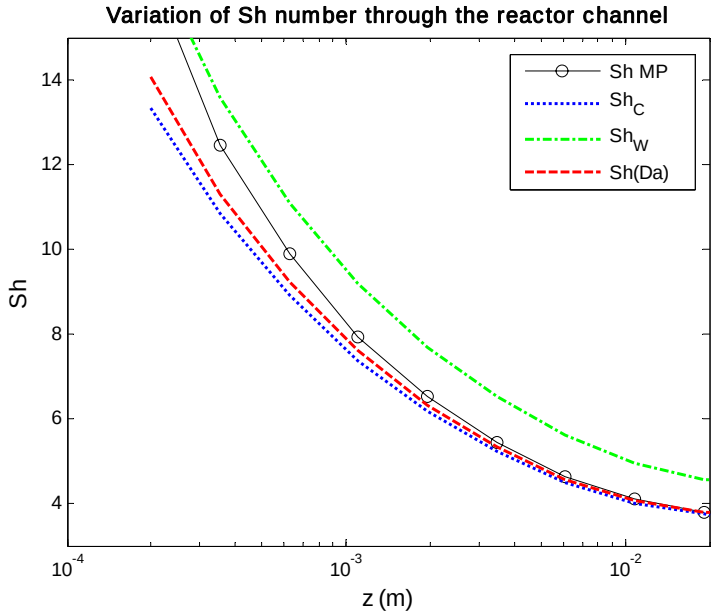

Fig 3.4-2 Comparison between predicted and real Sh number for a first order fast reaction.

Results of Sh are plotted in a semi-log(x) scale to display both the entry region and the asymptotic value.

Grigull's Sh_C and Sh_W represent respectively the lower and the upper limits of the Sh for each position. They run theoretically from and infinite value to their characteristic asymptotic value, with an exponential decrease. Sh(Da) places between them, as well as the exact solution, but the two values don't match. Sh(Da) keeps close to the Sh_C solution, but at the very beginning of the entry region it is somewhat higher because the concentration close to the surface has not reached its lower value, yet. It still is a mixed regime, since the chemical contribute is not negligible. The real solution runs even further away from the Sh_C, at the beginning, meaning that the chemical contribute is even higher than in the theory. Eventually, they meet at the asymptotes, where they both lay on the Sh_C. Indeed, after the entry region, this particular problem and the constant wall concentration case study are alike.

FIRST ORDER SLOW REACTION

A slow reaction determines a rather faint decay in the reactant concentration (Fig 3.4-3). We're here in chemical regime, where the concentrations on the bulk and on the surface are the same. No big change in concentration happens through the reactor.

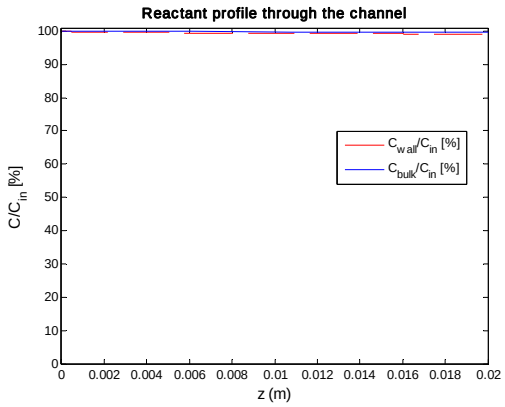

Fig 3.4-3 Profiles of the reactants in the middle of the channel and close to the surface, in terms of C/Cin, for a first order slow reaction.

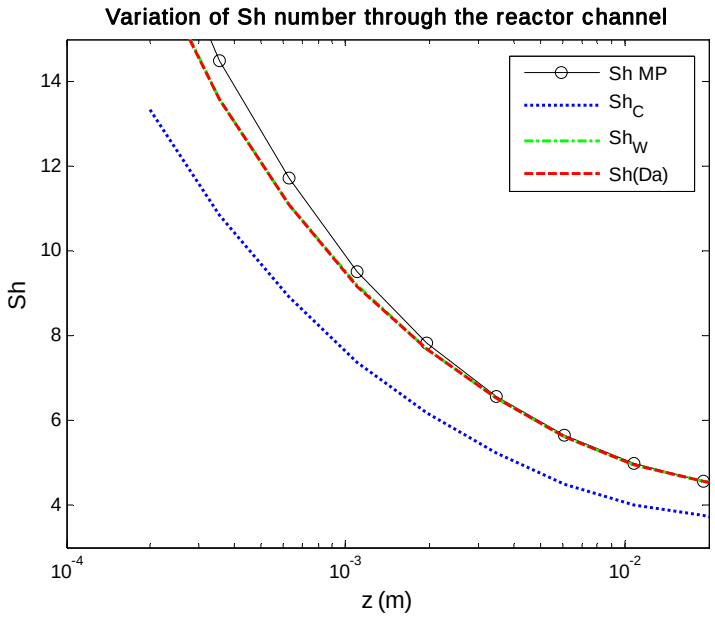

Fig 3.4-4 Comparison between predicted and real Sh number for a first order slow reaction.

This is a typical case of constant wall flux, linear function of the bulk concentration, which keeps constant along the reactor. As expected, Sh(Da) lies on the Sh_W curve (Fig 3.4-4). Here again, the real solution remain higher than that theoretical. Furthermore, it also stays outside the Grigull's formulas region. That means these two boundaries for heat transport are not properly applicable to the mass transport, in the presence of a chemical reaction. Apparently, with a reaction occurring at the wall, the transport is much more effective than that predicted by the heat transport analogy.

As an aside, the solution for a non developed velocity profile is given in Fig 3.4-5, where the reactant enters with a flat profile. Obviously, the developing velocity boundary layer allows a bigger transport of reactant from the bulk to the surface, and the resulting Sh is much higher. Where the entry region finishes, the asymptotic value converges again on the Sh_W solution.

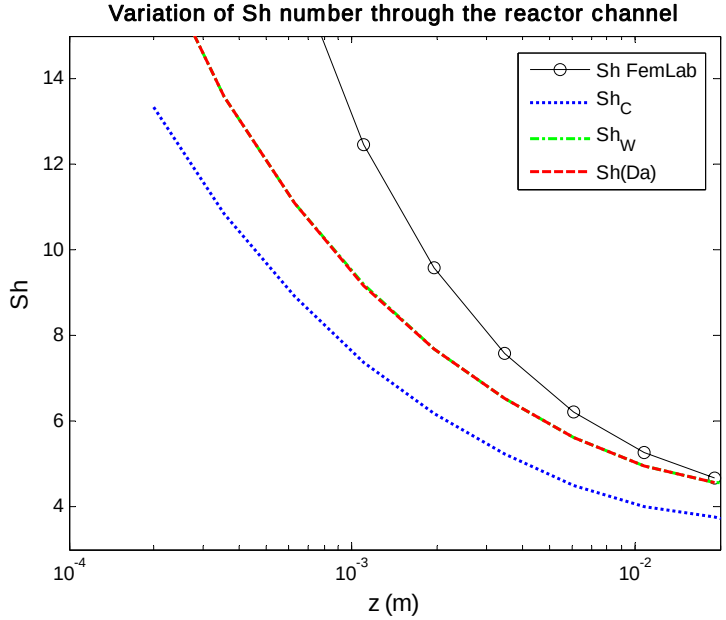

Fig 3.4-5 Comparison between predicted and real Sh number for a first order slow reaction, with flat velocity profile at the entrance.

FIRST ORDER NORMAL REACTION

Without seeking limiting cases, let's now have a look at the most common problem in which we have a mixed regime all along the reactor. That leads to a certain decrease in both the bulk and the surface composition, being neither the surface composition nor the difference zero (Fig 3.4-6).

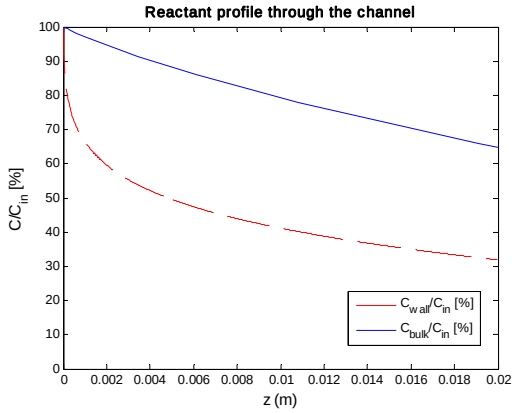

Fig 3.4-6 Profiles of the reactants in the middle of the channel and close to the surface, in terms of C/Cin, for a first order normal reaction.

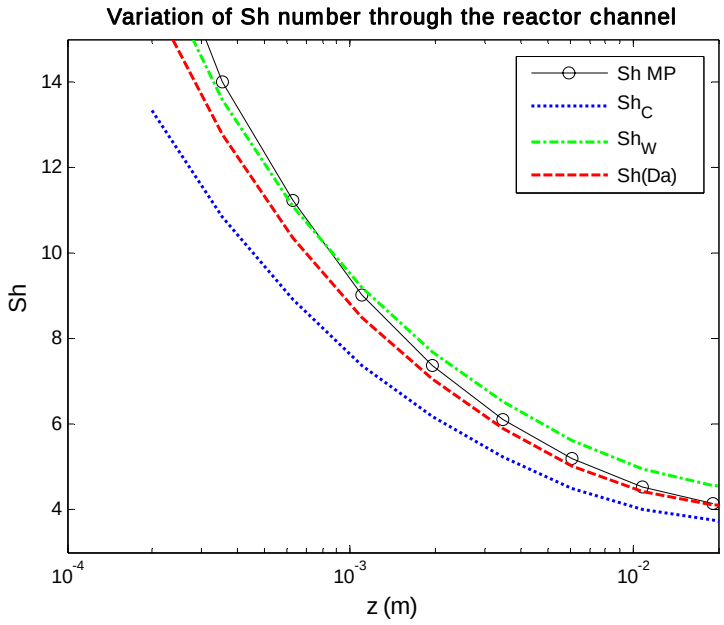

Fig 3.4-7 Comparison between predicted and real Sh number for a first order normal reaction.

The asymptotic Sh(Da) ends up in the middle between Sh_C and Sh_W. In the entry region its slope is here again higher than that of the Grigull's. The MP curve is even steeper, and even if its value crushes with the long distance Sh(Da), the entry region line lies above the ruled range.

3.4.2 Second order kinetics

When the actual reaction is second order, we're no longer in analogy with the heat transport, since there's no such law that describes any of the heat transport phenomena.

SECOND ORDER FAST REACTION

With a second order fast reaction, the concentration decay is even steeper than with a first order (Fig 3.4-8). Anyway, given the similarity in the concentration profile, the Sh should behave the same as in the first order fast reaction.

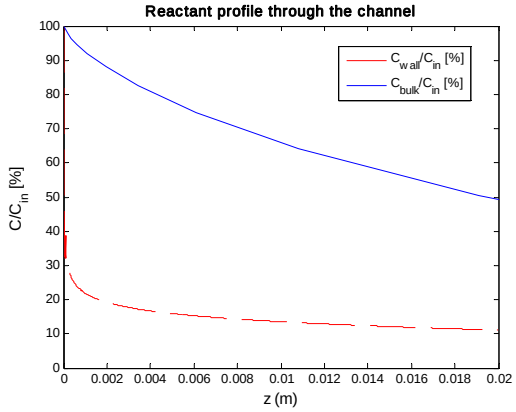

Fig 3.4-8 Profiles of the reactants in the middle of the channel and close to the surface, in terms of C/Cin, for a second order fast reaction.

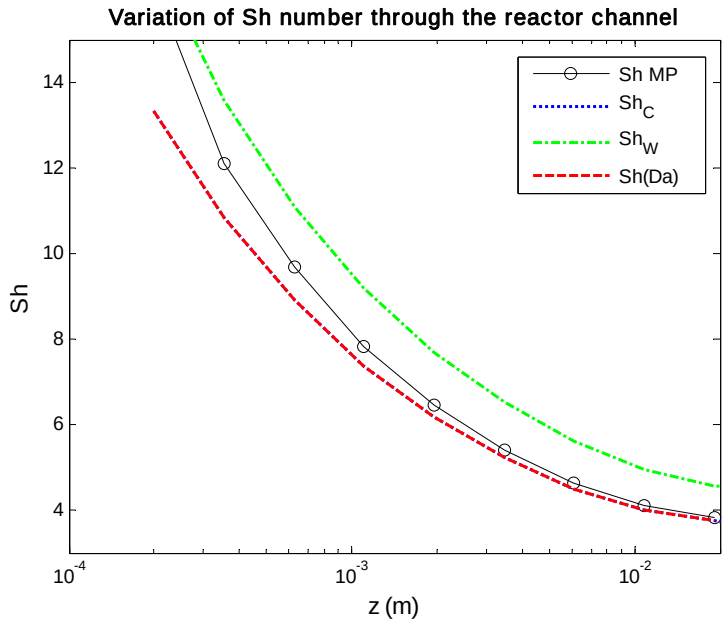

Fig 3.4-9 Comparison between predicted and real Sh number for a second order fast reaction.

As expected, the real Sh number ends up in the Sh_C curve far away from the entrance, while in the inner region is higher (Fig 3.4-9) Again it doesn't match with that calculated with Brauer's correlation, which in this case lay over the Sh_C all the way long.

SECOND ORDER SLOW REACTION

Also the second order slow reaction resembles the respective first order in the concentration profile, which is pretty flat for both the bulk and the surface concentration (Fig 3.4-10).

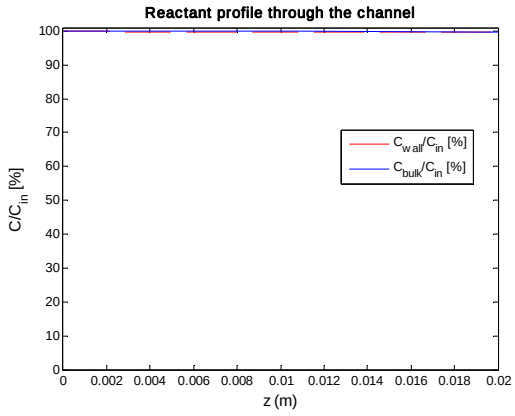

Fig 3.4-10 Profiles of the reactants in the middle of the channel and close to the surface, in terms of C/Cin, for a second order fast reaction.

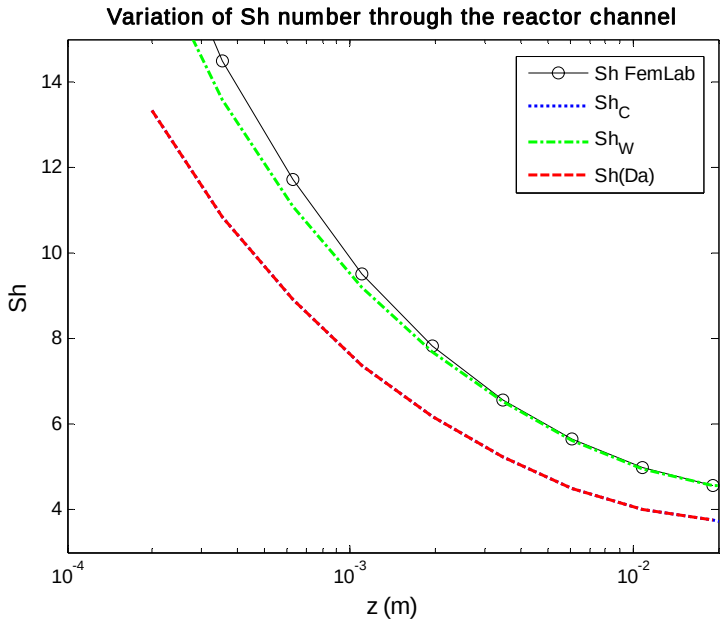

Fig 3.4-11 Comparison between predicted and real Sh number for a second order kinetic.

Again, the real Sh lays outside the boundaries set by Grigull's equations (Fig 3.4-11), meaning that a higher transport occurs in the inner region than that predicted from literature correlations. It is remarkable that the Brauer's solution lies again over the Sh_C curve, even though the physical interpretation would put it over the Sh_W line, instead.

3.4.3 Asymptotic Sh

Focusing only on the asymptotic values, let's analyze the variation of Sh with the velocity of reaction.

The reaction orders n=1,2,3 are investigated, with k varying between $1 \cdot 10^{-4}$ and $1 \cdot 10^{7}$. In Fig 3.4-11 all the results are plotted as a function of the kinetic constant, for different reaction orders and inlet concentrations.

For n=1 the trend agrees with the theoretical (see Fig 3.3-1).

For n>1 Sh is bigger, given the same k. This is consistent with the use of a low concentration of the reactant. Moreover Sh depends also on the inlet concentration.

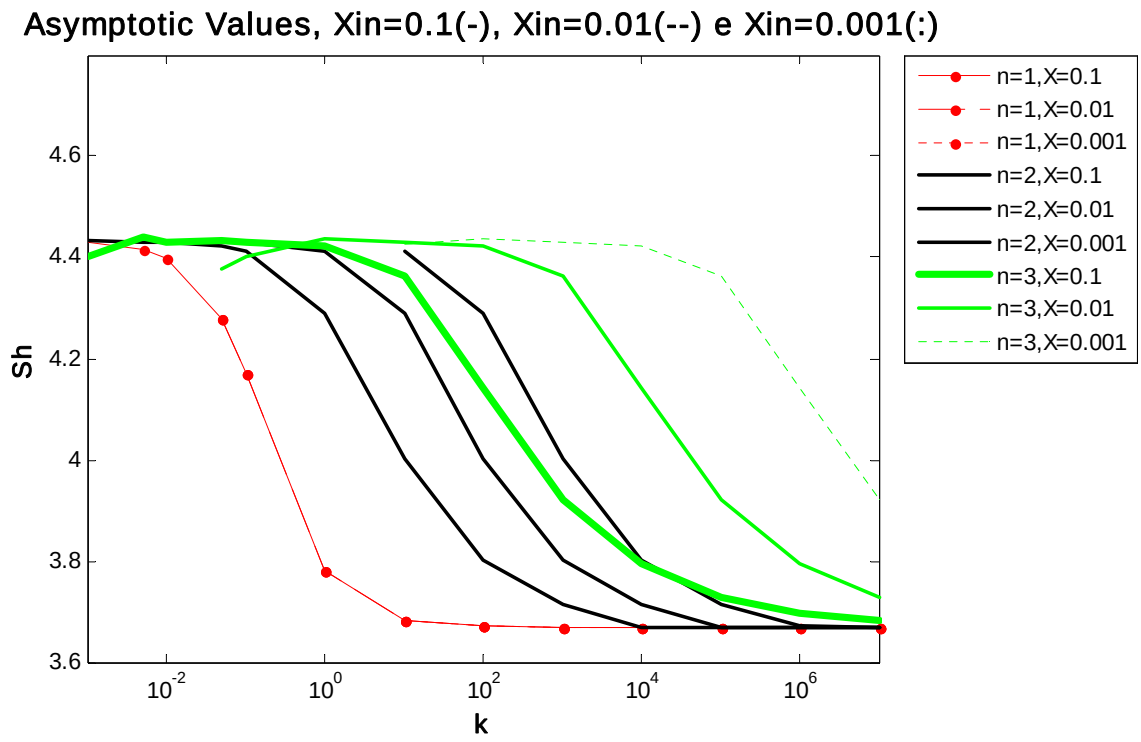

Fig 3.4-12 Asymptotic Sh values with respect to the kinetic constant for different reaction orders and inlet concentrations.

3.4.4 Asymptotic Sh, function of Da

In the attempt to generalize the behavior of the curves, we can go back to the definition of the Damköler number, that account for the reaction order: $Da = \frac{k \cdot c_A^{0(n-1)} \cdot R}{D}$. If we put the curves in a plot with the Da (or the $k \cdot c_A^{0(n-1)}$ product), we obtain a single curve for each reaction order (Fig 3.4-13).

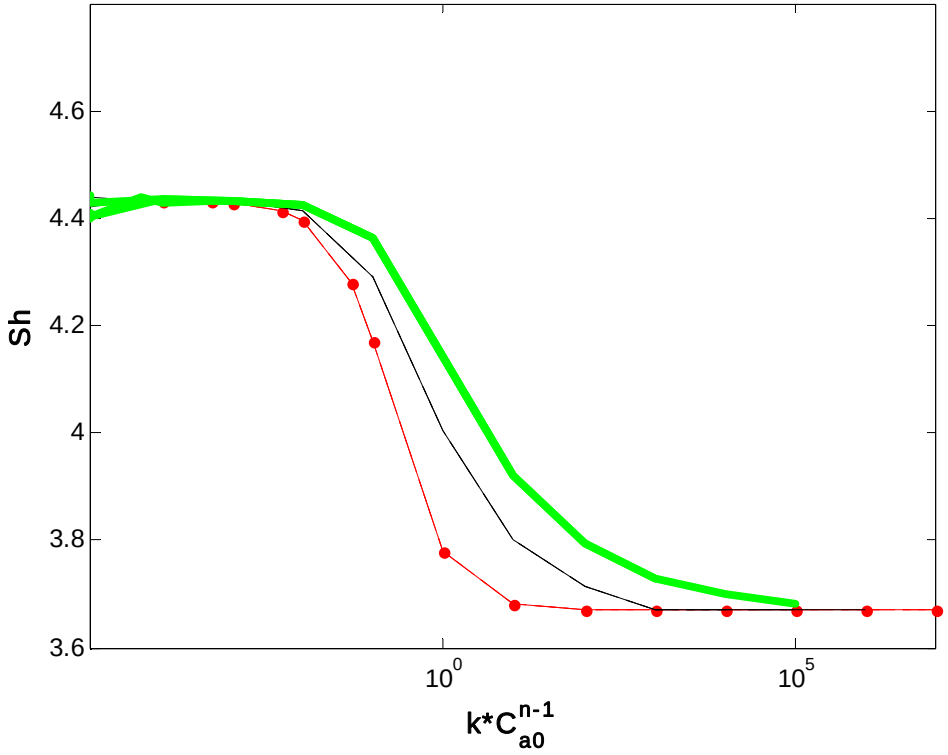

Fig 3.4-13 Asymptotic Sh values with respect to the Da for different reaction orders and inlet concentrations.

The behavior of Sh is still a monotonic function of Da, but with the higher orders the function is slightly different from that found by Brauer e Fetting in the 66.

To simplify, if for n=1 we've got:

$$Sh = \sqrt{(Da - a)^2 + b \cdot Da} - (Da - a)$$

where a,b are functions of Sh_C and Sh_W. The limit for Da→0 is 2a, while for Da→∞ is b/2.

The functions for n>1 have the same horizontal asymptotes.

The inflection point for n=1 is in Da=(b+4a)/3, while for the others is shifted upwards and the shape of the curves are distorted.

Still, the further generalization of this equation is beyond the objective of this thesis. As a matter of facts, with the use of a detailed mechanism, the actual order or reaction changes along the reactor, making a Sh(n) useless anyway.

3.5 Conclusions

The bases on transport coefficient approach are given, describing the dimensionless number approach and the heat transport analogy. Some analytical and numerical solutions of the reaction and diffusion problem are shown.

Correlating the real Sh number with the CFD, we see that in the entry region, the exact solution gives a higher value than the theory. The asymptotic values match for the extreme cases, both for n=1 and n=2: if the kinetics is fast, the wall composition approaches zero, and the Sh coincides with Sh_C (constant concentration); if the kinetics is slow, the wall composition is almost constant along the reactor, and the Sh coincides with Sh_W (constant wall flux). For the intermediate kinetics, the analogy is verified for the asymptotic values in case of first order, while for higher orders also the asymptotic value is mismatched. The approach of the Sh(Da) is valuable, but it should be extended to Sh(Da, n).

For kinetics not of the first order, Sh number should be calculated numerically, or a different reactor model is to be used – adopting CFD.

Chapter 4

1D Models – Variety and solution techniques

4.1 Coming to the point

A detailed kinetics is essential in the simulation of a catalytic reactor. A global mechanism often gives a not adequate prediction in the wide range of temperature and composition typical of the catalytic reactor. As discussed in Chapter 2, the up-loading of a multi-step kinetics, not strictly Arrhenius-shaped, is not trivial. Nonetheless, it's feasible. The resulting simulator is specialized on that mechanism and bound up with those chemical species. Instead, the use of a kinetic interpreter allows a free interchange between several mechanisms. The simulator only depends on the geometry, which might even be generalized but is easily implemented, anyway. Given a reactor set-up, the simulator will be able to predict the behavior of different chemical systems without any modification: only a new data sheet for the mechanism will be needed, which is in a standard format and possibly available in literature.

The main challenge is the coupling of the kinetic interpreter with a suitable reactor model. The simplest ideal PFR was taken at first. Complexity has been increased step by step, dropping one after the other the simplifications, and adding the more relevant physical features. It was a matter of reaching a good compromise. Eventually, the motto was: the best model you can solve is the model you *can* solve, which means the more detailed model you are able to solve with the actual computational resources.

4.2 PFR

The Plug Flow Reactor (PFR) is the simplest model that can be written for a system in flow. It states that convection of species, as well as of heat, is equal to its production/consumption. Physically, is assumes infinite radial diffusion, which turns out in a flat profile, and zero axial diffusion, that means a segregated volume of fluid flowing through the channel without exchanging anything with those beside it (Fig 4.2-1).

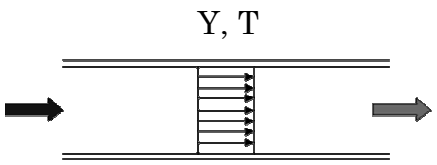

Fig 4.2-1 Composition and temperature radial profiles inside a PFR.

The mathematical formalization of this model follows. Note that neither here nor in the following any momentum balance will appear: all through this thesis the assumption of constant momentum will be made. Also, the equation $G=\rho v$ is generally true for steady-state systems.

MB:

$$\rho v \frac{dY_i}{dz} = r_i \cdot W_i \quad i = 1..Nsp \tag{4.2-1}$$

EB:

$$\rho v \cdot c_p \frac{dT}{dz} = \sum_j R_j \cdot \Delta H_{R,j} \quad j = 1..N\ reactions \tag{4.2-2}$$

This model is well applicable to systems in flow in which a homogeneous kinetic occur, and Pe>>1 (axial diffusion can be neglected). With heterogeneous kinetic, it's valid only where the chemical is the controlling regime, in comparison with transport.

Being a system of ordinary differential equations, it's easily solved with standard integration techniques, like those implemented in Matlab [31] in *ODEnn.m* functions.

4.3 Nusselt (Nu)

In heterogeneous catalysis a fence in the reactivity is caused by the availability of the reactant on the surface and the dissipation of the heat of reaction into the bulk of the gas. The issue of the transport of a property, either heat, composition or momentum, from the bulk to the surface, has been studied since the earliest times of the chemical engineering. A solution has been found for the simplest geometries and adopting the analogy between heat and mass transport (see Chapter 3). Even though this analogy is valid only for first order kinetics, it is still used because it allows writing 1D models with detailed kinetics. The frontier is the coupling of detailed kinetics and precise description of the flow field, through the use of CFD. This is not too far away, but it still requires huge computational efforts and today it's applicable to simple geometries only.

The traditional approach to transport coefficients lies on dimensionless numbers: from literature, relations can be found to calculate the transport coefficient (thermal in this context, K_T) for the actual system, given the Re and Pr numbers.

Focusing on the energy balance, this is split in two equations, because now two different temperatures are considered: that of the bulk and that of the boundary layer. As to say that there are two phenomena in series, the transport and the reaction, and with this mathematical tool we can handle this feature.

Bulk EB:

$$\rho v \cdot cp \frac{\partial T_G}{\partial z} = -S_V \cdot K_T \left(T_G - T_S \right) \tag{4.3-1}$$

BL EB:

$$S_V \cdot K_T \left(T_G - T_S \right) = S_V \cdot \left(\sum_{k=1}^{Nsp} h_k \cdot \dot{s}_k \right) \tag{4.3-2}$$

4.4 Conduction

The simplest conduction model (COND) is based on the PFR model, except that it includes the conduction through the solid substrate. Indeed, it turns out to be very useful in heterogeneous catalysis, where there is a solid structure that holds the catalyst, and this solid material might be a metallic high conducting material or a ceramic support, that is intrinsically not very conducting, but being exposed to high temperature gradients might allow some extent of heat passing through it.

From the Math point of view it is rather simple to add such feature into the energy balance:

EB:

$$\rho v \cdot c_p \frac{dT}{dz} + \frac{d}{dz}\left(\lambda \frac{dT}{dz}\right) = \sum_j R_j \cdot \Delta H_{R,j} \qquad j = 1..Nsp \tag{4.4-1}$$

When such equation is to put into a real model, though, the parameters definition and the boundary conditions setting are not trivial. As it is, this equation accounts for both gas and solid conduction, and a weighted conductivity λ has to be evaluated. Also, being a second order differential equation, boundary conditions are required at the inlet and outlet, which are physically hard to describe, being a pseudo-homogeneous model made by two phases.

For these reasons, this model, easy to write, is seldom used (I saw it used in a porous model, once).

4.5 Nu-Conduction

The coupling of the models described in §4.3 and §4.4 leads to a useful and quite widespread thermal model. With surface kinetics, the heat released or absorbed by the reaction locates on the solid surface. That means there'll be an uneven temperature distribution inside the catalyst. For example, it may happen that the surface, where the reaction takes place, is hotter than the mean section temperature, so that the actual kinetics is much faster (following an exponential function!) than that calculated without considering the temperature gradients.

The Nu model allows describing two different temperature profiles along the reactor: of the bulk gas and of the solid. The conduction model can now be properly applied to both the gas and the solid phase, adopting the corresponding heat conductivity and the proper boundary conditions. Even so, it's mostly restricted to the solid balance, being the conduction more important in it than in the gas (the gas conduction is usually neglected, unless the Pe number approaches unity). Observing this rule, as well as the intent to proceed in an orderly manner, only the solid conduction will be shown here.

For the gas phase heat balance, refer to eq. 4.3-1, while the solid temperature comes from the eq. 4.5-1. The funny coefficient in front of the conduction term arises from the fact that the catalyst section is occupied by the gas for a fraction ε (the "void" fraction) and the complement is the space taken up by the solid (1-ε being the "solid" fraction). Since all the equations I've written through this thesis are on "void volume basis", to turn the conduction term (pertinent only to the solid) into a "per void volume

basis" I needed to multiply it for the solid fraction and divide for the void fraction. Besides, to account for the resistance the heat has to overcome to pass through the twisted solid path, a "tortuosity" factor is included.

BL EB:

$$\frac{1-\varepsilon}{\varepsilon} f \frac{\partial}{\partial z}\left(\lambda_S \frac{\partial T_S}{\partial z}\right) = -S_V \cdot K_T \left(T_G - T_S\right) + S_V \cdot \left(\sum_{k=1}^{Nsp} h_k \cdot \dot{s}_k\right) \quad \text{4.5-1}$$

Being this a boundary value problem, a suitable solver has to be adopted, such as the *bvp4c.m* by Matlab.

4.6 Nusselt and Sherwood (Nu-Sh)

The Nu model, described in §4.3, is not strictly correct, nor is the Nu-Cond in §4.5, since they assume the transport is limiting for the heat, but not for the mass. Since both heat and mass are conveyed by molecules, a more rigorous model should take in account both the transport coefficients, respectively by means of Nusselt (Nu) and Sherwood (Sh) dimensionless numbers.

For heat transport see Eqq. 4.3-1 and 4.3-2.

For mass transport, the convection equals the transport from the bulk to the boundary layer, and, close to the surface, the transport equals the production rate.

Bulk MB:

$$\rho v \frac{\partial \mathbf{Y}_G}{\partial z} = -S_V \rho \mathbf{K}_C \left(\mathbf{Y}_G - \mathbf{Y}_{BL}\right) \quad \text{4.6-1}$$

BL MB:

$$-S_V \rho_{BL} \mathbf{K}_C \left(\mathbf{Y}_G - \mathbf{Y}_{BL}\right) = S_V \dot{\mathbf{s}} \mathbf{W} \quad \text{4.6-2}$$

This is a mixed differential-algebraic system of 2·(Nsp+1) equations. This kind of problem is quite challenging from the math point of view. It was solved in literature only with a Langmuir Hinshelwood mechanism [30], with a rather sophisticated DAE solver [5]. Others [2][3] found more convenient to skate over the Sh treatment by using an equivalent first order kinetic constant in finding an overall source term for each species that account for reaction and diffusion in series (see Chapter 1).

The use of this model, coupled with Cantera, is rather straightforward adopting the DAE solver by Matlab, which is anything but stable, though.

4.7 Nu-Sh-Cond

Given the application to the catalytic combustion, with very high heat release, the temperature gradients are such that solid conduction cannot be neglected, even if the monolith substrate is a ceramic material.

The complete model is made by eqq. 4.6-1 and 4.6-2 for the species balances, and by eqq 4.3-1 and 4.5-1 for the heat balances.

It turns out being a second order differential-algebraic equation system. The solving techniques adopted for the DAE system are not suitable, here, since it's an initial value solver, and we are before a boundary value problem. On the other hand, the BVP solver adopted earlier is not applicable to a DAE system. It looks like we ran out of solvers!

The usual procedure for dealing with such a problem is to discretize the derivatives and solve it as a non-linear algebraic equation system. Nevertheless, the number of variables is 16 (7 species and one temperature for each phase) and the minimum number of steps to describe the monolith is 50, so we would end up with a Jacobian matrix of the dimension of 800^2, even though sparse. The size and the nature of the algebraic problem discourage to solve it.

Instead, we preferred to use a homothopy continuation technique, choosing to face up to the full transient of the system, which is now an ordinary differential equation system in time. The Jacobian matrix is of the same size as the steady state model, but much simpler, and the ordinary differential eq. system is extremely stable. Thus, the method of lines was implemented, in which the space variable is discretized, transforming the problem in an Nv x Nstep variable problem.

Bulk MB:

$$\rho\frac{\partial \mathbf{Y}_G}{\partial t} = -\rho v\frac{\partial \mathbf{Y}_G}{\partial z} - S_V\rho\mathbf{K}_C\left(\mathbf{Y}_G - \mathbf{Y}_{BL}\right) \quad Nsp = 7 \tag{4.7-1}$$

BL MB:

$$\rho_{BL}\frac{\partial \mathbf{Y}_S}{\partial t} = \rho_{BL}\cdot S_V\cdot\mathbf{K_C}\left(\mathbf{Y}_G - \mathbf{Y}_{BL}\right) + S_V\cdot\dot{\mathbf{s}}\cdot\mathbf{W} \quad Nsp = 7 \tag{4.7-2}$$

Bulk EB:

$$\rho\cdot cp\frac{\partial T_G}{\partial t} = -\rho v\cdot cp\frac{\partial T_G}{\partial z} - S_V\cdot K_T\left(T_G - T_S\right) \tag{4.7-3}$$

BL EB:

$$\frac{1-\varepsilon}{\varepsilon}\rho_S\, cp_S\frac{\partial T_S}{\partial t} = \frac{1-\varepsilon}{\varepsilon}f\frac{\partial}{\partial z}\left(\lambda_S\frac{\partial T_S}{\partial z}\right) + S_V\cdot K_T\left(T_G - T_S\right) - S_V\cdot\left(\sum_{k=1}^{Nsp} h_k\cdot\dot{s}_k\right) \tag{4.7-4}$$

Needless to say, the transient itself is of no interest. Only the steady state solution is regarded, where the catalysis assumption of no deposition is fulfilled, since the $\mathbf{Y_{BL}}$ (and thus the surface coverages) are constant in time.

4.8 Nu-Sh-Cond-Diffusion-Radiation (Foam)

Where necessary, gas conduction and diffusion may be taken in account. It's when Pe, the ratio between convection and conduction or diffusion, is close to unity. It means that the transport due to molecular diffusion is no more negligible if compared to the convective contribution. Also, radiation among solid surfaces can contribute to the axial heat spreading, like and extra solid conduction. This is particularly the case

of non straight geometries. However, even if some extent of radiation absorption occurs in the gas phase, because of the presence of methane and water, this contribution is never accounted.

Although mentioned here, this model will be described properly in Chapter 6, together with the application to the foam catalyst, for which it was written.

4.9 Summing up

In the Table 4.9-1 you'll find the names of the models used through the next two chapters, together with the actual Matlab program name, that helps reaching the respective code in Appendix B.

"Application" refers to whether the model was applied to the square channel monolith (S) and/or to the foam monolith (F).

"Effort" is clearly the difficulty in solving the model. It is not surprising that the more detailed the model is, the trickier is the resolution.

"Algorithm" recalls the solution technique.

"Production" means "where" the production/destruction of the species is located, according to the model.

"G – convection" tells if the convection in the gas phase is considered. Notice that, as well as a production term, the gas convection term is included in all the models.

"G – D/λ" sais that the gas diffusion and conduction is important. Of the following two cases studied, only the foam requires these terms to be regarded.

"K_C" and "K_T" represent the transport coefficient approach.

"S – conduction" and "S – radiation" only refer to the conduction and radiation through the solid support.

Name	PFR	Nu-Cond	Nu-Sh	Nu-Sh-Cond	Foam
Application	S/F	S	S	S	F
Effort	1	2	3	4	5
Algorithm	ode	bvp4c	DAE	transient	transient
Production	G	G	S	S	S
G – convection	x	x	x	x	x
G – D/λ	-	-	-	-	x
K_C	-	-	x	x	x
K_T	-	x	x	x	x
S – conduction	-	x	-	x	x
S – radiation	-	-	-	-	x

Table 4.9-1 Name and main features of the 1D models.

4.10 Conclusions

Seven different 1D models are discussed here, of increasing detail, and hints on the solving techniques are given. Five out of seven are used in the following of this

thesis, to model the catalytic partial oxidation of methane in two different monolith geometries.

The argumentation in here might look a little dull, and quite didactic, but I experienced that not even the plainest model is useless, if you can critically read its results. Besides, increasing the complexity step by step, you should see the prediction improve from the (justified) bad results of the simplest model to the (hopefully) better prediction of the more complicated ones. You could find out that the former is not bad at all, making no sense in adopting something more complicated to solve. More realistically, you can sense which of the features you add is the most relevant in the actual situation. Furthermore, it guides you towards the right choices in approaching the CFD modeling, where it is applicable.

Chapter 5

The 1D model applied to the square channel monolith

5.1 A first case study

Improving methane combustion in short contact time reactors is important for being competitive towards other techniques, bulkier and less efficient. Using small reactors, even with the same productivity, allows using more precious catalysts, which lower the temperature and prevent NOx.

Short contact times (typical residence time of milliseconds) are either fixed bed or monolithic reactors, which could be shaped as a structured straight channel or as an unstructured foam support.

For kinetic studies, in which you'd like to model the reactor as closely as possible, the monolith is the best choice. It also gives the lowest pressure drop. On the other side, the foam and the packed bed are more efficient, since the flow pattern is messier and the transport is enhanced.

5.2 Experimental work

The experiments were carried out by Andrea Scarabello at KTH – Royal Institute of Technology – in Stockholm (SE). Only the details relevant for the modeling are reported here. For further insight his work is addressed [35].

5.2.1 Reactor set up

The reactor consists of a quartz tube schematically depicted in Fig 5.2-1 with a length of 450 mm, external diameter of 18.5 mm and inner diameter of 16 mm. The diameter, at the approximate distance of two thirds of overall length, reduces externally to 7.9 mm and internally to 6 mm.

The reactor is placed in the center of an electrically heated furnace in order to reach a uniform temperature. The furnace is governed by a programmable controller, which uses one thermocouple for measuring the temperature inside the furnace.

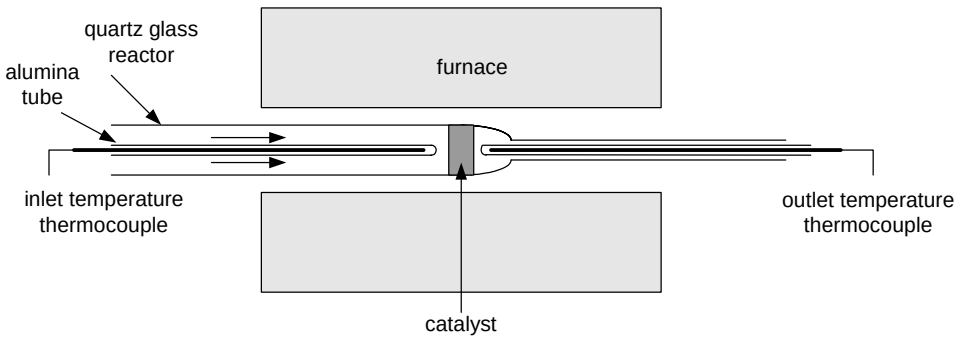

Fig 5.2-1 Reactor used for the activity tests.

The monolith is sketched in Fig 5.2-2, and in Table 5.2-1 the relative properties are given: geometry and composition of the substrate.

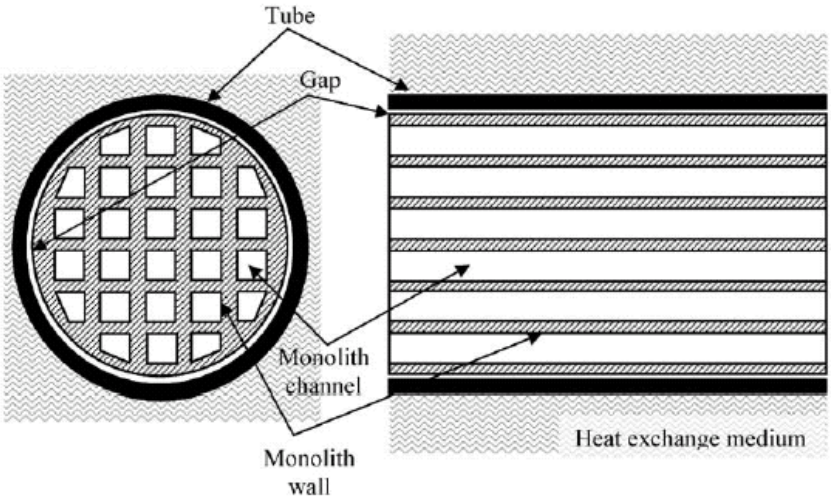

Fig 5.2-2 Sketch of the square channel monolith.

Monolith properties	
Monolith length [mm]	10
Monolith material	Cordierite
Composition	$2MgO \cdot 3Al_2O_3 \cdot 5SiO_2$
Cell density [cpsi]	400
Hydraulic channel diameter [mm]	1.07
Strut thickness [mm]	0.22
Square cells	89

Table 5.2-1 Monolith properties.

Thermal properties of cordierite were found in literature [20]:

$$\lambda(Wm^{-1}K^{-1}) = 1.132 \cdot 10^{-6} T(K)^2 - 3.228 \cdot 10^{-3} T(K) + 4.793$$

The activity of the rhodium catalysts was tested under fuel-rich conditions. Two supports were used (ZrO_2 and CeO_2-ZrO_2), but in the present work only one of them is taken as a yardstick to compare the numerical results of the different models: the 0.5 wt.% Rh/ZrO_2. Keeping the flow rate constant, the oven temperature was varied to scan different reacting temperatures (Table 5.2-2).

Pressure [atm]	Temperature range [°C]	GHSV [h^{-1}]	Total gas flow (20°C) [ml/min]
1	300-750	100000	2566.7

Table 5.2-2 Feedstock properties.

Even though different feed compositions were adopted, here again we focus on one of them, to have a unique case for the comparison (Table 5.2-3).

Mixture	CH_4 [%v]	O_2 [%v]	N_2 [%v]
mix1	3.33	1.67	95.00

Table 5.2-3 Feedstock composition.

5.3 The experimental data

The effects of conditioning of 0.5 wt% Rh/ZrO_2 on the CH_4 and O_2 conversion is reported in Fig 5.3-1. Eleven fast ramps were run followed by a slow ramp. The plot collects the conversion of seven (ramp 1, 2, 4, 5, 10, 11, 12) of the twelve ramps ran in different days. The last ramp is taken as representative of a steady functioning of the catalyst.

Methane conversion starts over 350°C, but keeps low. Only at about 450°C the catalyst lights off and suddenly the conversion jumps to about 50%, which means the methane reacted not only according to the total combustion reaction (which would lead to a 25% conversion), but some partial oxidation products must be forming, as well. Nonetheless, the kinetic fails to further increase with temperature, and a plateau appears after the light off temperature. Only after 550°C the conversion rises further, but with a gentler slope.

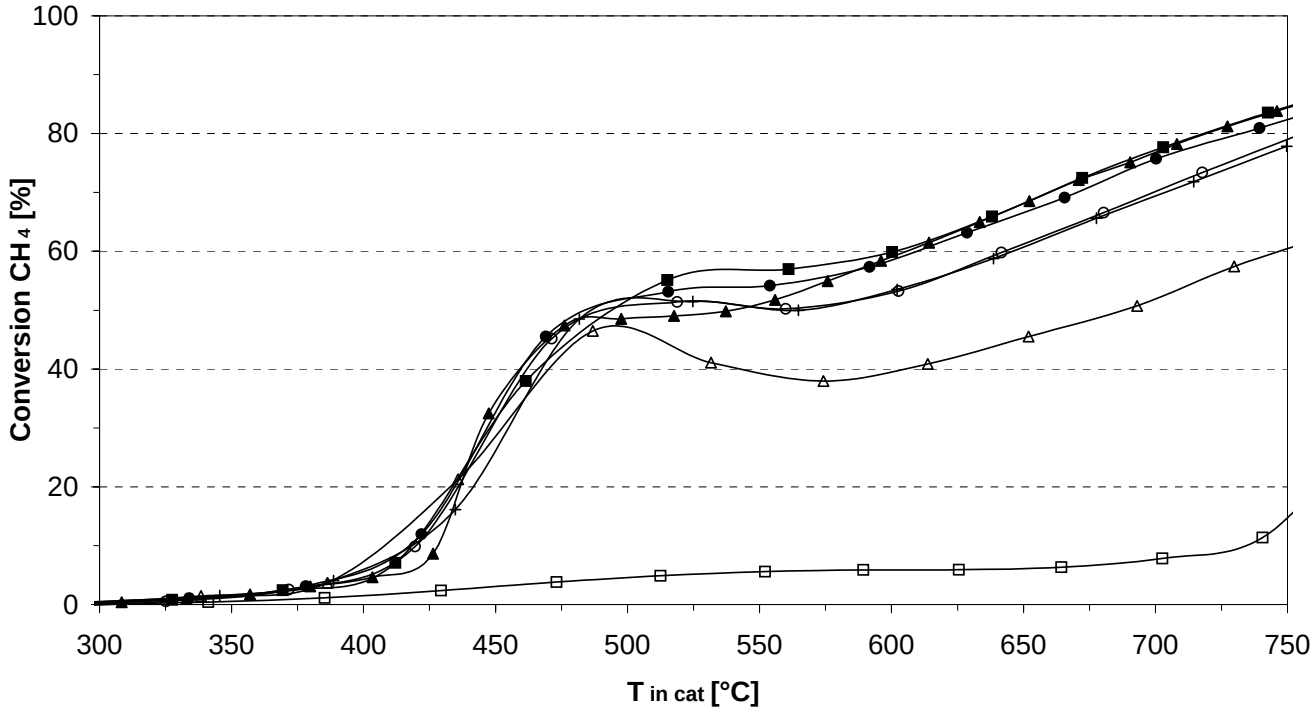

Fig 5.3-1 Typical path of experimental data, following many thermal cycles. Data for Rh/ZrO_2 catalyst, 3.33% CH_4 and 1.67% O_2 in N_2. (Ramps: 1 □, 2 △, 4 ○, 5 +, 10 ■, 11 ●, 12 ▲).

5.4 Equilibrium

Thermodynamic equilibrium sets the upper limit of conversion and the more stable products composition, by finding the combination of species whose composition assures the lowest Gibbs free energy of the system. A kinetic interpreter should profitably be used, since the minimization is not trivial. In Appendix B an example of equilibrium calculation with Cantera is shown: GRImech3.0 thermodynamic data were employed.

Even if the reactants ratio allowed the full consumption of methane, this might not occur. In Fig 5.4-1 the equilibrium for a CH_4/O_2=2 ratio is shown. The conversion is supposed to approach 100% only above 800°C, while at the lower temperatures some un-reacted methane is to be expected amongst the products.

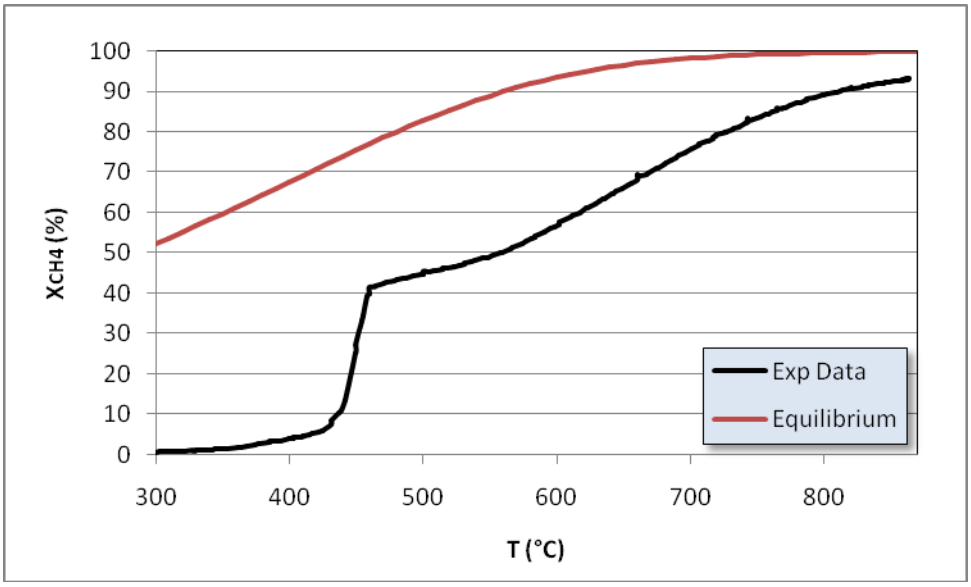

Fig 5.4-1 Equilibrium methane conversion, compared to the experimental data.

The conversion is an intuitive and concise way to represent the advancement of the reaction. But it's not fully exhaustive, since the carbon and hydrogen atoms deriving from the reacted CH_4 may either combine into oxidation species (CO_2 and H_2O) or to form partial oxidation species (CO and H_2). Other helpful parameters are the selectivities of one products with respect to all products or to some of them. In the following, the hydrogen selectivity is defined as the ratio of hydrogen to the sum of hydrogen and water. In that way, the complement to unity of hydrogen selectivity is water selectivity.

$$S_{H2} = \frac{H_2}{H_2 + H_2O}$$

Similarly, CO selectivity is:

$$S_{CO} = \frac{CO}{CO + CO_2}$$

These four species are related through the water gas shift reaction:

$CO + H_2O \leftrightharpoons CO_2 + H_2$

therefore the use of but one of these two selectivities is sufficient, together with the methane conversion, to fully represent the reaction. Hydrogen's is shown in Fig 5.4-2.

The H_2 experimental selectivity has a behavior quite dissimilar from that of methane conversion: the formation of H_2 doesn't start until the light off. It must be deduced that in the zone of low conversion methane turns to water preferably: and this is little wonder, since there's plenty of oxygen for the total combustion.

The equilibrium predicts that, at 300°C, 80% of the hydrogen atoms released by the reacted methane forms hydrogen molecules, and only 20% turns into water. Hydrogen selectivity should increase further with the temperature, until 100% of hydrogen atoms are trapped in H_2.

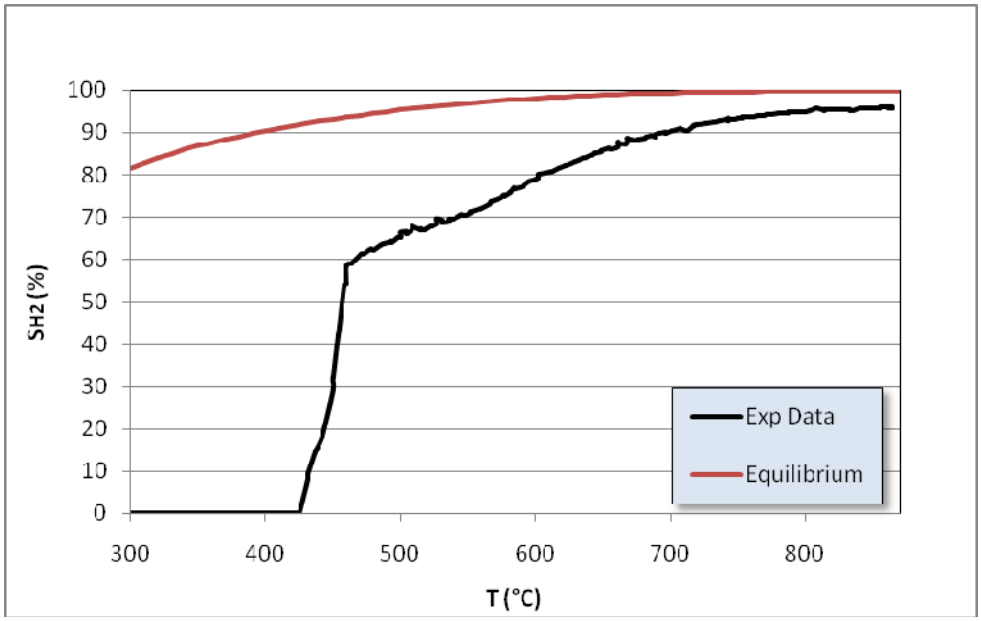

Fig 5.4-2 Equilibrium hydrogen selectivity, compared to the experimental data.

5.5 PFR results

In the first place, the reaction is modeled through an adiabatic PFR (see §4.2), that must be written for a heterogeneous kinetics:

MB:

$$\rho v \frac{dY_i}{dz} = S_L \, \dot{s}_i \, W_i \quad i = 1..Nsp \qquad \text{5.5-1}$$

EB:

$$\rho v \cdot c_p \frac{dT}{dz} = S_L \sum_i \dot{s}_i \cdot h_i \qquad i = 1..Nsp \tag{5.5-2}$$

The Deutschmann – Rh mechanism is used [37]. One of the limitations of this model is the specificity of the support, which is Al_2O_3. To extend the usability of the mechanism, a study was performed comparing the active catalytic surface area of Al_2O_3 with that of ZrO_2 or Ce-ZrO_2 [12]. According to it, for example, the ratio of Rh/ZrO_2's to Rh/α-Al_2O_3's active catalytic area is 1.333, thus we can simply use it to correct the surface site density in the mechanism. Furthermore, the presence of a washcoat largely increases the active surface area. To account for it, lacking any other indication, the surface to volume ratio, S_V, was corrected by a factor of 2. In Appendix B an example of PFR calculation with Cantera is shown.

In Fig 5.5-1 methane conversion is reported, varying the temperature, in comparison with the experimental data. Despite the simplicity of this approach in modeling the data, the results are terrific! The light off temperature is caught very precisely and the conversion at high temperature sticks up to the real solution. Being picky, though, there isn't the low conversion zone before the light off temperature, and the conversion right after the light off is a little too high (sometimes even +20%). That'll give me an excuse to try and go further with the other models, but first let's examine further the PFR results.

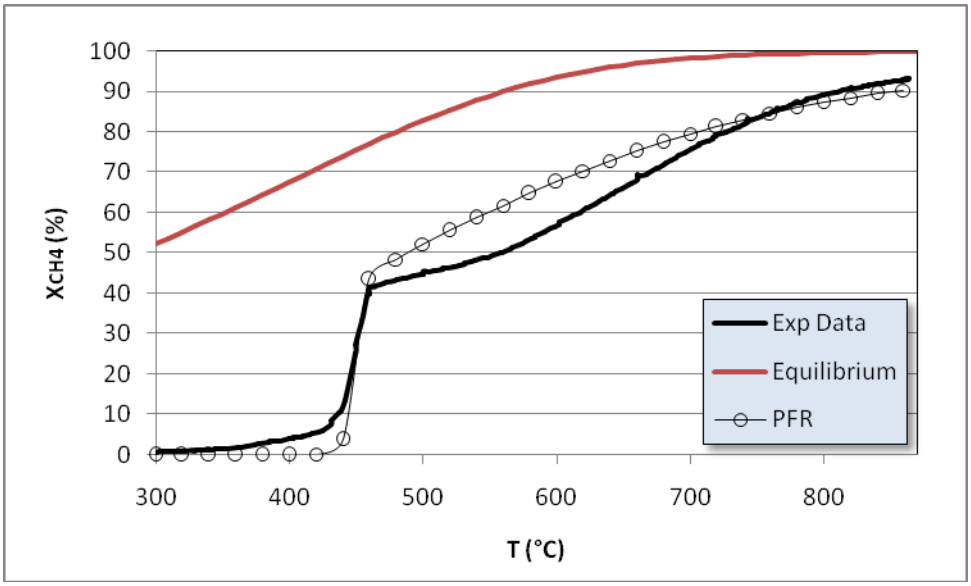

Fig 5.5-1 PFR methane conversion, compared to the experimental data.

The hydrogen selectivity (Fig 5.5-2) is neatly described by the PFR, as well. The raising, at the light off, is sudden, as in the experimental data, and the selectivity value is always very close to that experimental; though a little higher, justified by the PFR being an ideal reactor. Note that where the methane conversion is lower than the experimental (above 750°C), the hydrogen selectivity is still higher: the distribution of

the hydrogen atoms in the products is an intensive index and isn't affected by the actual amount of methane reacted.

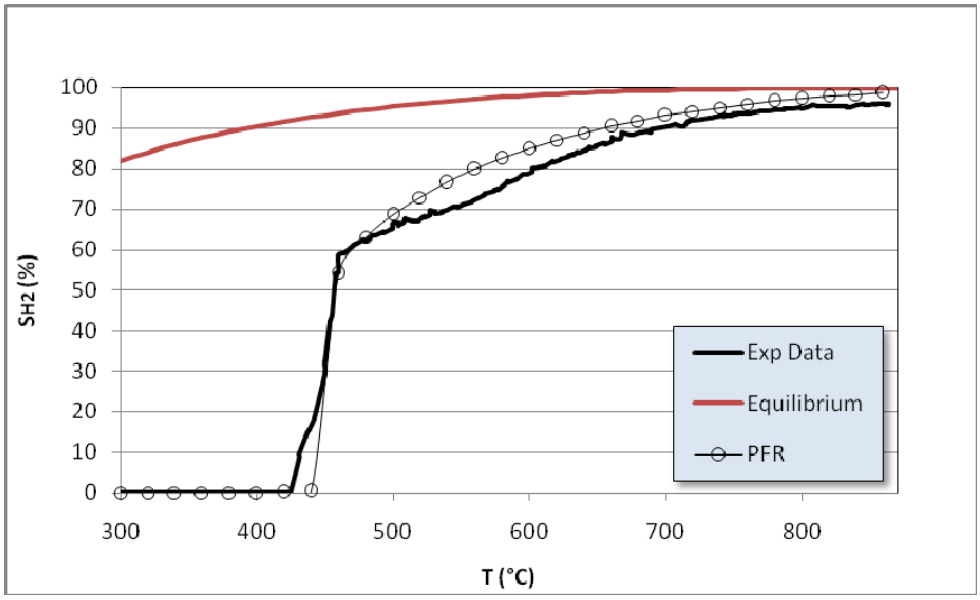

Fig 5.5-2 PFR hydrogen selectivity, compared to the experimental data.

5.5.1 Profiles along the reactor

The profiles along the reactor are quantitatively different at each temperature, but qualitatively alike. Tin=600°C was chosen as representative of the reactor behavior after light off.

Let's look at the temperature profile, first (Fig 5.5-3). Right after the entrance section there is a strong heat release, consistently with the idea of methane oxidation: the temperature gradient is 200°C/mm, and after 1 mm the temperature is little below 800°C. But at this position the temperature profile goes through a maximum and then decreases, more softly, meaning that an endothermic (slower) reaction is taking place.

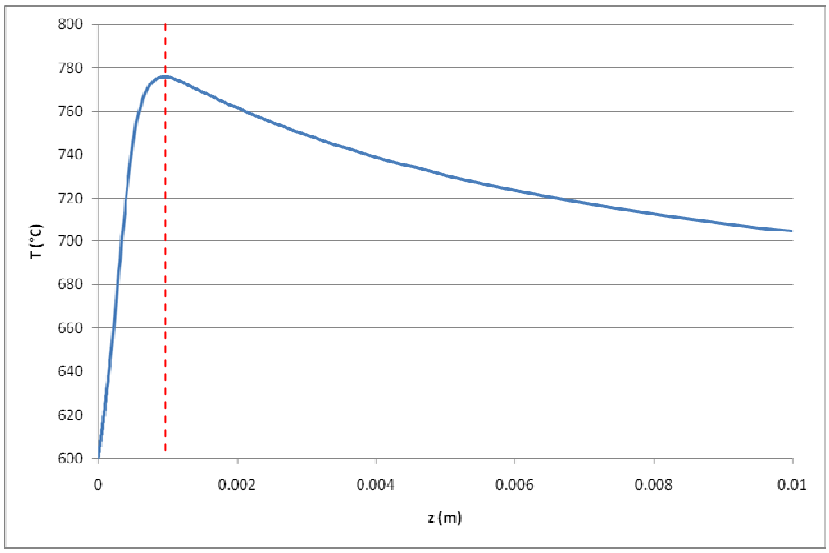

Fig 5.5-3 PFR temperature profile along the reactor. The position z=1 mm is emphasized as the point where there is a change in the chemistry.

The good of the PFR model is that the interpretation of the chemistry that occurs in each axial position is quite straightforward. Due to full segregation and lack of transport limitations of any kind, the kinetics liveals itself in a subsequent series of steps, involving the species present right in that position. Actually, also parallel reactions occur, which are less easy to discern, but anyway the cronological succession of species leading to the final products is very interesting in understanding the process.

Also for the composition profiles (Fig 5.5-4), the reactor can ideally be divided into two sections: one with the presence of oxygen (it is consumed after about 1mm), and the other without it. From the bending in the methane composition, we deduce its rate of consumption changes in the absence of oxygen. Pretty much the same occurs to all the species, since their behavior is different in the two zones. At the beginning, a lot of water comes up, but after the oxygen is gone, it's used as an oxidant and it decreases, reducising into hydrogen. Hydrogen starts to form at the very beginning, but after 1 mm its production rate increases. Carbon monoxide and dioxide are produced in presence of oxiden approximatively at the same pace, but then the former still increases, even if slowlier, while the second stops.

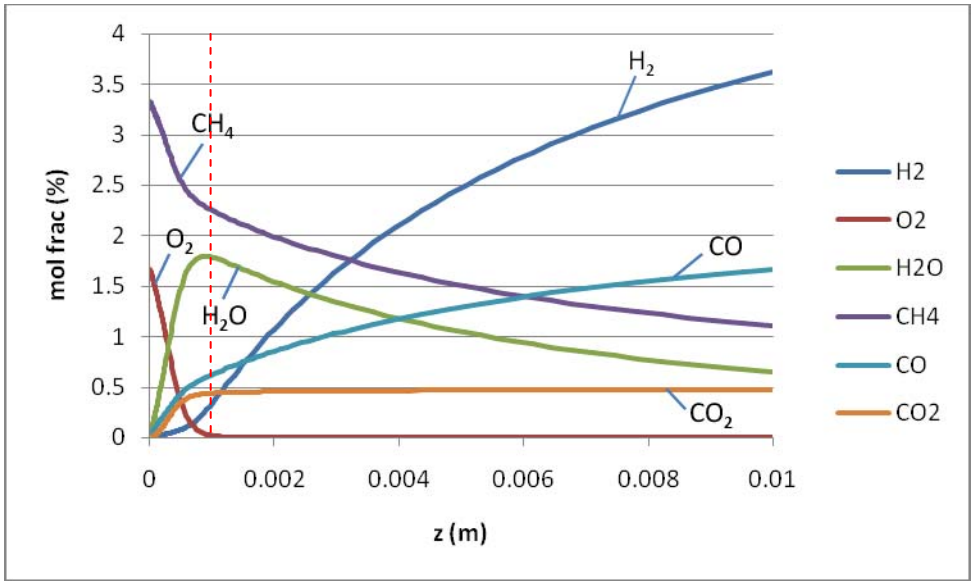

Fig 5.5-4 PFR composition profiles along the reactor. The position z=1 mm is emphasized as the point where there is a change in the chemistry.

Zooming in on the entrance (Fig 5.5-5), we see that the H_2O rises faster than every other species, with a slope around two times those of CO and CO_2. About these two, having the same initial slope, the CO_2 is delayed with respect to CO, meaning that it's produced in series after the CO (which is commonly aknowledged). H_2 grows with a non zero, but rather low velocity. No way to say whether it comes from a secondary reaction with water or from a direct production out of methane. Being a radical mechanism, though, this is maybe a silly question.

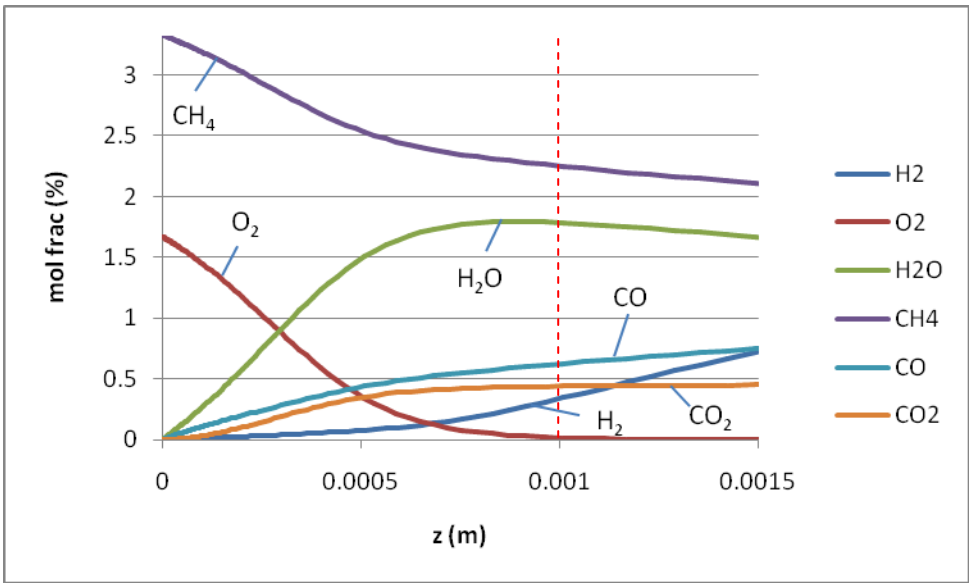

Fig 5.5-5 Zoom in of the PFR composition profiles along the reactor.

To inquire about the "effective" reaction taking place in each position, we can deduce the stoichiometric coefficients of a global reaction among the stable species:

$CH_4 + aO_2 \rightarrow bH_2 + cH_2O + dCO + eCO_2$

The stoichiometric coefficient is the slope of a species divided by the slope of methane (which stoichiometric coefficient is set to unity). In the region without oxygen, the stoichiometry of the steam reforming is rather settled (Fig 5.5-6):

$CH_4 + H_2O \rightarrow 3H_2 + CO$

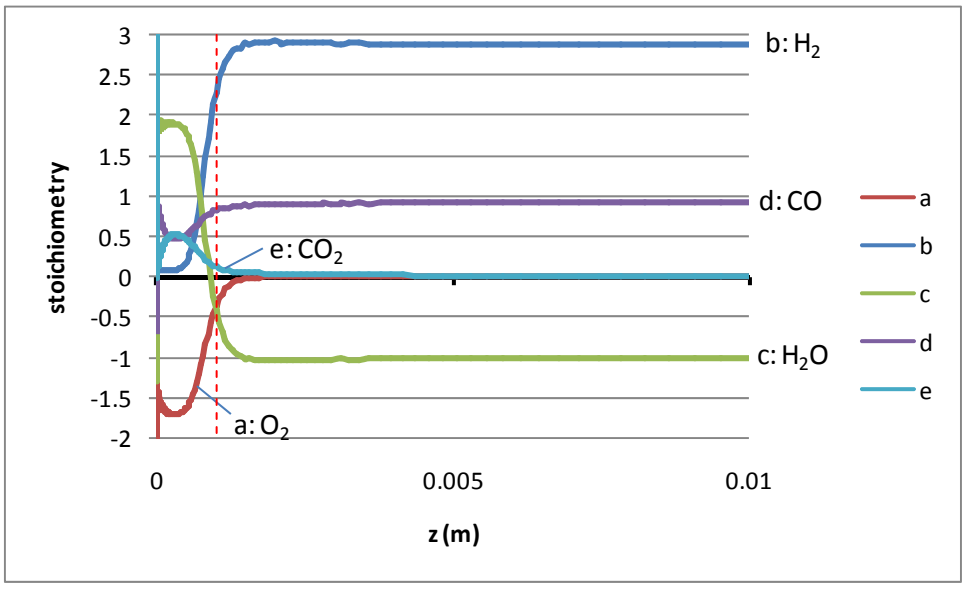

Fig 5.5-6 PFR stoichiometry along the reactor. The position z=1 mm is emphasized as the point where there is a change in the chemistry.

On the contrary, the kinetic in the first millimiter (Fig 5.5-7) is variable and not so simple to interpret. From the curves, I guess the following reaction, that is for sure the sum of several more elementary ones:

$CH_4 + 1.5O_2 \rightarrow 2H_2O + CO$

And after some CO is formed, the subsequent reaction starts:

$CO + 0.5O_2 \rightarrow CO_2$

There's also a very faint production of H_2, but I don't dare suggesting a route.

After half millimeter, the oxygen diminisces, and the kinetics go through a non well definite transient towards the already mentioned steam reforming stoichiometry.

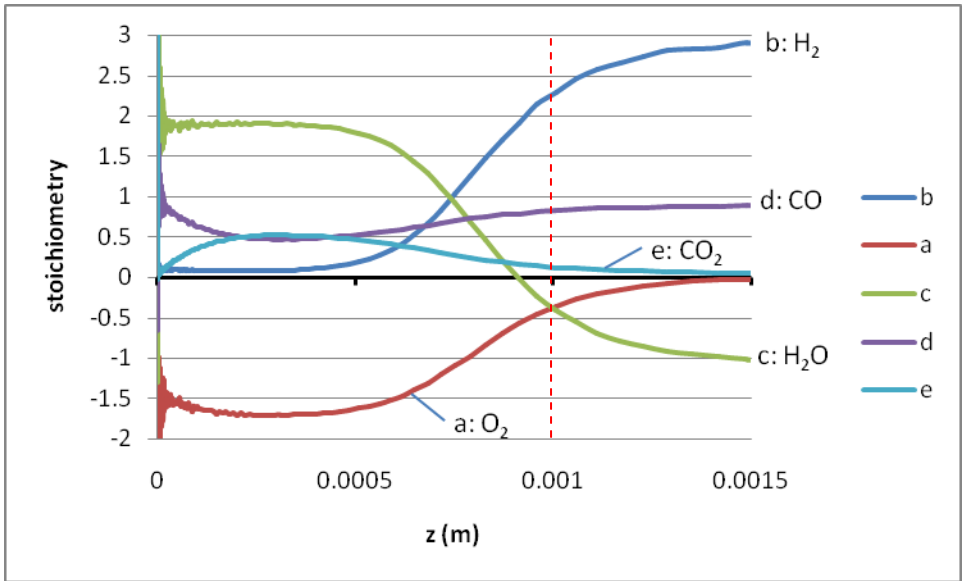

Fig 5.5-7 Zoom in of the PFR stoichiometry along the reactor.

After all, the PFR model turns out to be helpful in understanding the process and, even if not very accurate, it gives good insight in the kinetics. Besides, it also acknowledges the chosen mechanism might be not bad for the actual experimental set up.

5.6 Nu-Cond results

The Nusselt-Conduction model described in §4.5 is used in the description of the square channel monolith, for which the Shah and London [36] general correlation applies:

$$Nu = 2.977 + (8.827 \cdot (10^3 \cdot Z^*)^{-0.545}) \cdot \exp(-48.2 \cdot Z^*)$$

5.6-1

$$Z^* = \frac{z}{dcell \cdot Pe}$$

The mass balance is the same as in the PFR model (eq. 5.5-1). For the gas phase heat balance refer to eq. 4.3-1, while the solid temperature comes from the eq. 4.5-1.

Being a boundary value problem, the right boundary conditions should be adopted, in order to get the closest possible to the real physics of the system.

5.6.1 Full adiabatic monolith

Withstanding the adiabatic hypothesis on the oven side of the monolith, the new axial conduction term opens the issue about the heat losses in the axial direction. In practice, that determines the solid temperature derivative at the entrance and exit.

The simplest possible assumption states the monolith is fully adiabatic. That implies the heat of reaction keeps inside the pellet, no radiation leaves towards the incoming (and outgoing) gas stream and the temperature gradient at the edges is zero.

In Fig 5.6-1 the methane conversion predicted by the full adiabatic Nusselt-Conduction 1D model is shown. Above 450°C it is quite close to the PFR model, but a little lower. This is due to a combination of several factors: the conductivity smoothes the maximum but at the same time it produces a high surface temperature already at the entrance (see Fig 5.6-2).

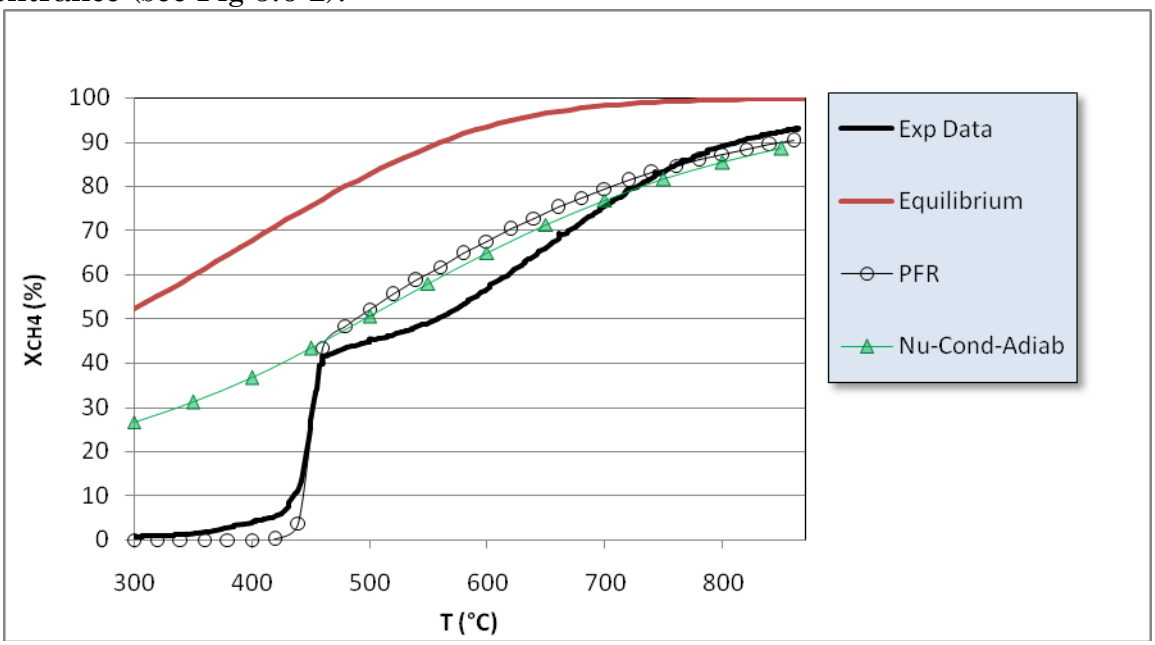

Fig 5.6-1 Methane conversion predicted by the Nu-Cond-Adiab model, compared to the PFR results and to the experimental data.

As soon as the reactants enter the reactor, they find a temperature higher than the light off, at the wall, thus the reactions start at once. Instead of having the induction time needed by the gas to absorb the heat of reaction, the reactants get immediately to the high reactivity zone. The composition profiles are not shown: they are alike the PFR results, because no diffusion resistance occurs.

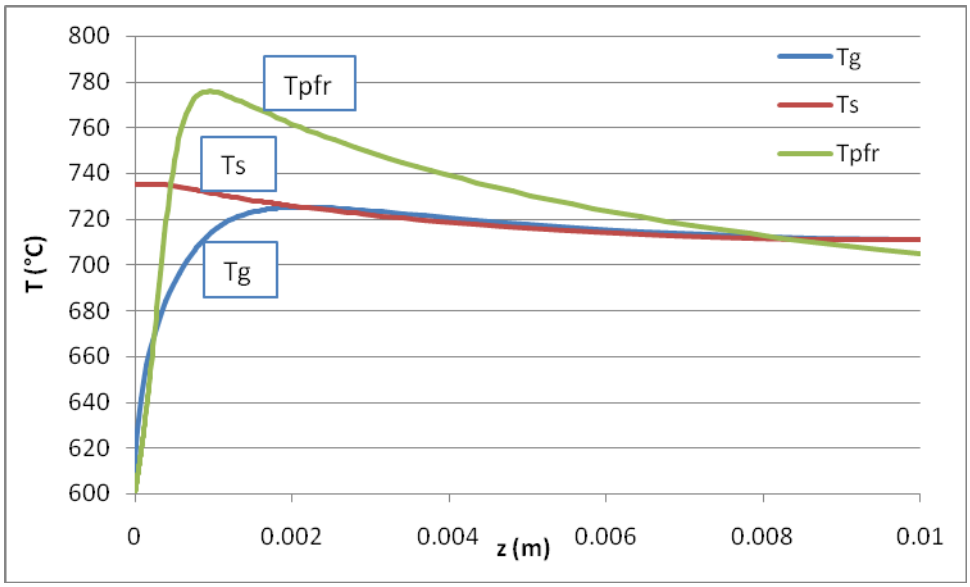

Fig 5.6-2 Temperature profiles along the reactor: solid and gas temperature profiles coming from the Nu-Cond-Adiab model compared to the unique PFR temperature profile.

The propagating of the heat due to conduction allows the light off of the reactor way before the inlet gas temperature reaches it. That explains the reactivity also before the 450°C. Of course this is a bad behavior, away from the reality, but reflects the lack of physical meaning in considering the resistance to the transport only in the heat balance and not in the species balances.

5.6.2 Irradiative faces

In contrast to the full adiabatic hypothesis, some radiation is likely to leave the solid towards the gas, which is more than 100°C colder than the front edge of the monolith. We can write the boundary conditions as follows:

$$\lambda_S \left.\frac{dT_S}{dz}\right|_{z=0} = -\sigma\,\varepsilon_g \left(T_{G,0}^4 - T_{S,0}^4\right)$$

$$\lambda_S \left.\frac{dT_S}{dz}\right|_{z=L} = +\sigma\,\varepsilon_g \left(T_{G,L}^4 - T_{S,L}^4\right) \qquad \text{5.6-2}$$

Being ε_g=0.8 the gas emissivity and σ the Stefan-Boltzmann constant.

In Fig 5.6-3 and Fig 5.6-4 the results, as methane conversion and hydrogen selectivity, can be seen. The light off is still lower than in the real world, but only 50°C. The conversion at the light off and until 650°C is basically identical to the exp data, while at higher temperature is underestimated.

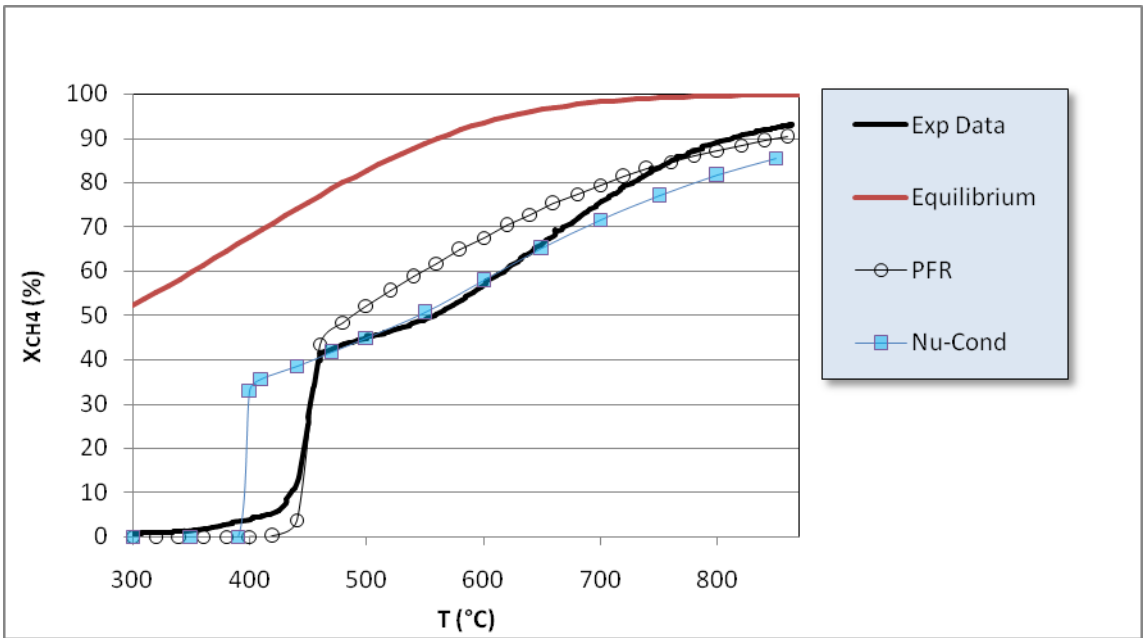

Fig 5.6-3 Methane conversion predicted by the Nu-Cond model, compared to the PFR results and to the experimental data.

Hydrogen production is predicted at lower temperature, as well, but always with the steep initial shape. It is always lower than the experimental selectivity, until 850°C, where the two meet.

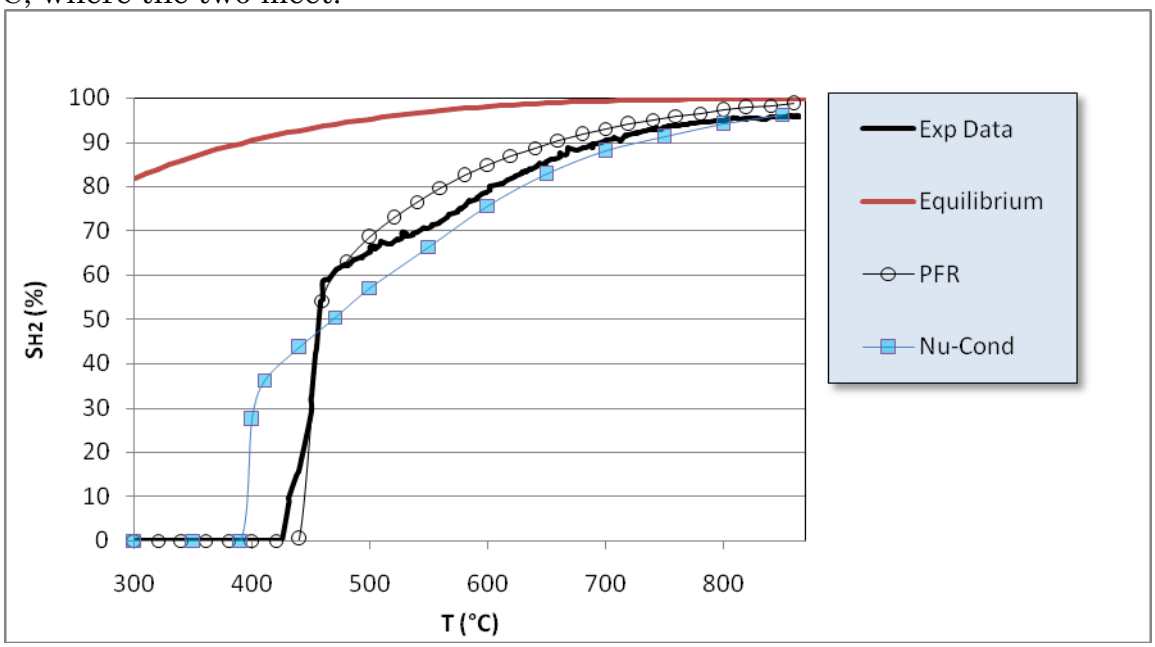

Fig 5.6-4 Hydrogen selectivity predicted by the Nu-Cond model, compared to the PFR results and to the experimental data.

Temperature profiles inside the reactor are qualitatively as in the adiabatic model, but much lower (Fig 5.6-5). Moreover, the initial slope of the Ts is now positive, because the radiation leaving the monolith causes a heat flux at the front cross section. The slope at the exit is nearly zero, being such a small temperature difference between the gas and the surface.

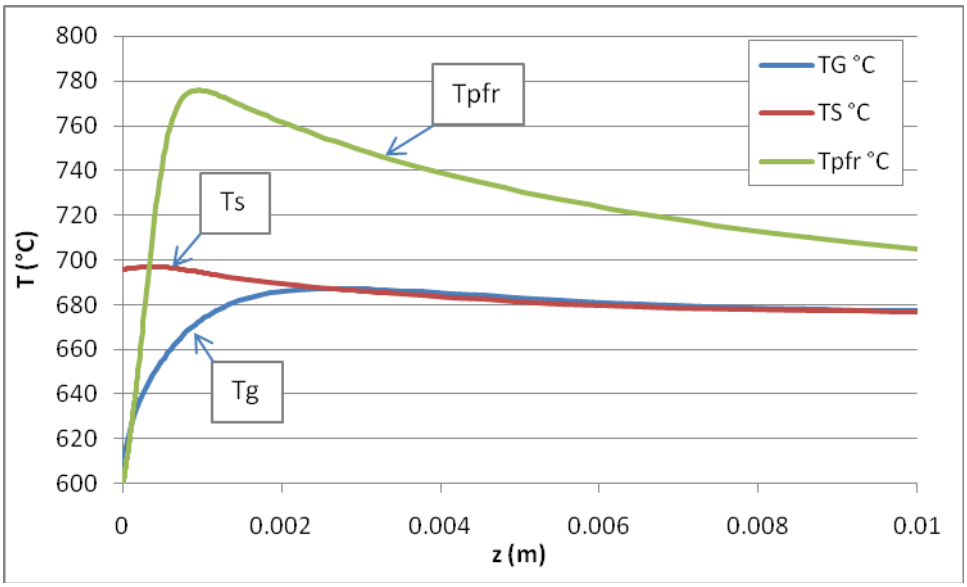

Fig 5.6-5 Temperature profiles along the reactor: solid and gas temperature profiles coming from the Nu-Cond model compared to the unique PFR temperature profile.

Zooming in on the entrance, we find the situation depicted in Fig 5.6-6: there is a so called "entrance region" where the heat boundary layer (BL) is developing, thus letting a bigger transport between the gas and the surface. The gas temperature slope reflects the path of the K_T: it is almost vertical at the entrance and gradually decreases afterwards. After the BL is established, the heat transfer coefficient keeps constant. This, of course, comes from a simplified analysis, that doesn't account for the change in properties due to the gas composition (other correlations include Pr dimensionless number to account for it).

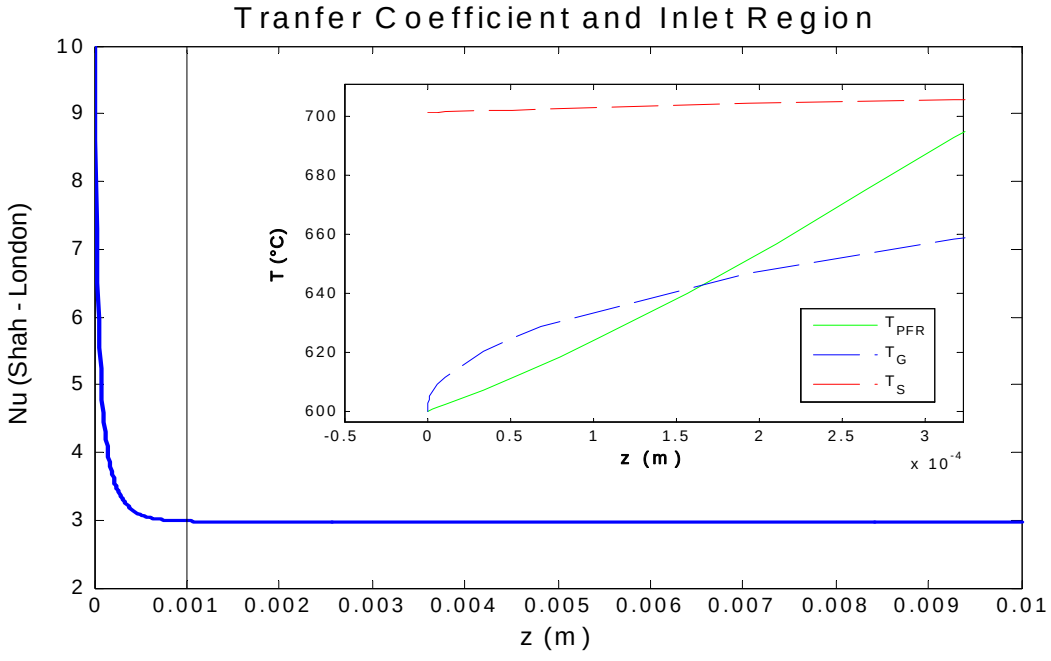

Fig 5.6-6 Zoom in on the temperature profiles along the reactor and heat transport coefficient.

5.6.3 Data pattern

It's not easy, so far, to judge the Nu-Cond model!

I want to strike a blow for it, even though I blame it of physical inconsistency for it assumes heat transfer to be important, neglecting mass transfer, while the two occur by means of the same phenomenon. This reflects in the results, because the light off temperature is way lower than in the experiments. Indeed, this model allows all the methane and oxygen reacting with the highest concentration, already at the entrance, where the wall temperature is high because of the conduction.

As I said, there's some good in the model, which you can see in Fig 5.6-7 analyzing the derivative of methane conversion with respect to the temperature. The experimental data show a peak, a hollow and a hill. The PFR reproduces the peak, but after that a monothonic decrease happens. The Nu-Cond-Adiab can only show the hill, while the Nu-Cond repeat the original sequence (peack-hollow-hill), only shifted at lower temperatures.

The Nu-Cond model is able to reproduce the bend in the conversion, not seen by the PFR. Since the reforming reaction are very temperature-sensitive, they occur in large extent only above certain temperature. In the PFR model, a high temperature peak develops, thus promoting the reforming reaction at each lighted off temperature. In the Nu-Cond model the temperature profile is more likely to be close to the actual profile inside the reactor. After the onset of the oxidation reactions (light off), the conversion slows down because the system runs out of oxygen (the only oxidant active at that temperature). Increasing the preheat temperature, water becomes an active enough oxydant, and the conversion of methane advances with a higher pace (the onset of the hill).

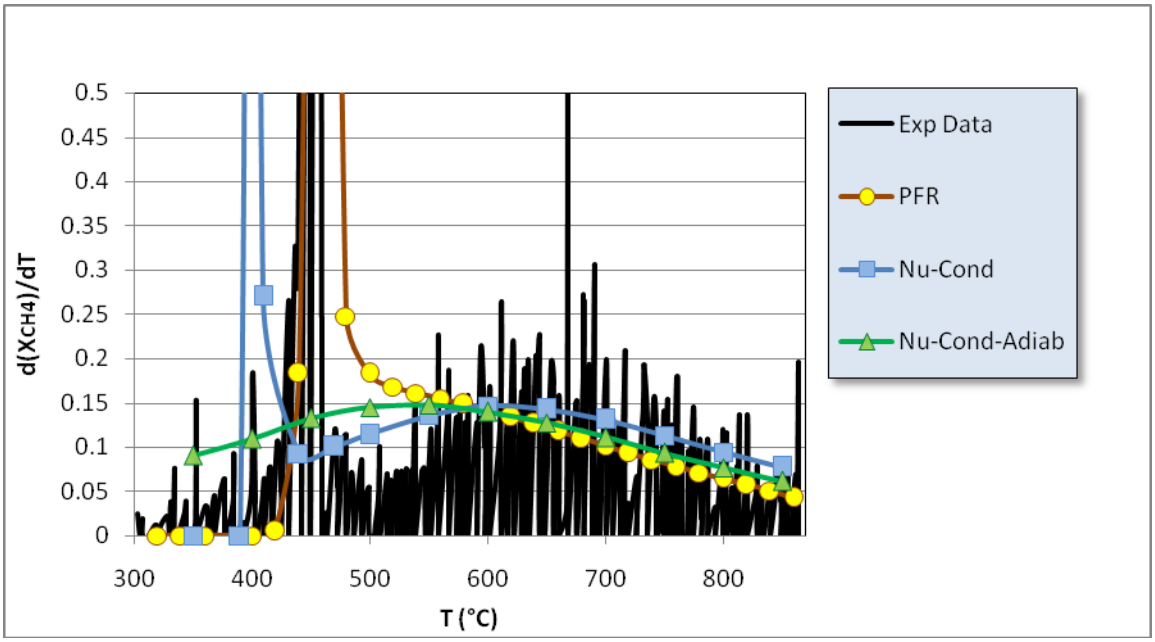

Fig 5.6-7 Methane conversion derivative with respect to the temperature. The two Nu-Cond models are compared to the experimental and to the PFR.

In Appendix B an example of Nu-Cond calculation with Cantera is shown.

As an aside, the b4p4c.m solver needs an initial guest. If usually a PFR is a good enough choice, sometimes an error like "unable to solve the collocation equations - - a singular Jacobian encountered" may occur. In that case, just solve the closest T0 possible with the PFR initialization, and then use the solution as an initial value for a T0'~T0. This usually makes it.

5.7 Nu-Sh results

The Nu-Sh model, mentioned in §4.6, was solved up to 436°C, resulting in a good agreement with the PFR model results (code is reported in Appendix B). Beyond this temperature the solver becomes irremediably unstable, so that the whole profile is not available. The point reached (see Fig 5.7-1) is clearly the onset of the fast chemistry regime, and a further increase in the production rate is not tolerated by the solver. The light off temperature is therefore well reproduced by the model, while no information is available on the "high conversion" region. The development of a more suitable algorithm is required, which is beyond the scope of this thesis.

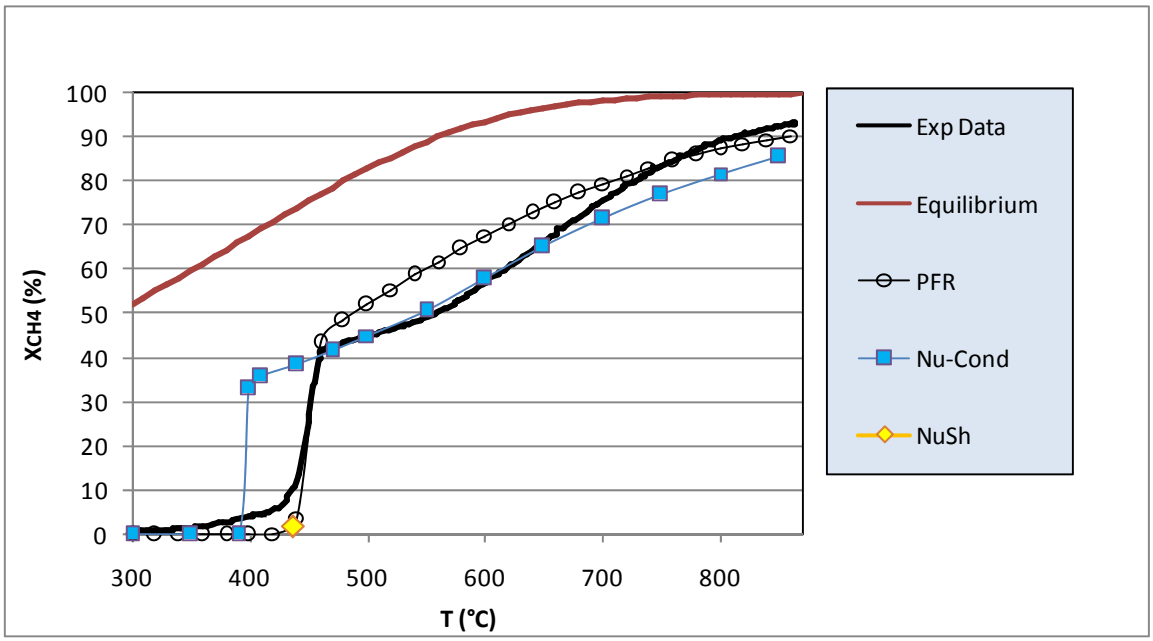

Fig 5.7-1 Methane conversion predicted by the Sh-Nu model, compared to the experimental data and to the previous models.

5.8 Nu-Sh-Cond results

The more accurate model adopted for this reactor set up includes both mass and heat transfer resistances in the bulk and the conduction in the solid substrate: the Nu-Sh-Cond model, if we want to follow the previous nomenclature. The constituent equations were reported in §4.7. Still, for details about the algorithm the reader is sent forward to Chapter 6. Here we only aim to present and discuss the results, in comparison with the other models.

The algorithm is quite slow to reach the convergence (depending on the starting point it takes 3 or more days of full CPU requirement in a modern PC). Here we want to focus on two points of the whole inlet temperature range: the light off temperature and a moderately high, full convergence, temperature. The 450°C and the 600°C were chosen.

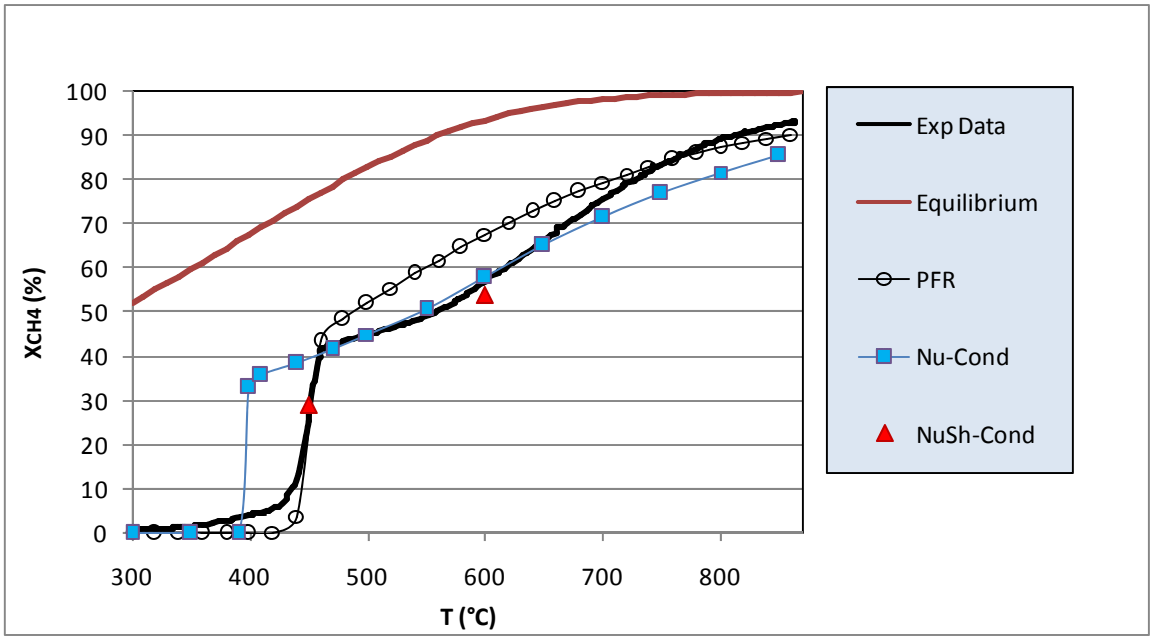

Fig 5.8-1 Methane conversion predicted by the Nu-Sh-Cond model, compared to the experimental data and to the other major models.

The light off temperature is now correctly predicted. Also the point at 600°C is acceptably close to the experimental: the conversion is underestimated only of 3 points %.

5.8.1 Profiles along the reactor

To analyze the axial profiles inside the reactor, the inlet temperature of 600°C is chosen, as usual.

In Fig 5.8-2 the temperature profiles along the reactor are shown, which are qualitatively similar to those presented in Fig 5.6-5 for the Nu-Cond model, but here the maximum of the T_S is more pronounced, and shifted downstream, because the reaction is spread in a longer zone after the entrance, due to the addition of the mass transfer resistance.

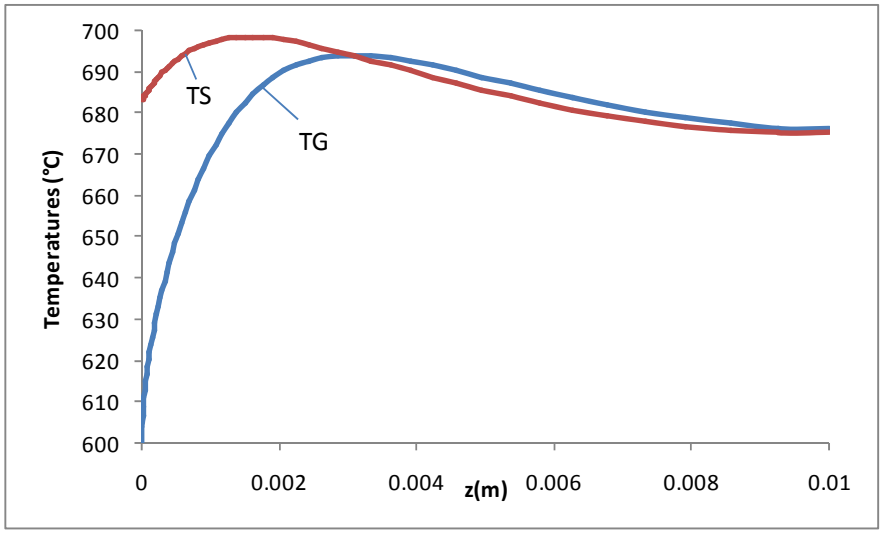

Fig 5.8-2 Temperature profiles along the reactor: solid and gas temperature profiles.

In Fig 5.8-3 the composition profiles are reported. There you can see both bulk and boundary layer mole fractions of all the species. The two reactants, CH_4 and O_2, have higher mole fractions in the bulk, while the reaction consumes them in the boundary layer, thus reducing their relative amount in favor of the products. On the contrary, the four products, H_2O, H_2, CO and CO_2 have higher mole fractions in the boundary layer, because the resistance to the mass transport limits their diffusion into the bulk. H_2O is an exception to this rule: after a maximum it decreases, becoming a reactant when the oxygen is consumed and ending with a boundary layer fraction lower than that in the bulk.

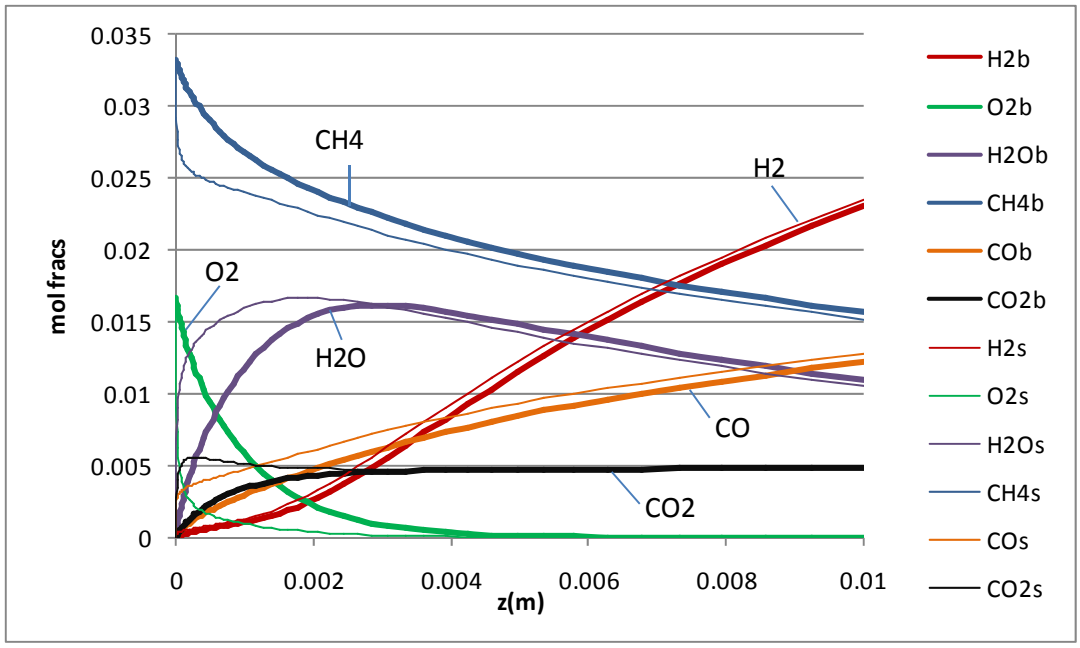

Fig 5.8-3 Composition profiles along the reactor: bulk (thick) and boundary layer (thin) mole fractions.

If we compare Fig 5.8-3 with Fig 5.5-4 we notice the main difference between this model and the PFR: in the latter there's no transfer resistance, and the oxygen is consumed after about 1 mm, while here more than 4 mm are needed to make it

disappear. I keep on looking at the O_2 because its behavior is paradigmatic of all the chemistry, but every species of the system reacts much more slowly than in the ideal reactor, because the kinetics is affected by the availability of the reactants on the surface. As a consequence, the exit conversion is lower (68% → 64%) as well as the H_2 selectivity (84% → 68%).

The slowdown of the chemistry in presence of transport resistance is enforced by the comparison between the real stoichiometry, from the PFR model (Fig 5.5-6), and that apparent, from this model (Fig 5.8-4). The stoichiometric coefficients of all the species have essentially the same behavior in both the models, but here their development along the reactor takes much longer.

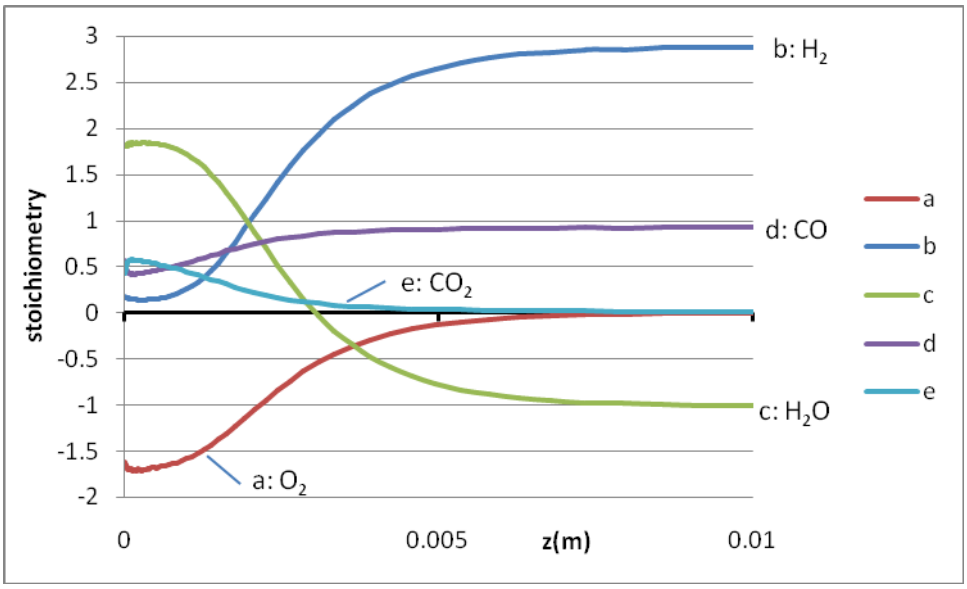

Fig 5.8-4 Apparent stoichiometry along the reactor.

5.9 Conclusions

Several 1D reactor models were used to simulate the square channel monolith for POM, and results were compared to the experimental data.

The PFR model is able to predict the light off temperature of the catalyst, but over-predicts the conversion at the higher temperatures. An analysis of its results is useful to get more insight in the chemistry adopted, without any interference of the physical phenomena.

The Nu-Cond model adopts more plausible temperatures; therefore it leads to a conversion pattern closer to that experimental. Also, the prediction of the conversion is better, after the light off. Yet, because of the lack of the mass transport, the light off temperature is badly reproduced.

The Nu-Sh model is potentially an interesting model, but we could only verify its ability in obtaining the right light off temperature, after which the solver became unstable.

The Nu-Sh-Cond model presents the capacity of reproducing both the light off temperature and the higher temperature conversion. The strong difference between the simplest and the most complicated model presented is the different spatial profiles inside the reactor: comparing the real stoichiometry with that apparent, we notice that the transfer phenomena strongly affect the conversion.

Chapter 6

Modeling Spatially Resolved Profiles of Methane Partial Oxidation on a Foam Catalyst with Detailed Chemistry

6.1 Case study number two

Partial Oxidation of Methane (POM) in monolithic reactors showed competitive in converting natural gas into syngas, an intermediate for the syntheses of higher hydrocarbons and methanol or a new form of energy vector. A millisecond contact time reactor reaches the aim with undoubted benefits. Noble metal catalysts lead to high performance in small volume and little metal load. Besides, active at lower temperature, this technology is cleaner from the NO_X point of view. Among the three possible geometries – straight channel monolith, packed bed and foam – the latter showed the high porosity typical of the first (causing low pressure drop) and the good radial mixing of the second, which improves the transport efficiency. Being widely tested through experiments, it still represents a challenging task for the modeling.

The single channel can't be modeled in its actual shape and, unless adopting oversimplified assumptions on the geometry, the CFD hardly applies. For this particular foam, which porosity is rather small, the lattice assumption is way too far to be applied. Since the low pressure POM reaction occurs predominantly on the surface11, a lumped model can here be adopted [34]: it's based on empirical correlations to find the transport coefficients; therefore it applies to whatever geometry.

The transport coefficients approach, coupled with a PFR model, was often adopted in the literature related to the catalytic combustion. A remarkable example was set by reference [30], which models in this way the foam, the honeycomb monolith and the packed bed, although using Langmuir-Hinshelwood-Hougen-Watson kinetics. The interplay between chemical and physical processes has been several times underlined in literature, being a fundamental issue of the modeling, one for all reference [27], although a fundamental account for heat and mass transport requires CFD capabilities [7]. After two introductory works to investigate the relative weight of transport limitation over the conversion ([1],[2]), the effort of using detailed surface kinetics was carried out by reference [3], in which both heat and mass transfer coefficients are adopted, though using an equivalent first order kinetic constant in finding an overall source term for each species that accounts for reaction and diffusion in series. A third example of such a model applied to POM is included in reference [39], where they model a triangular channel monolith. Here they are mostly interested in describing the reactor start up. They also implement the thermodynamic and transport coefficients, as well as the kinetics. The present work is aimed to be more flexible regarding the parameters calculations. Through the use of a kinetic interpreter, the model becomes easy to apply to any reacting system, with no further

programming. The chemistry is handled in a very flexible way. The model only needs to be adjusted for the geometry and the boundary conditions.

6.2 Experimental Data

An extensive presentation of experimental set up was given in references [22],[23],[24],[25]. The actual data set used in this work, included in [9], are the spatial profiles of POM at steady state which include the concentration of the main gas species and both gas and surface temperatures. The reactor is adiabatic and autothermal. Given the inlet composition and temperature of the feed, there are no more degrees of freedom, and the system evolves accordingly to the mass and energy conservation laws. Thus, a single data set is available for each inlet composition. The data presented are for a carbon to oxygen ratio: C/O = 1. The reactor set up consists in three α-Al_2O_3 foam monoliths; each of them has the geometry defined in Table 6.2-1. Those external are heat shields, and that in the middle is loaded with 6 $\%_{wt}$ Rh, without washcoat.

Property	Value
Foam type	80 ppi
Pore diameter (dpore)	0.5 mm
Porosity (ε)	0.53
Surface to void volume ratio (S_V)	8000 m^{-1}
Monoliths length (L)	10.0 mm
Monoliths diameter (D)	16.5 mm
Tortuosity factor (f)	0.6

Table 6.2-1 Geometric properties of the foam monolith.

Composition profiles of species CH_4, CO, CO_2, H_2 and O_2 were measured with a capillary technique. H_2O profile was not measured; it could be obtained from H and O balances, but we chose not to show it here, since it implies some arbitrary assumption. In Fig 6.2-1 the catalyst measured profiles are shown, extended 1 mm into the up- and downstream heat shields (elsewhere they keep constant).

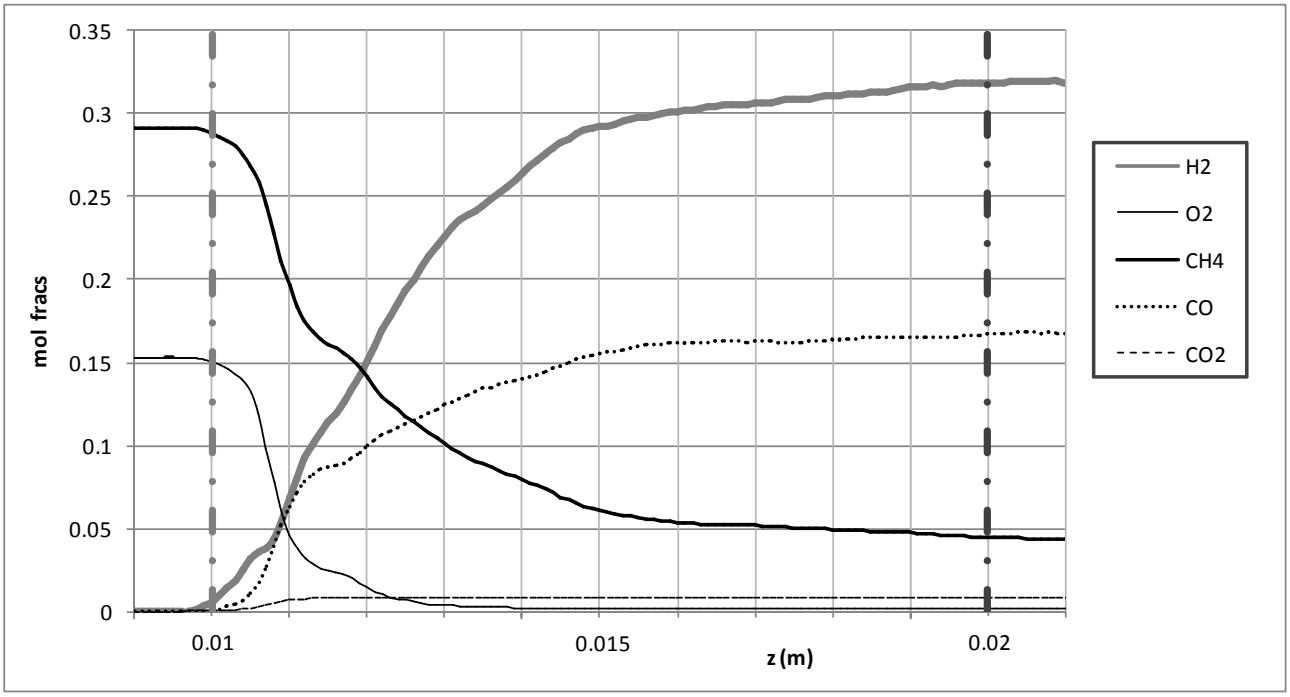

Fig 6.2-1 Spatial profiles of experimental composition. Boundaries of the catalytic foam are shown.

The catalyst inlet and outlet are sketched in the plot, as well. CH_4 and O_2 react to produce CO, CO_2, H_2 and H_2O. CH_4 conversion is 80% at the catalyst exit, after reacting first with oxygen and secondly with water; CO_2 reforming seems negligible on Rh catalyst, since no maximum is evident in its profile. On the contrary, CO_2 forms only in the presence of a large amount of oxygen. H_2 and CO grow monotonically, up to a final molar ratio of about 2. H_2O profile (not shown) has a maximum located after about 2 mm of catalyst bed.

Kinetics is faster in the first half of the reactor, and much slower in the remaining. This might be due to the decrease of reactants, or to the proximity to equilibrium or to lower temperatures, as will be clear in the next paragraph. The system is still not at equilibrium, but get quite close to it. Equilibrium results are listed in Table 6.2-2: thermodynamics predicts a higher methane conversion, achieved through the still active endothermic reforming reaction, with a consequent lower temperature. CH_4 should be lower than in the experimental products, as well as H_2O, with a higher amount of H_2 and CO. Looking at the composition paths, equilibrium is likely to be reached with a longer catalytic monolith (higher contact time).

Property	Equilibrium	Experiments	Abs. Diff.
Temperature	700 K	758 K	+58 K
CH_4 conversion	87 %	80 %	–7 %
Mole Fractions:			
H_2	.352	.319	–.033
O_2	.000	.002	+.002
H_2O	.022	.036	+.014
CH_4	.028	.045	+.017
CO	.170	.167	–.003
CO_2	.017	.009	–.008

Table 6.2-2 Adiabatic equilibrium results and absolute difference between equilibrium and experimental data.

A thermocouple measurement is available, which is likely close to the bulk gas temperature, and a pyrometer reads the catalytic surface temperature exposed to the probe. Depending on the relative direction of the flow with respect to the probe insertion, the pyrometer gave two measurements, which are the same as temperature value, but differ for the position (Fig 6.2-2). The normal flow curve refers to the probe moving co-current with the flow, while in the reverse flow the probe move counter-current.

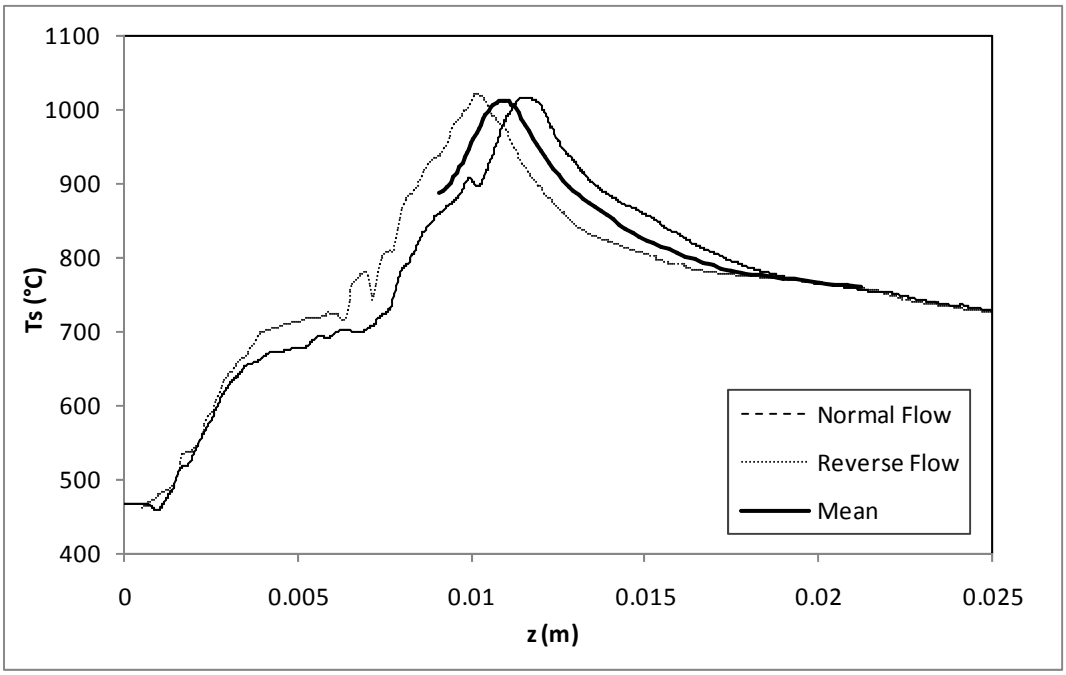

Fig 6.2-2 Pyrometer measurements for normal and reverse flow, and their mean.

We resolved to mean the axial position at which the corresponding temperature value of the two measurements was taken, obtaining a third curve in between the former two. In Fig 6.2-3 the gas and the solid temperatures are shown.

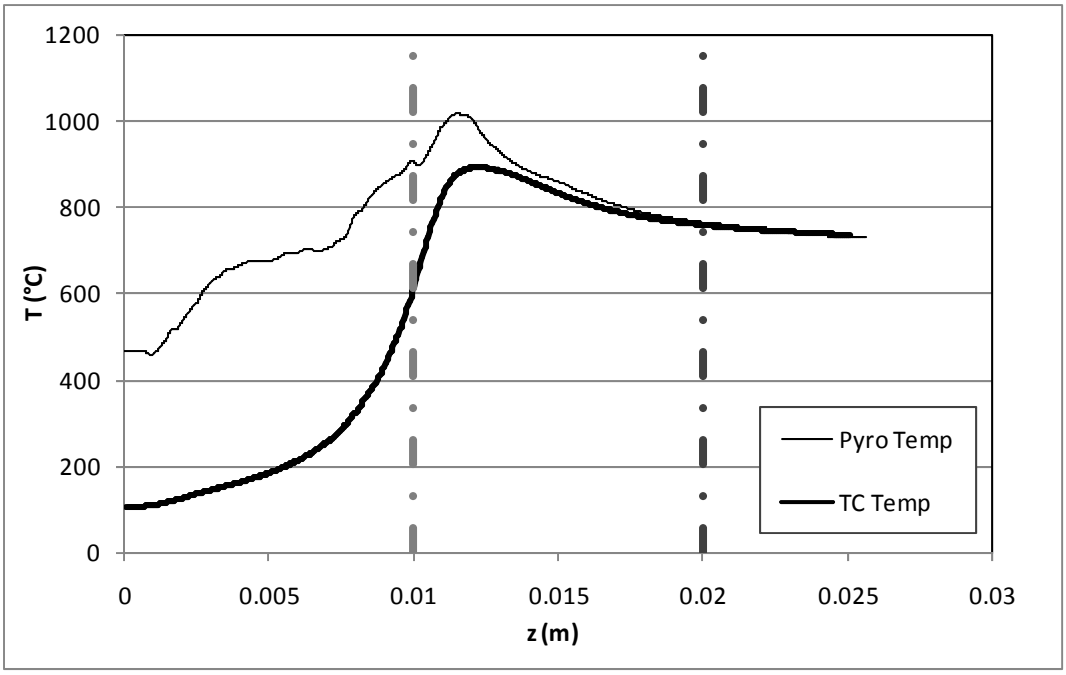

Fig 6.2-3 Spatial profiles of experimental temperature.

The feed mixture enters the front heat shield (FHS) at about 100°C. At the same position, the solid is at about 450°C, due to the combination of solid conduction and heat transport towards the gas. The radiation leaving the face of the FHS is negligible, given the horizontal slope of the curve. The gas heats up and enters the catalytic section at 600°C, where a temperature difference of about 300 °C exists between the gas and the solid temperature, and that testifies the existence of a limitation in the heat transport. Both temperature profiles increase strongly in the first few millimeters inside the catalyst, due to the oxidation reactions, pass through a maximum and decrease, more softly, meaning that an endothermic (slower) reaction is taking place. The two profiles run into each other at the end of the reactor, which means the kinetics slows down and no more heat of reaction is released. The maximum read by the pyrometer is at 1015 °C. The gas exits the catalyst at 760 °C.

Fig 6.2-4 shows a section of an 80 ppi foam monolith: an uneven pore distribution is responsible for the fine structure in the profiles.

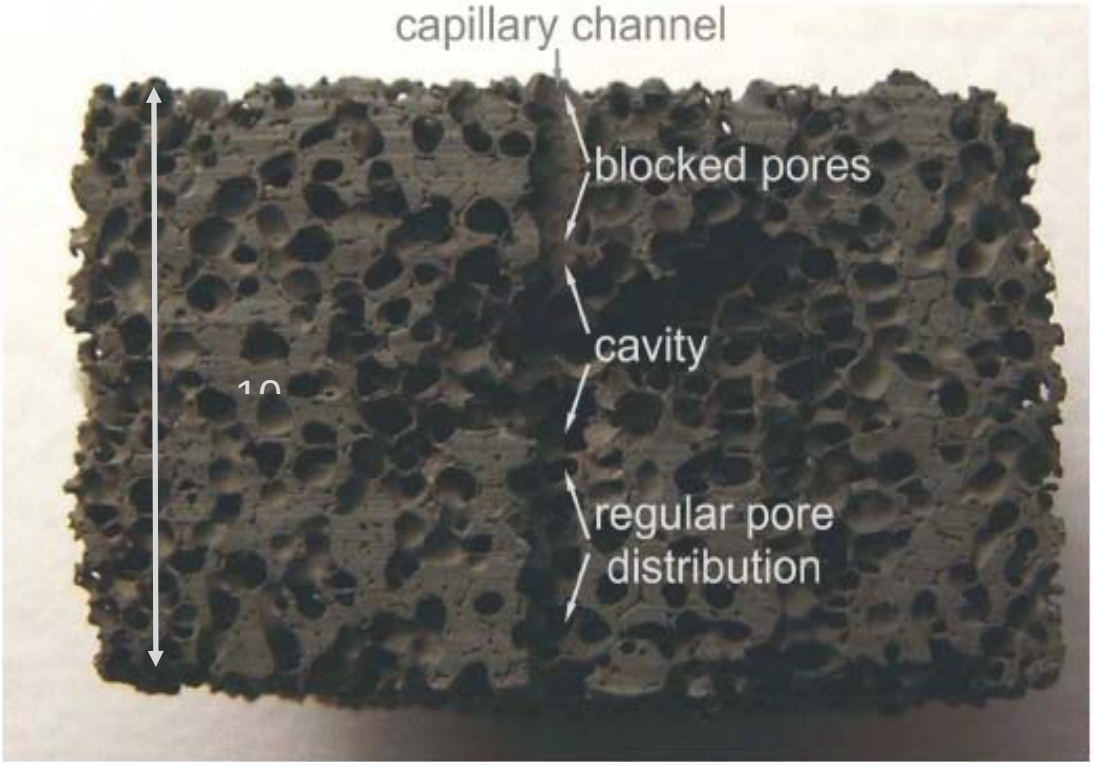

Fig 6.2-4 Example of pore structure: an uneven distribution of pores produces a fine structure in the spatial profiles.

In particular, it explains the behavior of the experimental data, shown in Fig. 1. In the first half millimeter of the catalytic monolith the conversion of both reactants is pretty low, while it drops quickly after that, to continue with a more likely exponential decay. Even though the radial mixing in the foam is generally so good, that the cross section profile can be considered flat, the pores exposed to the capillary channel might be blocked and therefore the probe might not be in contact with the real local mean composition. As a proof of that, note that the delay in the conversion of CH_4 and O_2 has the same extension as a single pore diameter (half millimeter); the real internal profile is more likely exponential-like from the beginning, although not seen by the probe.

To date, in modeling a reacting system only a few information were available; therefore a big chance is now given. Thanks to the data obtainable by the capillary technique, the modeling of this reacting system can be validated in great detail.

6.3 Model Equations

6.3.1 An ideal model: the PFR

The Plug Flow Reactor (PFR) is the simplest model that can be written for a system in flow. It states that convection of species, as well as of heat, is equal to its production/consumption. Physically, is assumes infinite radial diffusion, which turns out in a flat profile, and zero axial diffusion, that means a segregated volume of fluid flows through the channel without exchanging anything with those beside it.

The mathematic formalization of this model follows.

PFR MB: $\rho v \frac{dY_i}{dz} = \dot{r}_i \cdot W_i \quad i = 1..Nsp$

PFR EB: $\rho v \cdot c_p \frac{dT}{dz} = \sum_j R_j \cdot \Delta H_{R,j} \quad j = 1..N\ reactions$

This model is well applicable to systems in flow in which a homogeneous kinetic occur, and Pe>>1 (axial diffusion can be neglected). With heterogeneous kinetic, it's valid only where chemistry is the controlling regime, in comparison with transport.

6.3.2 The model including the transport phenomena

The reactor model consists in transient one-dimensional balances for heat and species. The reactor is represented as a straight channel, where the bulk gas has certain composition and properties, while there is a thin layer of gas close to the solid surface with its own composition and properties: we conventionally labeled these quantities as BL, Boundary Layer. In the following, we'll refer to this model as the "foam" model, for simplicity.

The equations are written on a void volume basis. Symbols are explained in the Notation.

Bulk MB: $\rho_G \frac{\partial \mathbf{Y_G}}{\partial t} = -\rho_G \mathrm{v} \frac{\partial \mathbf{Y_G}}{\partial z} + \rho_G D \frac{\partial^2 \mathbf{Y_G}}{\partial z^2} - \rho_G S_V \mathbf{K_C} \left(\mathbf{Y_G} - \mathbf{Y_{BL}} \right) \qquad Nsp = 7$

BL MB: $\rho_{BL} \frac{\partial \mathbf{Y_{BL}}}{\partial t} = \rho_{BL} S_V \mathbf{K_C} \left(\mathbf{Y_G} - \mathbf{Y_{BL}} \right) + S_V \dot{\mathbf{s}} \cdot \mathbf{W} \qquad Nsp = 7$

Bulk EB: $\rho_G \mathrm{cp} \frac{\partial T_G}{\partial t} = -\rho_G \mathrm{v}\, \mathrm{cp} \frac{\partial T_G}{\partial z} + \lambda_G \frac{\partial^2 T_G}{\partial z^2} - S_V K_T \left(T_G - T_S \right)$

Solid EB: $\frac{1-\varepsilon}{\varepsilon} \rho_S cp_S \frac{\partial T_S}{\partial t} = \frac{1-\varepsilon}{\varepsilon} f \frac{\partial}{\partial z} \left(\lambda_S \frac{\partial T_S}{\partial z} \right) +$

$+ S_V K_T (T_G - T_S) - S_V \left(\sum_{k=1}^{Nsp} h_k \dot{s}_k \right) - S_V \sigma \left(T_S^4(z) - \frac{K}{2} \int_{-\infty}^{+\infty} T_S^4(z + z^*) e^{-K|z^*|} dz^* \right)$

The Bulk MB contains the terms of accumulation, convection, diffusion and flux from the bulk to the surface for the species H_2, O_2, H_2O, CH_4, CO, CO_2 and Ar. In the BL MB accumulation equals the flux from the bulk to the surface plus the production or consumption at the catalytic surface. No homogenous reactions are accounted for [17]. Transient balances were written to simplify the solution, as will be clear in the following, and not because the system is dynamic. At steady state each accumulation term goes to zero; also, from the continuity equation we obtain G=const. It could be

proved that the time scale of the first three equations is much lower than the energy accumulation in the solid, so that the system goes through pseudo-steady states for composition and bulk temperature in relationship with the T_S at each instant. This helps in the simulations, because the heat capacity of the solid might be decreased, being a convergence parameter, and the time for reaching the steady state is shortened. The Bulk EB is analogous to the Bulk MB: it contains accumulation, convection, conduction and the heat flux from the bulk to the solid. In the solid EB the accumulation and conduction terms have to be written on a solid volume basis. For this reason they must be divided by the void volume and multiplied by the solid volume, e.g. introducing the term $(1-\varepsilon)/\varepsilon$. Since the solid structure of the monolith has a discontinuous nature, the heat conduction in the axial direction finds high resistance (taken in account through a porosity factor). At high temperature, though, the presence of a pore is no more an obstacle to the heat transport, which can now occur by radiation. Thus, the equation contains a radiation term, which becomes important in the catalyst region, where the surface temperature reaches values above 1000 °C. Radiation reflects from a pore face to the others: since the gas is considered transparent to radiation, it doesn't modify the gas temperature, and it reaches the solid completely. Radiation turns out in an extra – conduction effect, strongly dependent on the temperature.

To determine whether axial mass diffusion and temperature conduction in the gas phase are to be included or not in the model, Pe numbers must be evaluated. For the temperature, Pe_T reaches unity at the highest temperatures. For Re lower than 5, the dispersion coefficient is very close to the molecular diffusion [29], thus we use the latter to calculate Pe_M. For H_2 Pe_M is close to unity, even a little lower, while for the other species it's somewhat above 1 (meaning the conduction is more important, for them). As a consequence, the contributions of gas conduction and diffusion have to be included in the model.

6.3.3 Boundary conditions

Since the model contains second order differential equations, the system needs to be solved as a boundary value problem. Boundary conditions are listed below.

Front Heat Shield inlet (z=0):

The gas temperature and composition are those in the feed. These result in Nsp+1 Dirichlet boundary conditions:

$$\mathbf{Y}_G = \mathbf{Y}_{G,feed} \text{ and } T_G = T_{G,feed}$$

The gas diffusivity is assumed zero because no concentration gradients are expected one centimeter far from the catalyst and, for the presence of a heat shield, no radiation leaves the reactor. Another Nsp+1 Neumann boundary conditions apply:

$$\left.\frac{\partial \mathbf{Y}_G}{\partial z}\right|_{z=0} = 0 \text{ and } \left.\frac{\partial T_S}{\partial z}\right|_{z=0} = 0$$

Back Heat Shield outlet (z=0.03 m):

At the exit, there's no radiation leaving the back heat shield, as well. Furthermore, since there isn't a big difference between gas and solid temperature, the gas temperature gradient is low and there's no conduction in the gas at the exit. Even if unnecessary, the gas zero diffusivity is set also at the exit, since it is physically reasonable, and numerically stable. In the outlet we come out with Nsp+2 Neumann boundary conditions:

$$\left.\frac{\partial \mathbf{Y_G}}{\partial z}\right|_{z=0.03m} = 0\,,\ \left.\frac{\partial T_G}{\partial z}\right|_{z=0.03m} = 0 \ \text{and}\ \left.\frac{\partial T_S}{\partial z}\right|_{z=0.03m} = 0$$

Initial guess (t=0):

The start up of the system is simulated in a way it could likely happen in the real world: starting from a cold reactor, in which the feed flows without reacting, the central catalytic monolith is artificially heated up to the light off temperature of the catalyst, where the reaction begins. The heater is then switched off, and the reactor runs autothermally towards the steady state. A changing in the operating conditions (like for example the switching from a composition to another) starts from the previous steady state, being it a physical state of the system, and moves to another steady state. Interestingly, the dynamic model allows predicting conditions (i.e. pre-heating temperature) for self-sustainability of the reactor.

6.3.4 Equations' Parameters

As in reference [23], the solid component of the foam was considered polycrystalline alumina, which intrinsic thermal conductivity was taken as a function of temperature [26]. Pore diameter and porosity was measured with image analysis [9]. Tortuosity factor was taken from reference [14].

Transport coefficient correlations for foam of our pore size were not available in literature. Other formulas, extrapolated from their real validity range, turned out to overestimate transport: with the great detail of our reactor characterization we could see that the temperature profiles calculated with such correlations were too close one another to represent the real operation of the reactor. This behavior is also in agreement with some previous work ([28],[33]), in which Re was kept very low, so exiting from the validity of the standard theories, based on transport around a sphere or in single cylinder: they found that for Re<10 correlations for heat and mass transfer should have a Re exponent higher than the 0.5, usually valid for higher Re.

Experiments were carried out with a model reaction (CO oxidation), at adiabatic conditions and with a CO lean mixture, which is a well established benchmark ([15],[17]). Details of our measurements can be found in [9]. The correlations that we obtained for our 80ppi foam, where the characteristic length used in dimensionless numbers is the inverse of the geometric surface to total bed (thus the not void) volume, $1/S_V'$ are the following:

$$Sh' = 0.0483\ Re'^{0.753}\ Sc^{1/3}$$

$$Nu' = 0.0483\ Re'^{0.753}\ Pr^{1/3}$$

All numbers marked with a prime indicate that are based on the total bed volume.

The kinetic mechanism was initially developed by the authors [21] and subsequently improved by others [37], to a final 38 steps detailed surface mechanism, involving 7 gas species and 12 surface species. It contains adsorption and desorption reactions, as well as the proper surface reactions. Since the kinetic model was developed on a 3 $\%_{wt}$ Rh loading, half the amount adopted in the present work, the surface site density was doubled.

6.4 Numerical resolution

6.4.1 Choice of the solution method

Although we need to solve a steady state problem, the use of transient equations simplifies the solution and closely follows the physics.

The analogous model, written for a steady state problem is an ADE system (Algebraic Differential Equation System), including a second order differential equation, which requires the solution of a BVP (Boundary Value Problem). The usual procedure to solve such a problem is to discretize the derivatives and solve it as a non-linear algebraic equation system. Nevertheless, the number of variables is 16 (7 species and one temperature for each phase) and a reasonable minimum number of spatial elements to describe all the three monoliths is 100, we would end up with a Jacobian matrix of the dimension of more than 1600^2, even though sparse. The size and the nature of the algebraic problem discourage its solution.

Instead, we preferred to use a homothopy continuation technique, choosing to solve the full transient of the system, which is now an ordinary differential equation system in time. The Jacobian matrix is of the same size, but much simpler, and the ordinary differential equation system is extremely stable.

6.4.2 Mesh and derivative discretization

The derivatives have been discretized with respect to a non-uniform spatial grid of 130 elements spanning the three foam pieces. The mesh is thinner where the gradients are larger: at the front heat shield entrance and exit, and at the catalyst entrance. The growth is geometric: each step is bigger than that former by a constant growth factor, gf.

$$a = L\frac{gf\text{-}1}{gf^{(nsteps+1)\text{-}1} - 1}$$

$$z_1 = 0$$

$$z_i = z_{i\text{-}1} + a \cdot gf^{(i\text{-}1)\text{-}1} \qquad i = 2 \ldots nsteps + 1$$

The front heat shield is divided in 45 steps, the catalyst in 60 steps, while the back heat shield has a uniform mesh of 25 steps.

The 4 steps Lagrange polynomials were used in approximating the first and second derivatives.

They follow the general definition:

$$P(x) = \sum_{j=0}^{k} y_j l_j(x)$$

$$l_j(x) = \prod_{i=0, i\neq j}^{k} \frac{x - x_i}{x_j - x_i}$$

For k=4:

$$P^n 4(x) = l_0^n(x) \cdot y_0 + l_1^n(x) \cdot y_1 + l_2^n(x) \cdot y_2 + l_3^n(x) \cdot y_3$$

Where for n=0, it's the interpolation function, for n=1 its first derivative and for n=2 the second. For example:

$$l_0(x) = \frac{x - x_1}{x_0 - x_1} \frac{x - x_2}{x_0 - x_2} \frac{x - x_3}{x_0 - x_3}$$

$$l_0'(x) = \frac{3x^2 - 2x_1 x - 2x_2 x - 2x_3 x + x_1 x + x_2 x + x_3 x}{(x_0 - x_1)(x_0 - x_2)(x_0 - x_3)}$$

$$l_0''(x) = \frac{6x - 2x_1 - 2x_2 - 2x_3}{(x_0 - x_1)(x_0 - x_2)(x_0 - x_3)}$$

A 3 step Lagrange polynomial was substituted in the T_S^4 inside the integral, so that the integral itself was calculated analytically, and the resulting formulas were introduced in the algorithm, to make it more efficient than the numerical integration.

$$P3(x) = \frac{(x - x_2)(x - x_3)}{(x_1 - x_2)(x_1 - x_3)} y_1 + \frac{(x - x_1)(x - x_3)}{(x_2 - x_1)(x_2 - x_3)} y_2 + \frac{(x - x_1)(x - x_2)}{(x_3 - x_1)(x_3 - x_2)} y_3$$

$$I(z) = \int_{-\infty}^{+\infty} T_S^4(z + z^*) \cdot e^{-K|z^*|} dz^*$$

where:

$$T_S^4(z+z^*) = \frac{(z+z^*-x_2)(z+z^*-x_3)}{(x_1-x_2)(x_1-x_3)} T_S^4(x_1) + \\ + \frac{(z+z^*-x_1)(z+z^*-x_3)}{(x_2-x_1)(x_2-x_3)} T_S^4(x_2) + \frac{(z+z^*-x_1)(z+z^*-x_2)}{(x_3-x_1)(x_3-x_2)} T_S^4(x_3)$$

The first piece of the integral becomes:

$$I_1(z) = \int_{-\infty}^{+\infty} \frac{(z+z^*-x_2)(z+z^*-x_3)}{(x_1-x_2)(x_1-x_3)} T_S^4(x_1) \cdot e^{-K|z^*|} dz^*$$

Constant terms can be extracted from the integral:

$$I_1(z) = \frac{T_S^4(x_1)}{(x_1-x_2)(x_1-x_3)} \int_{-\infty}^{+\infty} (z+z^*-x_2)(z+z^*-x_3) \cdot e^{-K|z^*|} dz^*$$

which turns out to be very straightforward to solve analytically.
Let A be the constant term in front of the integral.

$$I_1(z) = A\int_{-\infty}^{+\infty} \left(z^*\right)^2 \cdot e^{-K|z^*|} dz^* + \\ + A\left[\left(z-x_2\right)+\left(z-x_3\right)\right]\int_{-\infty}^{+\infty} z^* \cdot e^{-K|z^*|} dz^* + \\ + A\left[\left(z-x_2\right)\left(z-x_3\right)\right]\int_{-\infty}^{+\infty} 1 \cdot e^{-K|z^*|} dz^*$$

Each term can be solved using the basic integral rules:

$$I_{11}(z) = A\int_{-\infty}^{+\infty} \left(z^*\right)^2 \cdot e^{-K|z^*|} dz^* = A\left\{\int_{-\infty}^{0} \left(z^*\right)^2 \cdot e^{Kz^*} dz^* + \int_{0}^{+\infty} \left(z^*\right)^2 \cdot e^{-Kz^*} dz^*\right\} = \frac{4A}{K^3}$$

$$I_{12}(z) = A\left[\left(z-x_2\right)+\left(z-x_3\right)\right]\int_{-\infty}^{+\infty} z^* \cdot e^{-K|z^*|} dz^* = 0$$

$$I_{13}(z) = A\left[\left(z-x_2\right)\left(z-x_3\right)\right]\int_{-\infty}^{+\infty} 1 \cdot e^{-K|z^*|} dz^* = \frac{2\left(z-x_2\right)\left(z-x_3\right)A}{K}$$

Therefore:

$$I_1(z) = \frac{T_S^4(x_1)}{(x_1 - x_2)(x_1 - x_3)} \cdot \frac{2}{K^3} \cdot \left(2 + (z - x_2)(z - x_3)K^2\right)$$

$$I_2(z) = \frac{T_S^4(x_2)}{(x_2 - x_1)(x_2 - x_3)} \cdot \frac{2}{K^3} \cdot \left(2 + (z - x_1)(z - x_3)K^2\right)$$

$$I_3(z) = \frac{T_S^4(x_3)}{(x_3 - x_1)(x_3 - x_1)} \cdot \frac{2}{K^3} \cdot \left(2 + (z - x_1)(z - x_2)K^2\right)$$

The analytic result of the integral (since $z \equiv x_2$) is:

$$\frac{K}{2}\int_{-\infty}^{+\infty} T_S^4(z + z^*) \cdot e^{-K|z^*|} dz^* = \frac{1}{K^2}\left[\frac{2 \cdot T_S^4(x_1)}{(x_1 - x_2)(x_1 - x_3)} + T_S^4(x_2) \cdot \left(\frac{2}{(x_2 - x_1)(x_2 - x_3)} + K^2\right) + \frac{2 \cdot T_S^4(x_3)}{(x_3 - x_1)(x_3 - x_2)}\right]$$

6.4.3 Jacobian matrix pattern

The Jacobian matrix is the matrix of all the first-order partial derivatives of a vector-valued function. In particular, our unknown vector is: $\boldsymbol{\varphi} = [\mathbf{Y_G}, T_G, T_S, \mathbf{Y_{BL}}]$, where each entry of the vector is discretized and has a dimension that equals the number of points in the mesh: for example, $Y_{G,1}=[Y_{G,1}(z_1), Y_{G,1}(z_2), ...]$. The dimension of $\boldsymbol{\varphi}$ (2080) results from the product of the number of variables (16) times the points in the mesh (130). The i^{th} and j^{th} entry of the Jacobian matrix is defined as $J_{ij} = \partial\varphi_i/\partial\varphi_j$, resulting in a 2080^2 matrix, which is required both in the solution of a differential equation problem and by the algorithms that solve a system of nonlinear equations.

The Jacobian matrix is made by blocks, each of them has the same dimension of the mesh, of derivatives in space of each variable, regarding to itself and to the other variables in different positions. Non-diagonal blocks are identity blocks, since each balance contains no derivatives regarding to other variables, but are only function of them in that point in space. Diagonal blocks are diagonal matrices if the variable is governed by an algebraic equation (Y_S), are tri-diagonal matrixes if the balance is a first order differential equation (none for this model), are penta-diagonal matrixes if balances are second order differential equations (Y_G, T_G and T_S). It results in a very sparse Jacobian. Implementing the Jacobian Pattern (which means the non-zero positions of the Jacobian matrix) the computational time required by the program is strongly reduced.

6.4.4 The kinetic interpreter

The chemistry is dealt with the free software Cantera [6]. In particular, Cantera is used as Matlab routines and easily coupled with the main Matlab **Errore. L'origine riferimento non è stata trovata.** program, to give thermodynamic and transport properties and to calculate species production rates. It allows handling mechanisms in Chemkin format, which is the most common way to publish and distribute a kinetic mechanism, formed by elementary steps. It also supports the typical features of surface mechanisms, like coverage dependences, sticking coefficients, and so on. Also, equilibrium was calculated using Cantera "equilibrate" routine.

6.5 Results and discussion

6.5.1 Predictions by a simpler model, the PFR

With the aim to better understand the role of the chemistry and the transport phenomena, as to say, to discover if the system is in the chemical or diffusion regime, a simpler calculation might be helpful. Indeed, the use of a PFR model is really affordable. We reckon that it's a highly ideal model, in which, at each axial position, conduction equals production and no transport resistance of any kind interferes with the kinetics. Since the heat model required to describe this reactor set up is rather complicated and may lead to some uncertainties, we delete the heat balance from the model and use instead the experimental surface temperature. This way, we want to reveal only the effect of ignoring the transport resistance in the mass balances.

In Fig 6.5-1profiles of the four species CH_4, CO, O_2 and H_2 are shown, compared to the experimental data.

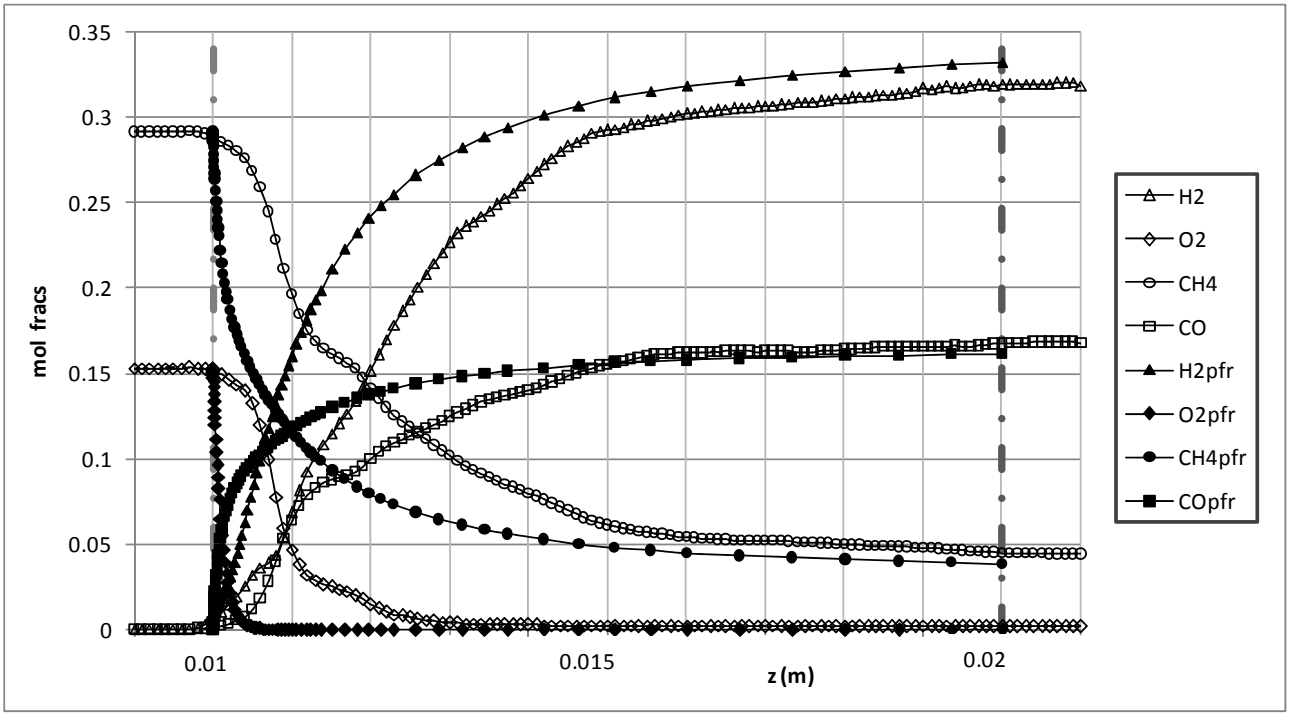

Fig 6.5-1 Gas phase composition along the reactor: calculated by a PFR model with the real surface temperature (filled symbols), and experimental measurements (empty symbols).

If we compare the exit compositions, the prediction of the model is very good for all the species, with a CH_4 conversion of 82%, only 2 points higher than measured. Nonetheless, the experimental exit composition is close to equilibrium and every reactor model, with whatever kinetics inside, would have brought to an analogous good result. On the other hand, some surplus was expected, since the reactor is strongly idealized, and there is more contact between the reactants and the surface.

Interestingly, almost universally the experimental composition is collected at the reactor exit; in that case, we'd have argued that the PFR model, with this kinetic mechanism, almost perfectly describes the experimental data. On the contrary, looking at the pattern of the composition profiles, we become aware that the initial slopes of all the species are very badly reproduced. In the PFR the reactivity is too high; therefore the slopes are too steep. For example: the probe detects the presence of oxygen up to 3-4 mm, while the PFR model predicts total consumption O_2 before 0.5 mm.

To inquire about the "effective" reaction taking place in each position, we can deduce the stoichiometric coefficients of a global reaction among the stable species:

$$CH_4 + aO_2 \rightarrow bH_2 + cH_2O + dCO + eCO_2$$

The stoichiometric coefficient is the slope of every other species divided by the slope of methane (which stoichiometric coefficient is set to unity). The stoichiometic coefficients relative to that of a single species are also called "reactivity ratios", because we calculate the relative production rate of the species.

Even though the global reactions we might write are the results af several elementary ones, an effort in writing the major reactions can help understanding the chemistry of the system. For example, at the very beginning of the catalyst zone we expect the total oxidation reaction to take place (Fig 6.5-2):

$$CH_4 + 2O_2 \rightarrow 2H_2O + CO_2$$

This is quite right, except that the system is better described by the following two, in which the CO forms first and then the subsequent oxidation to CO_2 occurs:

$$CH_4 + 1.5O_2 \rightarrow 2H_2O + CO$$

$$CO + 0.5O_2 \rightarrow CO_2$$

After half millimeter, the oxygen diminisces, and the kinetics goes through a not well definite transient towards the steam reforming stoichiometry:

$$CH_4 + H_2O \rightarrow 3H_2 + CO$$

Since three independent reactions are needed to describe the kinetics among the 6 species, we complete the set with the water gas shift reaction:

$$CO + H_2O \rightarrow CO_2 + H_2$$

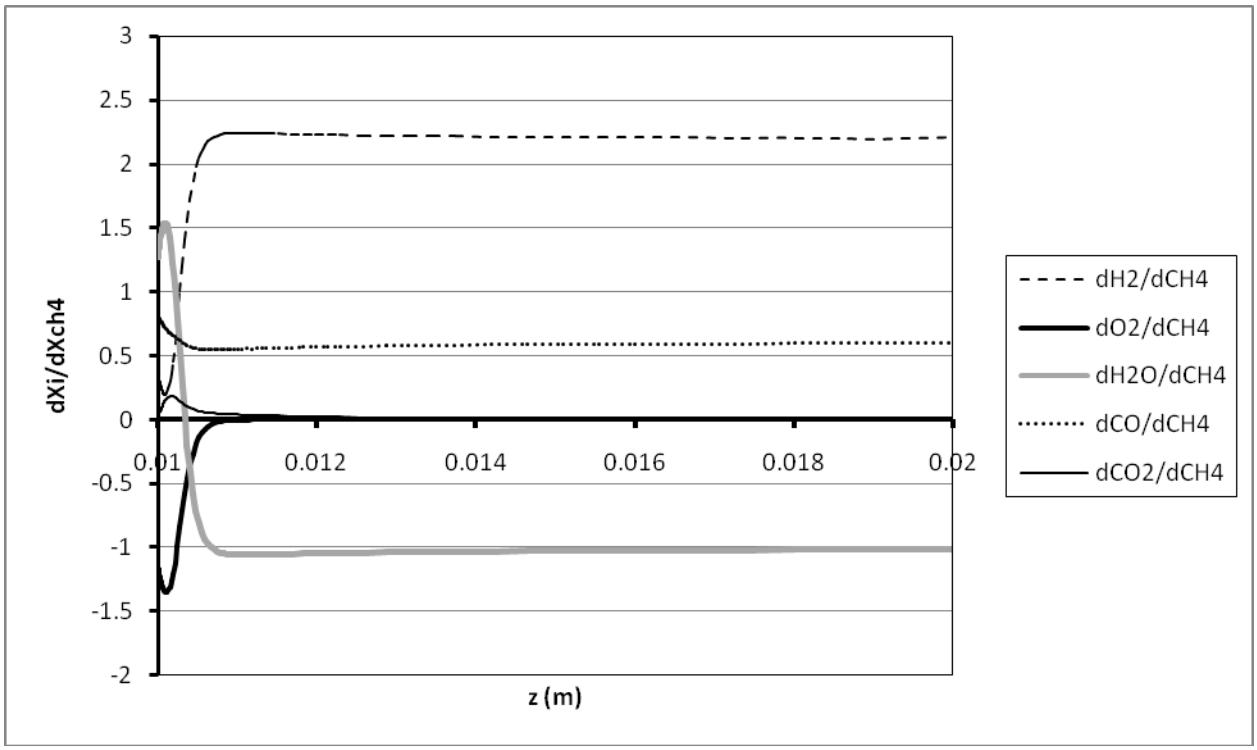

Fig 6.5-2 Stoichiometric coefficients in the PFR model.

In general, discrepancies say that consumption/production of all the species is diffusion limited (the reaction is much faster than diffusion). In other words, the composition near the surface is sensibly different from that in the bulk of the gas. But to properly describe the reacting system, the real production rate at the surface must be calculated with the concentration at the surface. Ascertained that a diffusion regime prevails in a significant part of the foam, the PFR model is not a suitable reactor model. That's where the effort in writing a model involving transport coefficients finds its justification.

6.5.2 Results from the "foam" model

Results from the "foam" model are shown Fig 6.5-3 and Fig 6.5-4, in comparison with the experimental data.

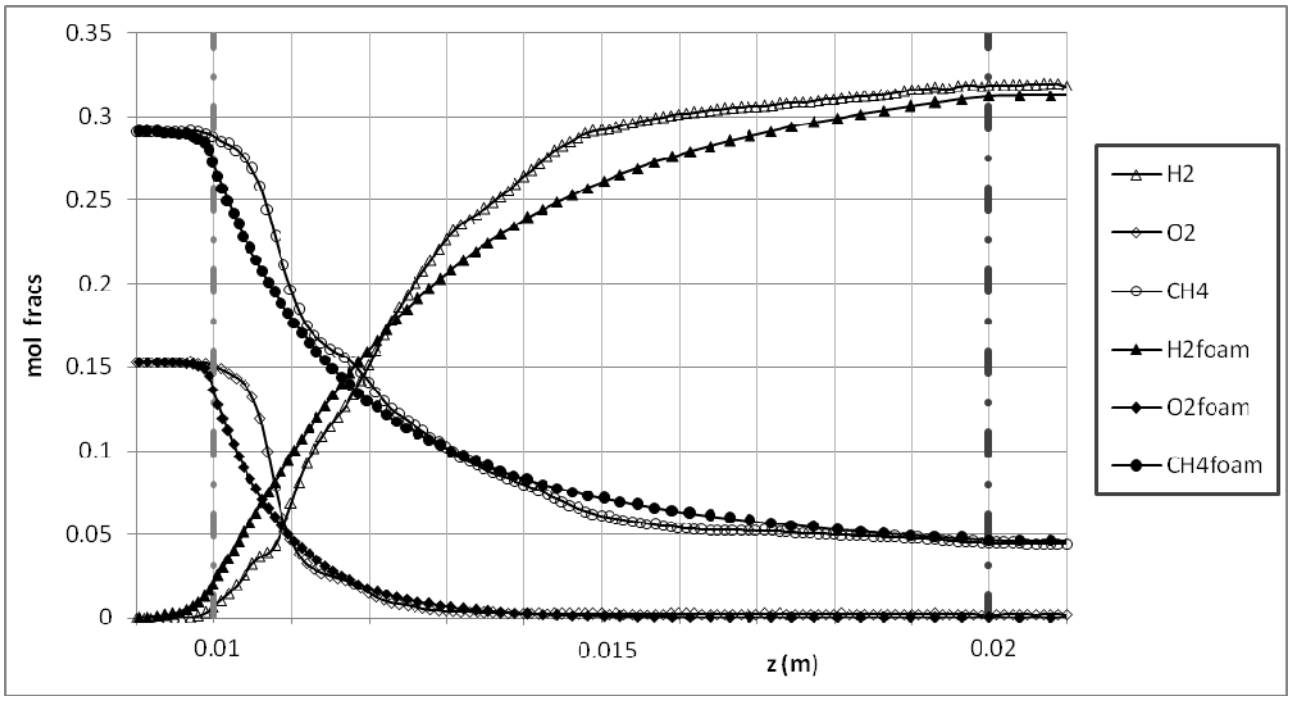

Fig 6.5-3 Mole fractions of H_2, O_2 and CH_4 predicted by the "foam" model, compared with those experimental.

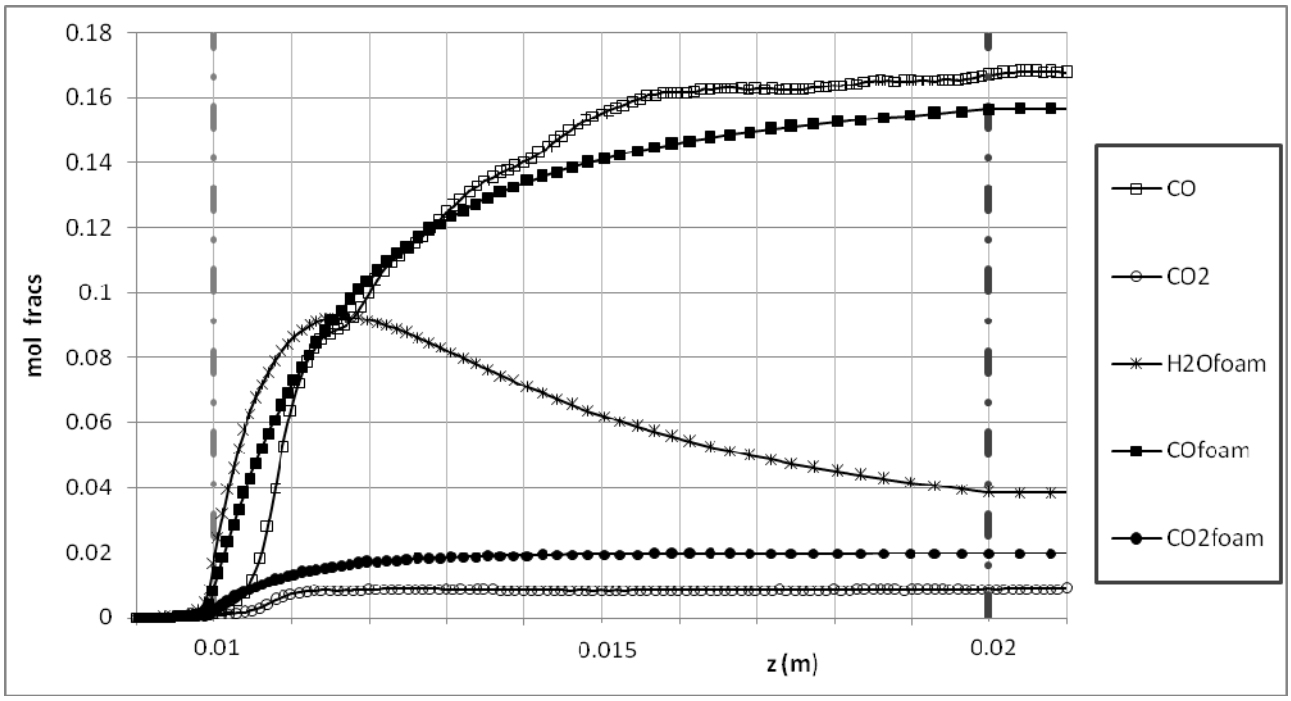

Fig 6.5-4 Mole fractions of H_2O, CO and CO_2 predicted by the "foam" model, compared with those experimental.

In the first half millimeter, as already mentioned, the pore structure is likely uneven and constituted by a blocked pore: the real composition is masked to the probe, which still sniffs the feed taken along by the convection. Note that the composition profiles catch up with those experimental after 1 mm, which corresponds to two pore diameters, and the predicted composition matches much closer the experimental data

along the reactor. This enforces the hypothesis that only the pore structure impedes some sort of exponential profile to set up. The slopes are close to the experimental curves and the final composition of all the species have less than 0.01 absolute errors in the mole fraction. In these pictures the adopted mesh around the catalyst section can be recognized through the markers in the simulated curves.

In Fig 6.5-3the predicted mole fractions of O_2, CH_4 and H_2 are reported. The reactants undergo some axial diffusion, so that their concentration at the catalyst inlet is slightly lower than in the feed. Inside the catalyst, their decay is exponential, as expected. Remarkably their initial slope is the same, confirming once again that we are in a diffusion regime, because the reaction occurs with an apparent "reactivity ratio" O_2 to CH_4 of 1 (Fig 6.5-5), instead of the 2, typical of the case of the total oxidation reaction.

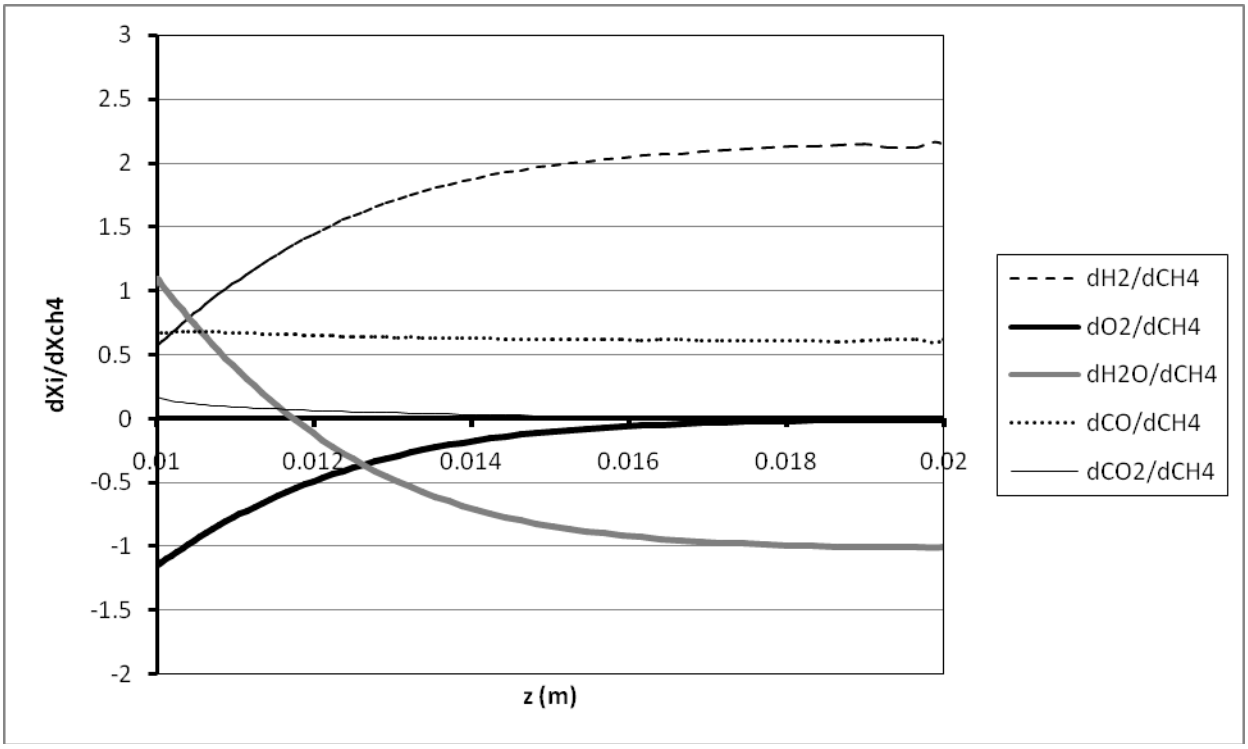

Fig 6.5-5 Apparent stoichiometry coefficients in the "foam" model.

Also H_2 appears before than in the experimental profile, but its high back-diffusivity partly compensates the delay due to the blocked pore, and a gap lower than half a mm is initially present between the predicted and the measured curve. Indeed, the curve of H_2 presents the earliest variation, among all the 6 species involved. Thanks to a big amount of water in the boundary layer, as will be clearer in the next paragraph, some steam reforming is already present at the entrance, where H_2 initial stoichiometric coefficient is 0.5 and grows up to 2 towards the exit.

Predicted CH_4 conversion and H_2 production at the reactor exit are only slightly lower than the measured values.

The other stable species - H_2O, CO and CO_2 - are shown in Fig 6.5-4. Here again we find the delay of half millimeter at the catalyst entrance. The exit CO is lower than expected, but does not appear to relate to the much smaller underestimation of CH_4

conversion; rather a lower CO concentration in the outlet is likely connected to the overestimation of CO_2 at the exit. This is likely due to some deficiency in the kinetic mechanism, although inadequacies in the foam model might contribute. CO and CO_2 exhibit a similar stoichiometry with respect to the full chemical regime of the PFR, but the curves are smoothed and the chemistry of these two species vary more slowly in the presence of a diffusive regime.

The H_2O profile is also shown in Fig.5b: note that it goes through a maximum. H_2O switches from being a product to a reactant, after the O_2 is totally consumed. Even more interesting, CH_4 appears to react in parallel with both O_2 and H_2O even when oxygen is still available. H_2O stoichiometric coefficient starts from +1 and ends to –1. While in the PFR this reactivity ratio changes abruptly in correspondence of the disappear of O_2, where the kinetics turns from a total oxidation into a partial oxidation, in the foam model it varies constantly from the entrance to the exit.

The stoichiometric coefficients are based on the bulk concentration. What we see from the probe tell us that the chemistry in the "foam" model is rather different from the intrinsic kinetics, seen in the PFR. Even though the two models adopt the same kinetics mechanism, the stoichiometry that we deduce from the gas composition is different.

Fig 6.5-6 shows the temperature profiles only in the catalyst, even if the model predicts all the temperature profiles in the three pellets.

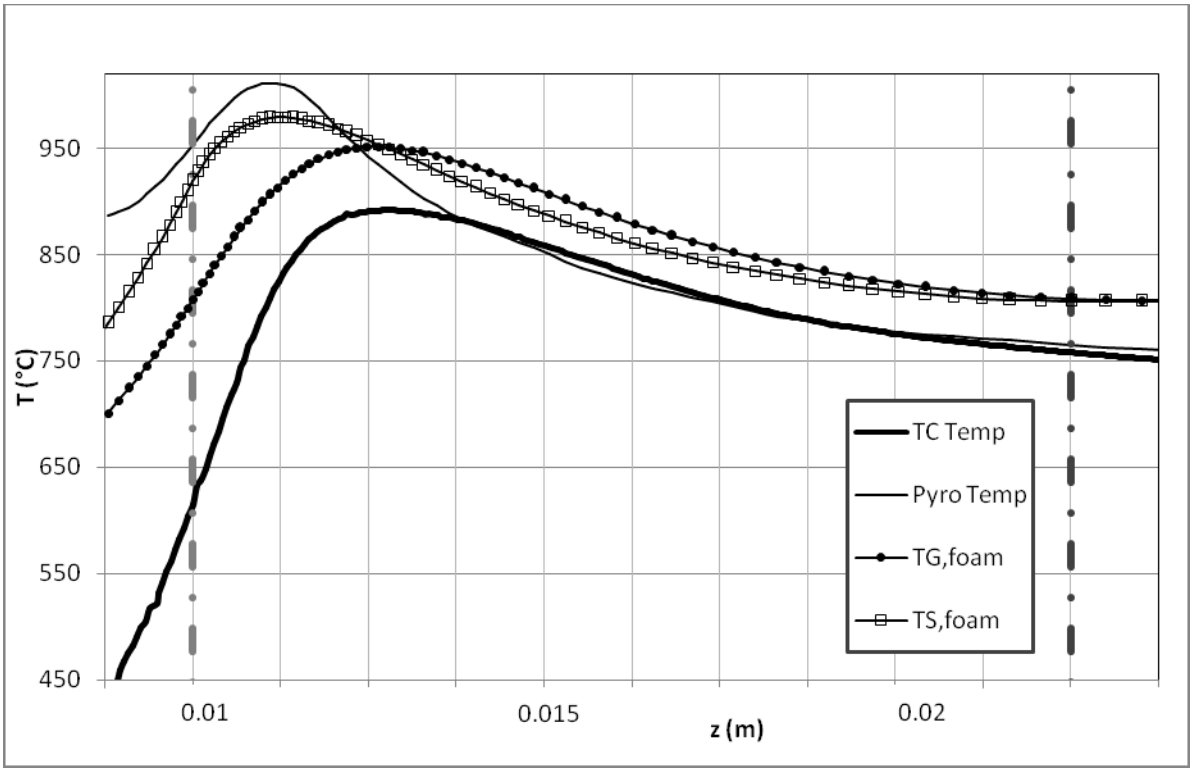

Fig 6.5-6 Gas and surface temperature profiles predicted by the foam model, compared with the experimental. Catalytic foam boundaries are also reported.

In the FHS the T_S grows monotonically up to the value at the catalyst entrance. Heat transport by convection, conduction, radiation and transport between the phases is responsible for the gas heating in the inward direction and the solid cooling in the outward direction. In the catalyst section there is the heat of reaction that keeps the two temperatures – T_S and T_G – different. At the catalyst entrance the strongly exothermic reactions make the solid hotter than the gas. After the oxygen is disappeared, on the solid only the endothermic reaction occurs, thus its temperature is lower than the gas: the heat transport limitations impede the two phases to gain the same temperature, as far as some reactions take place on the surface. In the portion of back heat shield (BHS) not shown here the two temperatures keep equal and constant, since there is no more driving force for the heat to pass through the solid or transfer between the phases.

Up to the maximum, the calculated solid temperature keeps lower than in the experiments: the maximum itself is 35 °C below. However, the position of the maximum is approximately the same as in the real monolith, which confirms the agreement of the chemistry, but also tells us that the description of solid conduction and radiation heat transfer are consistent with the real physics. Besides, this justifies the use of the mean pyrometer temperature profile, instead of those normal or reverse. Indeed, the composition profiles are predicted with high accuracy, so the enthalpy of reaction is reliable, and the position of the maximum is trustworthy (not its absolute value, which depends on many transport features). This position corresponds to that of the mean temperature profile, and this is evidence in favor of this choice.

If the maximum in the solid is determined by a switch from exothermic to endothermic reactions, the maximum in the gas is only due to heat transport from and to the solid, since no production exists in the bulk. Also the position of the maximum in the gas temperature is properly predicted, but now the value is higher than the experimental. As a consequence of the heat transport limitation and the contemporary convection in the gas phase, the maximum in the gas temperature is located downstream that in the solid. Note that in the calculated profiles the gas temperature maximum takes place exactly where the two temperatures cross: among the contributions to the gas heat balance, the accumulation term is zero at the steady state, the radial transport there is null because no temperature difference exists between the two phases, the gas conduction has a minor role in the heat transport because around the maximum the gradients are low, thus the convection term almost equals zero, meaning that the temperature gradient is nearly zero, and the temperature profile pass through a maximum. The crossing of the experimental temperature profiles is far away from the location of the experimental maximum, which gives some suspects on the accuracy of the experimental measurements. For the purpose of this study, though, we are more pleased with the agreement of the surface temperature, since it actually rules the chemistry, which is indeed purely heterogeneous.

An integral heat balance of the whole reactor closes to about 1% error. The adiabatic assumption, carried out through the heat balances, is satisfied. Since the balances are conservative, we don't need to superimpose the adiabatic temperature at the T_G, with a Dirichlet-like boundary condition, at the exit: the Neumann-like boundary condition is enough, together with the conservation of energy, to guarantee that the model is adiabatic. It's interesting to note that the predicted output temperatures are a little higher than those experimental. Of course the actual reactor

is very close to be adiabatic, but some losses are likely to occur by conduction, through the quartz tube which contains the monoliths, and also through the insulation, because of the high temperature reached inside the reactor. However, these losses are really low and neglect them constitutes a minor simplification.

The gas temperature in general is overestimated all along the reactor. A reason is that the transfer coefficients were derived for the mass transport, and extended to the heat transport with the Chilton-Colburn analogy. However, as shown in reference **Errore. L'origine riferimento non è stata trovata.**, the analogy is questionable in presence of a fast reaction, when mass transfer coefficients are sensibly higher.

6.5.3 Limitations by heat- and mass-transport

Once the model has been validated for gas composition and both gas and solid temperatures, it can be used to speculate on those variables that cannot be measured, like the gas species at the surface.

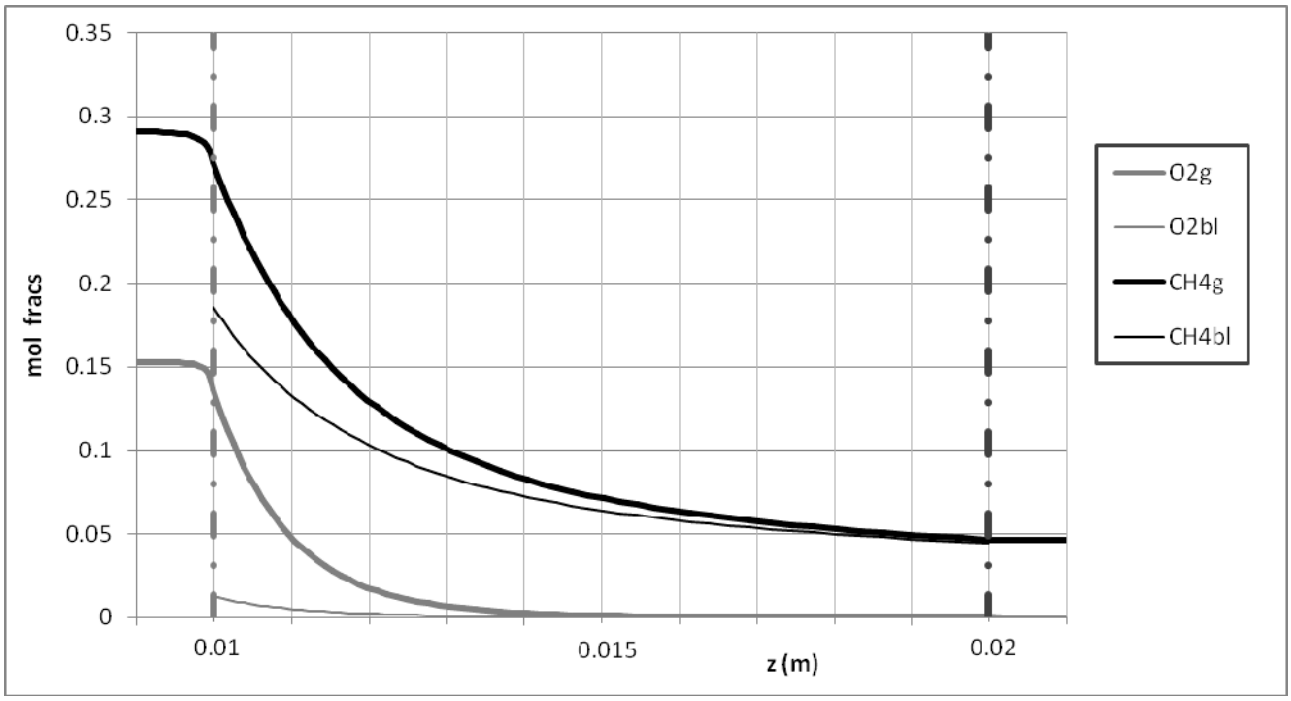

Fig 6.5-7 Composition (mole fractions) in the bulk (thick lines) and at the catalytic surface (thinner lines) of the species O_2 and CH_4.

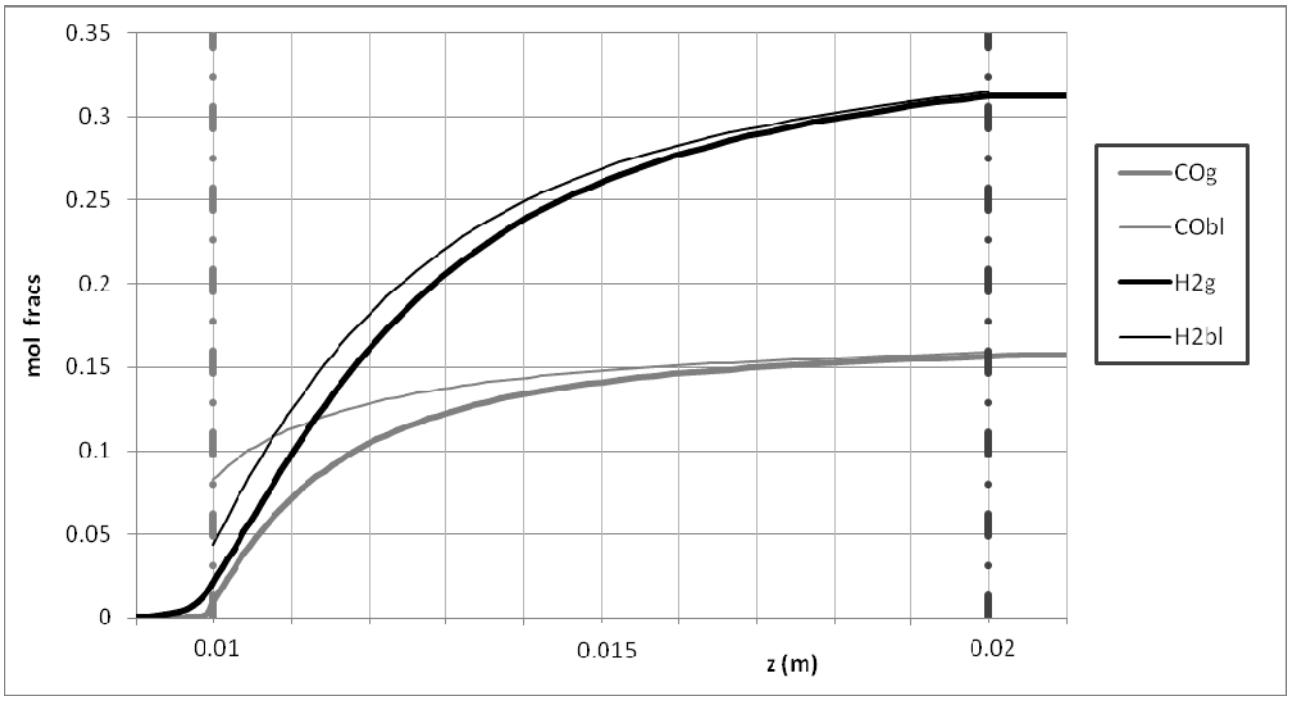

Fig 6.5-8 Composition (mole fractions) in the bulk (thick lines) and at the catalytic surface (thinner lines) of the species CO and H_2.

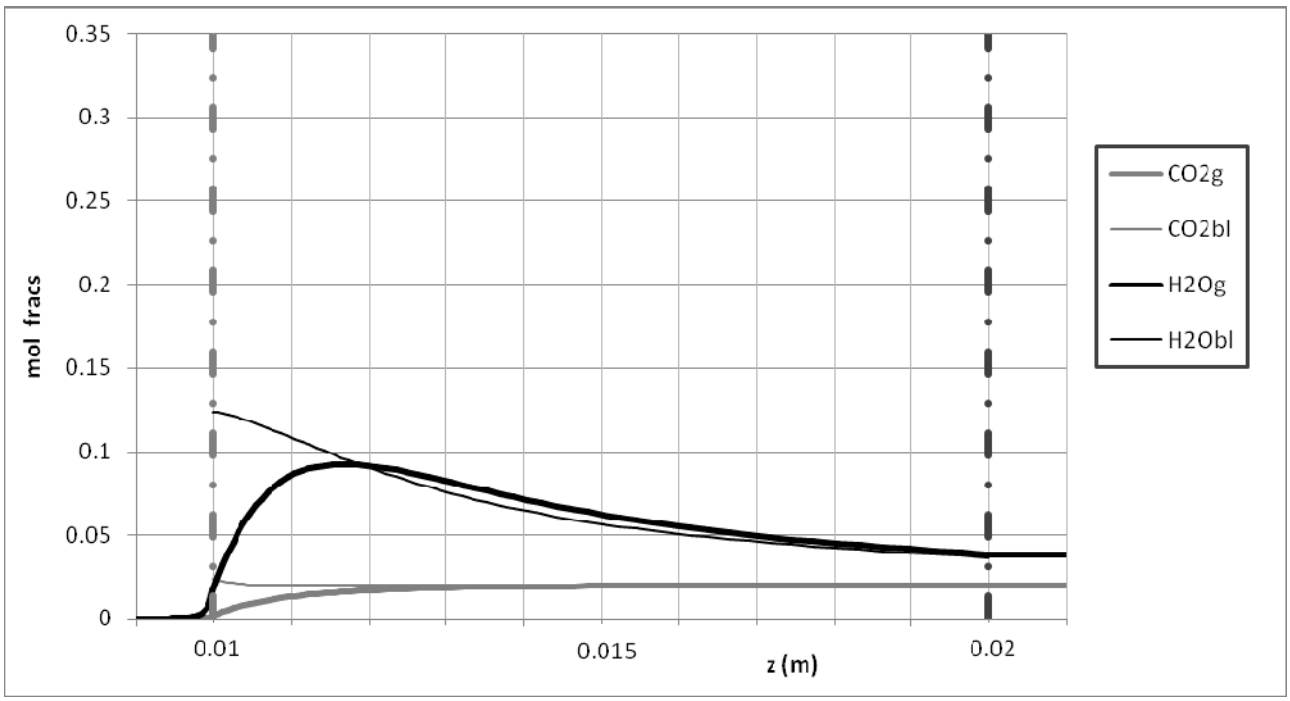

Fig 6.5-9 Composition (mole fractions) in the bulk (thick lines) and at the catalytic surface (thinner lines) of the species CO_2 and H_2O.

In Fig 6.5-7, the two reactants are compared. Their concentration at the surface is quite different from that in the bulk, at the same axial position, and particularly at the beginning, where total oxidation (a faster reaction) takes place. Note that the difference between the concentration at the surface and in the bulk is larger for O_2 than for CH_4; O_2 concentration at the surface is very low already at the entrance. The

surface is apparently "starving" for O_2 because the reaction consumes it very quickly and the diffusion cannot provide for the needs of the kinetics. After 3 mm the oxygen mole fraction on the surface is negligible, even if the corresponding bulk mole fraction is still significant.

Fig 6.5-8 shows the same comparison for CO and H_2. Both species are continuously produced and their profiles are monotonously increasing. As expected, the fast diffusing H_2 results in a smaller difference between bulk and surface while for CO the difference is more substantial.

CO_2 and H_2O are compared in Fig 6.5-9 with the same scale. To understand these curves, we should reckon that the BL composition refers to a thin layer of gas close to the surface, where the composition is the direct consequence of what is consumed and produced by the reaction, locally. It's not surprising to find such a big mole fraction of water, since this representation shows not the quantitative amount of water formed, but the "quality" of the gas inside a small volume. The high concentration of water at the beginning, and even more its slope, reinforces the statement that CH_4 reacts in both oxidation and reforming reactions in parallel from the beginning of the reactor. Note that no maximum exists in the boundary layer composition of H_2O: its maximum production is at the entrance, where the oxygen is higher. There is a crossing between the bulk and the boundary layer mole fraction, meaning that water turns from product (when the $Y_{BL}>Y_G$) to reactant ($Y_{BL}<Y_G$): in the latter, the reaction rates are much slower than in the beginning, and also the composition difference is lower. Also CO_2 has a relatively high mole fraction at the beginning, which decreases and clash to the value of the bulk mole fraction after about 3 mm, that is the same position where there's no more O_2 in the gas close to the surface. After that position, the production rate of CO_2 is near zero, and no difference exists between bulk and boundary layer composition. The fact that also the CO_2 surface concentration decreases at the entrance means not necessarily that it reacts to form something else: it's the natural decrease due to the diffusion into the bulk (a part from the natural decrease in the mole fractions when the reaction has an increase of the mole number). In general, for all the species the difference is more pronounced at the entrance and decreases gradually towards the end. The kinetics is slowing down, for several reasons: the fast oxidation reactions run out, and the reforming is much slower; the kinetics turns from exothermic to endothermic, with a temperature decrease; the reactants run out; the system is approaching the thermodynamic equilibrium.

From the boundary layer species balance (the BL MB), we obtain that the difference between the composition in the bulk and that in the boundary layer is proportional to the ratio of the production rate to the transport coefficient:

$$\Delta X_i \propto \frac{\dot{s}_i}{K_{C,i}}$$

Fig 6.5-10 shows a comparison of the three quantities $\dot{s}$, K_C and $\Delta X=|X_G-X_{BL}|$, all scaled to the values of CH_4, at the catalyst entrance. The mass transfer coefficient is directly related to the species diffusivity as $K_{C,i} \propto D_i^{2/3}$, according to the *Sh'* correlation used.

Note that CH_4 and O_2 have comparable diffusivity, but O_2 reacts with a higher molecularity, thus:

$\Delta X_{O2} \approx 1.5\, \Delta X_{CH4}$.

On the other hand, H_2 and CO_2 have the same composition difference, even if the $K_{H2} = 3\, K_{CO2}$: indeed, also $\dot{s}_{H2} = 3\, \dot{s}_{CO2}$ applies, since the ratio $\dot{s}_i / K_{C,i}$ is the same.

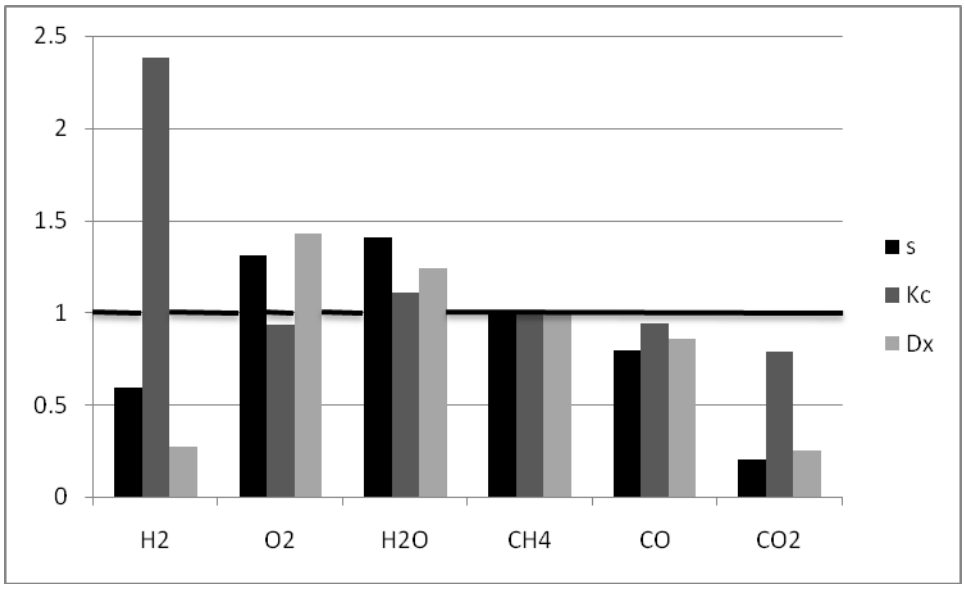

Fig 6.5-10 Difference between bulk and superficial mole fractions (ΔX), transport coefficient (K_C) and production rate ($\dot{s}$) for each species, all scaled with respect to the values of CH_4.

Results confirm that the transport limitation depends both on diffusivity and reactivity of a species: the difference between gas and surface concentrations will be larger for a species with low diffusivity, but also for another with high reactivity. Transport rate, as already mentioned elsewhere, are very sensitive to the actual rate of reaction of a species. For this reason, we are brought to two substantial conclusions; 1) a representative model must include bulk-surface transport of both heat and mass 2) caution in applying the Chilton –Colburn analogy for the case of reacting systems, particularly with fast heterogeneous kinetics (see Chapter 3), must be exercised.

Through the model we can also calculate the residence time inside different monolith sections. It depends both on the local temperature and on the variations of moles due to the reaction. For the FHS results 5.56 ms, in the catalyst 2.90 ms and in the BHS 2.86 ms, strongly confirming that it is a ms contact time reactor.

6.6 Conclusions

We used spatially resolved measurements of temperature and concentration to critically analyze the chemistry and transport limitations in the POM reaction carried out on Rh supported on a foam catalyst. Analysis is based on two models, PFR and foam model, both sharing a detailed surface chemistry but differing by the account of gas-surface transport processes.

Experimental data include axial profiles of bulk concentration and of both gas and solid temperatures. The simulation with a PFR model predicts outlet concentrations very close to the measured one, but apparently because of the approach to equilibrium, given that large disagreement between PFR prediction and measurements are observed along the catalyst, particularly in the initial region. That proved the existence of regions where strong diffusive limitations prevail, requiring the extension of the simple PFR model to account for transport limitations.

We developed a pseudo-1D model ('foam' model), which differentiates the species and temperature in the bulk of the gas and at the surface and describe heat and mass transport through correlations with ad hoc parameters based on dedicate experiments. The solid heat balance contains a solid conduction term, as well as a term describing the radiation transmitted through the porous structure. A Pe number close to unity imposes to add the diffusion also in the gas phase.

The foam model is able to correctly predict slopes and values of all the species. CO_2 is the only species which yield is unfairly high, allegedly due to some weakness in the chemical mechanism. The solid temperature is well reproduced, as well, while the gas temperature has a correct behavior, but is higher than the experimental, possibly due to an overestimated heat transport coefficient. Using the insight given by the model, an analysis of the transport limitations was carried out, showing that the O_2 concentration is everywhere very low near the surface, because of its main involvement in the total oxidation which is a very fast reaction. H_2O concentration close to the catalytic surface is always very high, also at the catalyst entrance, and its slope suggests that the oxidation and the reforming reactions work in parallel from the beginning.

Otherwise sometimes in the literature the differences in composition are ascribed only to the different transport coefficients of the species, as a matter of fact the limitations are stronger for those species whose diffusivities are low, or for those whose net production rates are high. Indeed, transport phenomena are very dependent on the actual rate of reaction of a species. Besides, this is also a warning in the use of the Chilton–Colburn analogy for the case of reacting systems, particularly with fast heterogeneous kinetics.

Chapter 7

About the monolith thermal model

7.1 A single representative channel

The ceramic monolith hosting a combustion process certainly behaves in a mixed thermal regime. Surely it isn't an isothermal reactor, or an adiabatic one. Nevertheless, when we approach it with modellistic purposes, the proximity of one of these two conditions would highly simplify the task. As a first instance, therefore, we try to see what condition is closer to better describe the thermal behavior of the reactor set up, just to decide which one of the models – if the isothermal or the adiabatic – we should more profitably adopt in describing just one of the channels, as representative of the whole monolith. The alternative would be to model the monolith as a pseudo-continuum, with no radial discontinuities on the substrate, thus on the temperature.

7.2 Explaining the experimental evidences

The experimental evidence [38] shows the reactor monolith as an isothermal reactor. When total oxidation is performed in it, no temperature increase is measured, despite the high preheating temperature or the almost full conversion.

7.2.1 Different fluid dynamic of the cells

One explanation that matches the adiabatic hypothesis with the experimental evidence is a different fluid dynamic of each cell. In the quartz tube the reactants flow towards the catalyst, preheating, with a Re~100. A laminar profile develops in the quartz tube, which might cause a different flow rate inside each channel. The laminar profile corresponding to a mean velocity of 1.07 m $\cdot s^{-1}$ at 475°C is sketched in Fig 7.2-1. In the channel axis the velocity is twice that mean, and at the wall it's zero. If the gas hits the catalyst with the same profile, we expect a different flow rate in each channel.

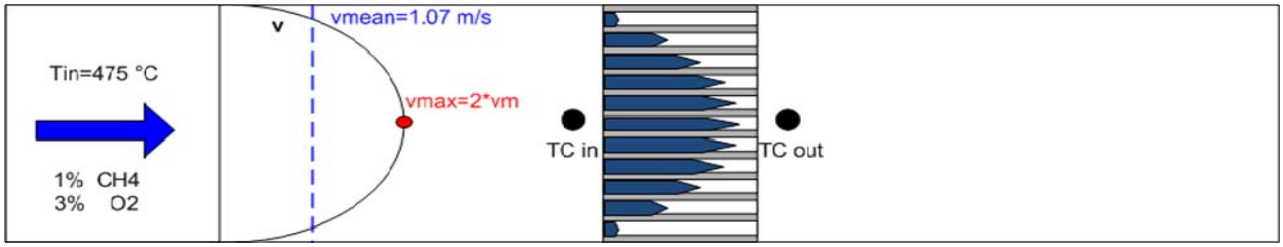

Fig 7.2-1 Velocity profile inside the quartz tube and in the catalyst.

At the chosen temperature the Rh catalyst is active, but not too fast. A lean mixture is sent in the reactor, to qualitatively reproduce the experimental conditions. The monolith section is divided in 11 channels, as it is in the real world. Two

thermocouples measure the inlet and the outlet temperature. Each channel is modeled as an adiabatic PFR, with an inlet velocity corresponding to its radial position. The outlet temperature and conversion are reported in Fig 7.2-2.

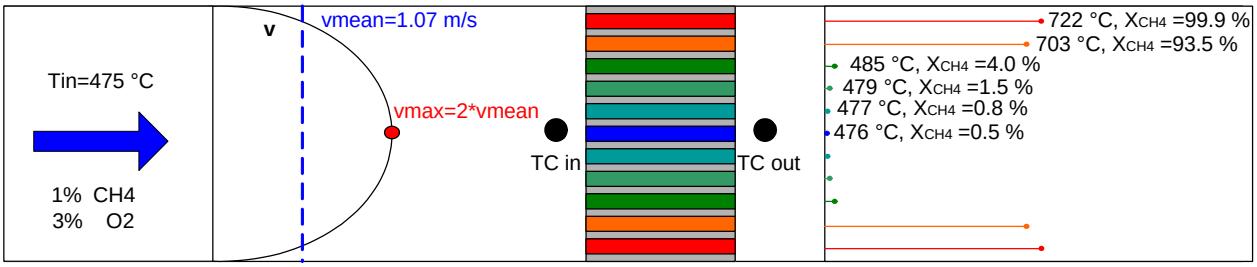

Fig 7.2-2 Conversion inside the monolith, in the hypothesis of the gas flowing with laminar velocity profile.

In the outer channel the conversion nearly reaches 100%, while in the middle it's less than 1%. This behavior could explain why the TC^{out}, which is very close to the pellet, doesn't notice a temperature increase, even if the catalyst is adiabatic.

Temperature and composition profiles are shown in Fig 7.2-3: after the light off the reaction is very fast, because of the high temperature increase.

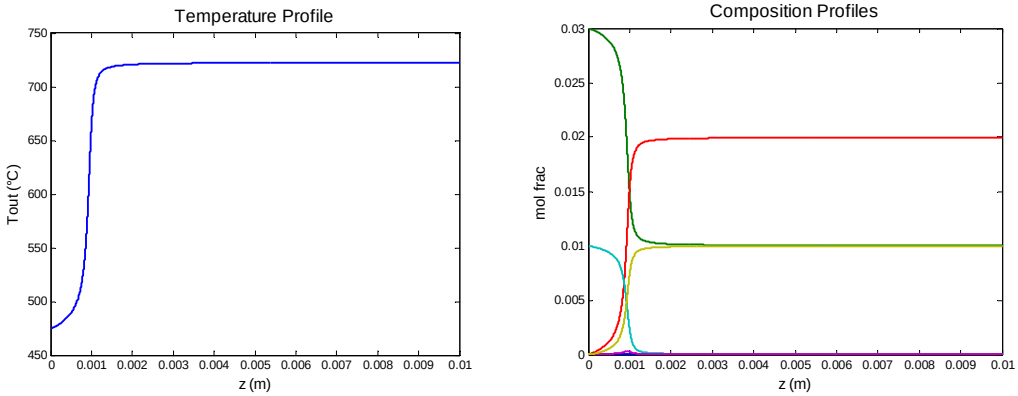

Fig 7.2-3 Temperature and composition profiles of methane total oxidation with high conversion.

7.2.2 Radiation hitting the inlet thermocouple

Temperature profile, after light off, is very steep. Thus, the heat can radiate outward and hit the inlet thermocouple, located very close to the monolith. This way, the TC doesn't measure the preheated gas temperature, but something in the middle between it and the catalyst surface temperature.

As shown in Chapter 5, surface temperature has a peak a few millimeters after the inlet section. The maximum temperature, for this kind of systems, is way much hotter than that adiabatic, and the catalyst is likely to light around heat. On the other hand, the reaction becomes slow approaching the monolith exit, and no big temperature gradients are expected near the outlet section. Assuming that the middle channels are representative of the behavior of the whole pellet, the outlet thermocouple gives a more reliable measurement.

An analysis should be done, that enlightens the role of solid conduction in this situation. Once the adiabatic hypothesis has been checked, the right coupling should be between conversion and temperature of TC^{out}, not TC^{in}, like so far.

7.3 Deep insight into the fluid dynamic

In this situation, CFD calculations aim to understand, at least qualitatively, the profile with which the gas reaches the monolith and enters the channels. The quartz tube is long enough to develop a steady laminar profile, like that shown in §7.2.1. On the other hand, the pellet is a major obstacle for the flow, even if the honeycomb monolith gives a relatively low pressure drop.

An empty tube's been modeled, followed by a porous pellet, representative of the monolith. A first move is to characterize the monolith, through a single channel analysis. Eventually, a long piece of quartz tube, representative of a fully developed region for velocity, can be linked to the 1 cm porous section.

7.3.1 Characterization of the square channel

The square channel can't be simulated using a 2D axial symmetric model: a 3D model is required. However, its 3 symmetry axes allow reducing the dimension of the problem: the simulation of an octant is enough to describe the whole section (Fig 7.3-1).

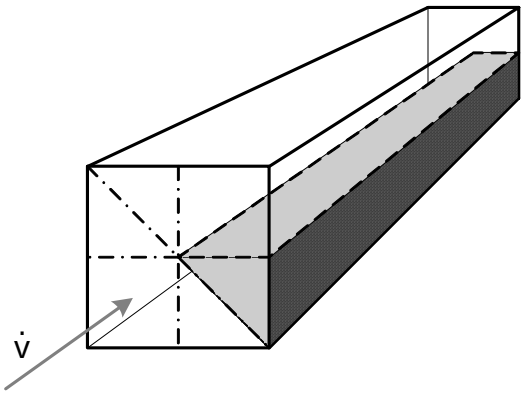

Fig 7.3-1 Square channel symmetry axes and an example of octant.

We are interested only in the flow field, in a qualitative way; therefore a simple model based on incompressible Navier-Stokes equation's been used. For the only purpose of finding the pressure drop the channel is considered isothermal, and a mean temperature of 600°C was chosen.

Geometry refers to Fig 2.2-1. The section of the octant is $A_{\angle} = 1.431 \cdot 10^{-7}$ m^2, and the corresponding velocity is $v = 1.251$ m·s^{-1}. The non-reacted mixture of 3.33% CH_4 and 1.67% O_2 in nitrogen is assumed to flow through the channel, and properties were preventively calculated at the chosen temperature using Cantera: density $\rho = 0.3864$ kg·m^{-3} and viscosity $\mu = 3.772 \cdot 10^{-7}$ Pa·s. Inside the channe Re ~ 14. The resulting flow field is shown in Fig 7.3-2.

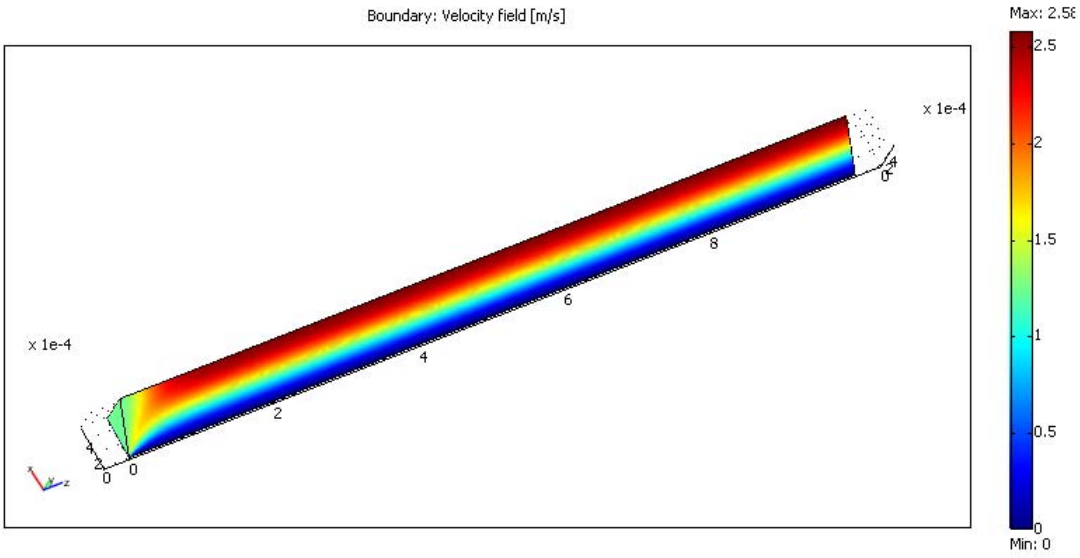

Fig 7.3-2 Flow field in the channel. Here, half a diagonal section is shown. The inlet section is on the left-hand side of the figure. The channel corner is on the bottom and the axis is on the top of the stick.

The non-slip condition on the wall makes the flow pattern parabolic-like. Keeping the other properties constant, the velocity field develops in about 1 ½ mm, which is clearer if we take a look at the axial velocity (Fig 7.3-3). Being the entry region more than 1/10 of the total reactor length, a correlation accounting for it should (and was) used in a 1D Boundary-Layer model.

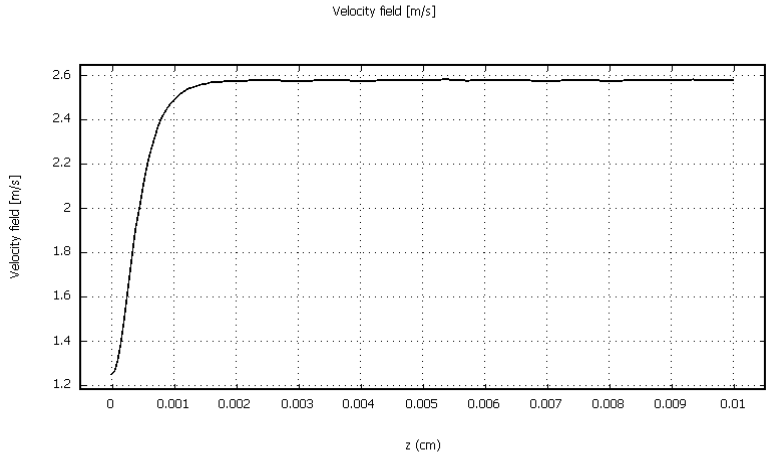

Fig 7.3-3 Velocity field in the channel axis. The profile takes more than 1/10 channel to get flat.

The main advantage in using a structured catalyst is its low pressure drop. In Fig 7.3-4 it's possible to sense this very low pressure decrease: some stress is located at the entrance, by the wall, but the bulk gas has an almost imperceptible difference from the entrance to the exit.

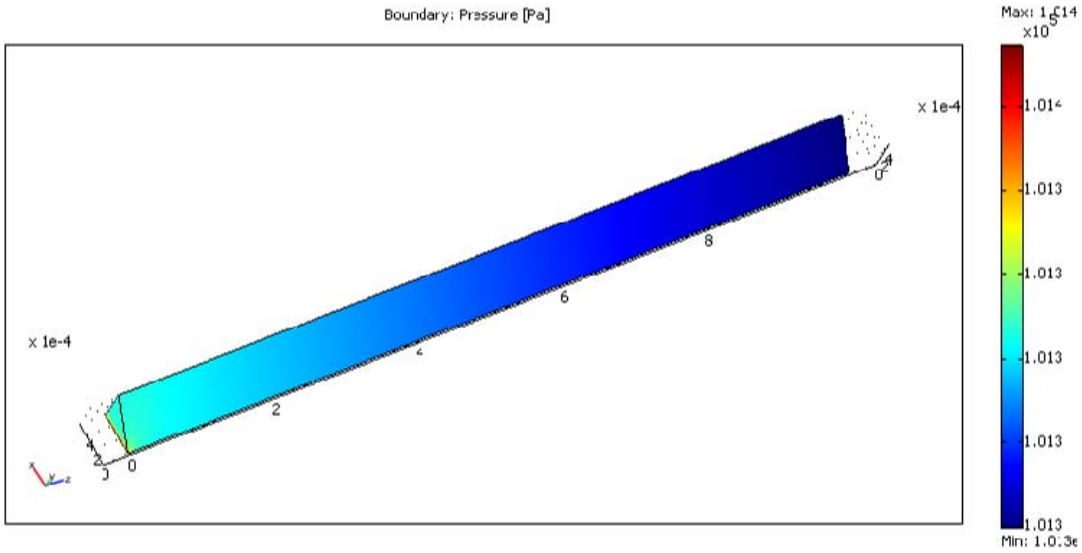

Fig 7.3-4 Pressure field in the channel. Here, half a diagonal section is shown. The inlet section is on the left-hand side of the figure. The channel corner is on the bottom and the axis is on the top of the stick.

Let's evaluate the actual pressure drop and the permeability factor of the equivalent porous structure, according to the Darcy's law. The surface integral of pressure is 0.014501 N in the outlet section and 0.14503 N in the inlet one, giving a difference of $-2 \cdot 10^{-6}$ N. Times the $A_{\angle}$ it becomes 14 Pa.

We recall the Darcy's law:

$$v = -\frac{k}{\eta}\nabla P \qquad \text{7.3-1}$$

where, as usual, v is the interstitial velocity, rather than the superficial, and ∇P is the pressure gradient. Since the monolith is 1 cm long, the permeability turns out to be $k=3.4 \cdot 10^{-8}$ m^2.

7.3.2 Simulation of the quartz tube

The quartz tube's been simulated as an empty tube and a porous pellet in series. A 2D axial symmetric model can here be used. A representative length of 20 cm of quartz tube is analyzed, to be sure to reach a full developed profile before reaching the pellet. The incompressible Navier-Stokes equation models the empty region while the Darcy's law represents the porous zone. The zero gauge pressure is set at the monolith exit. At the interface between the two zones, the Darcy's equation reads the inlet

velocity incoming, while the Navier-Stokes equation sees the front pressure from the porous edge. All the other BCs are trivial for this problem.

In Fig 7.3-5 the trend of the velocity in the empty tube is shown, that proves a full developed profile is reached before reaching the porous zone.

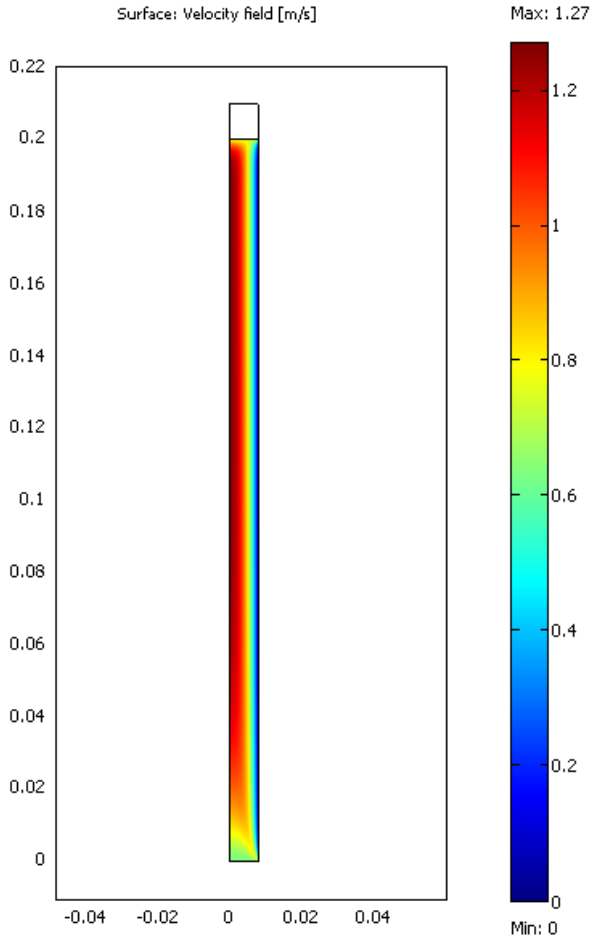

Fig 7.3-5 Developed velocity profile in the empty quartz tube.

Thus, after a parabolic profile stabilizes inside the tube, the even high porosity monolith disturbs the flow, flattening the velocity profile right in front of its entrance (Fig 7.3-6).

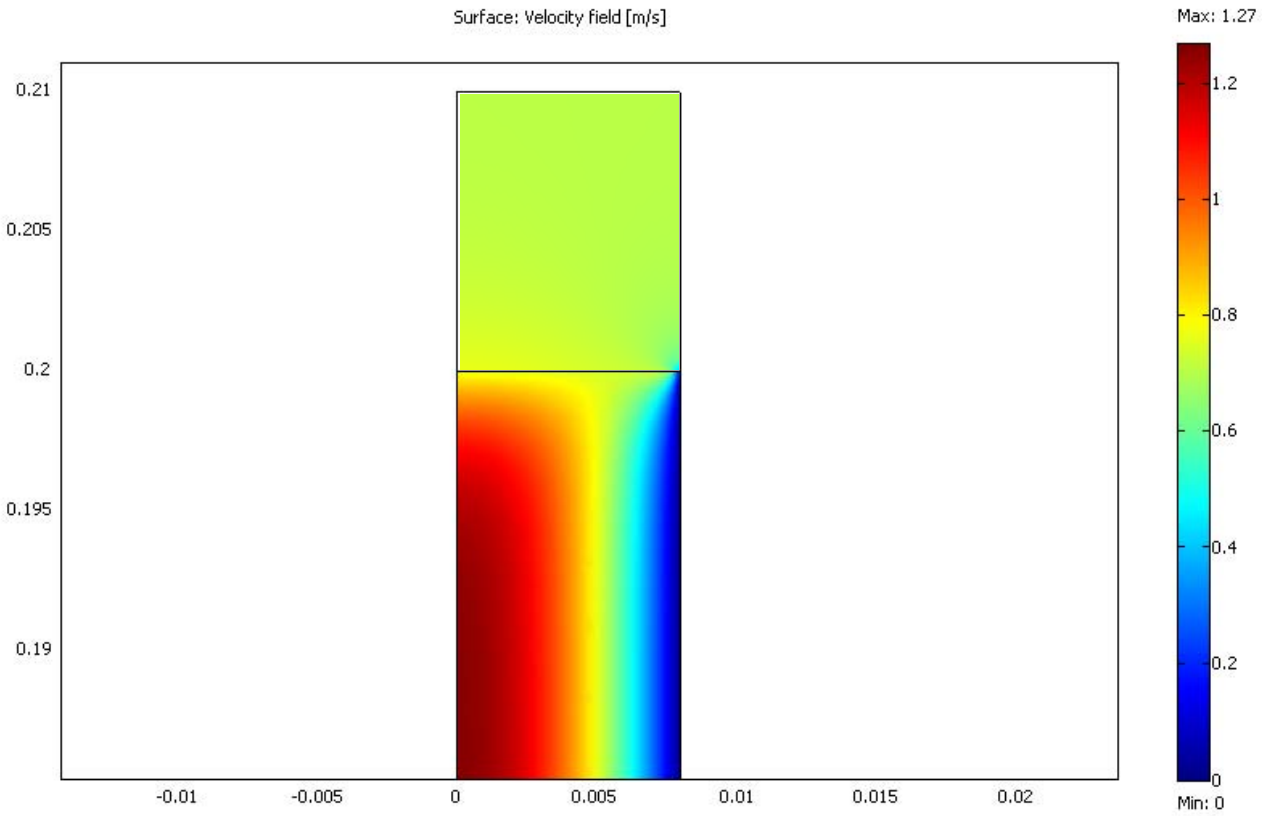

Fig 7.3-6 Axial symmetric velocity field in the empty zone and in the porous region.

As a further proof, the velocity profile at the entrance of the porous region is shown in Fig 7.3-7. Only the peripheral channel might be influenced by the profile, while the others are fed with almost the same flow rate.

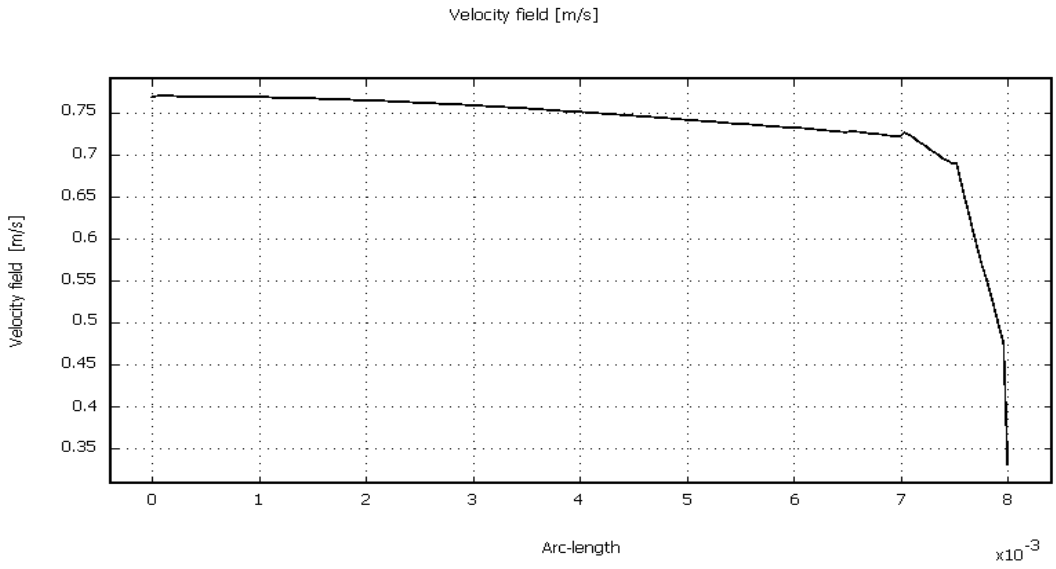

Fig 7.3-7 Velocity profile at the interface between the empty and the porous zone.

In conclusion, the explanation about the different fluid dynamic of the cells is not consistent. This doesn't mean the monolith is isothermal, though. Other explanations could be found, consistent with the adiabatic hypothesis.

7.4 Heat highways through the solid?

7.4.1 Hot gas flowing in a channel with cold external wall

An important statement against the isothermal hypothesis is the cordierite has such a low conductivity that it can't dissipate all the heat of reaction in that milliseconds contact time length.

To verify this statement a simple calculation is required. Let's suppose to flow a hot gas (T^{in}=600°C) inside one channel, which wall is exposed to a 300°C outside temperature. If the channel were adiabatic, a negligible temperature decrease would be expected at the outlet. Otherwise, if it were isothermal, the gas outlet temperature (T^{out}) should be close to 300°C. In general, T^{out} could vary in the range 300-600°C, but hopefully it'll be closer to one extreme of this interval, and we'll have an evidence of whether the channel is more likely adiabatic or isothermal. For simplicity, the velocity field is supposed fully developed at the entrance already, with a mean of v_m = 1.251 $m \cdot s^{-1}$and a parabolic profile with a maximum of 2 $\cdot v_m$, being a laminar stream. A conductive model is assumed for the cordierite wall, with a constant thermal conductivity of 2.75 $W \cdot m^{-1} \cdot K^{-1}$. A convective–conductive model describes the gas phase, here again with constant properties (velocity, density, heat capacity and thermal conductivity). Temperature boundary conditions are set at the entrance of the channel and at the outside of the wall. The front and rear wall edges are supposed adiabatic. The outlet gas section has a "convective flux" boundary condition. At the interface between the two phases, a temperature coupling is enough to allow the heat through the internal surface.

In Fig 7.4-1 half a channel is shown, together with the wall. The upper edge corresponds to the outside of the wall and the lower one is a symmetry axis. The gas flows rightwards.

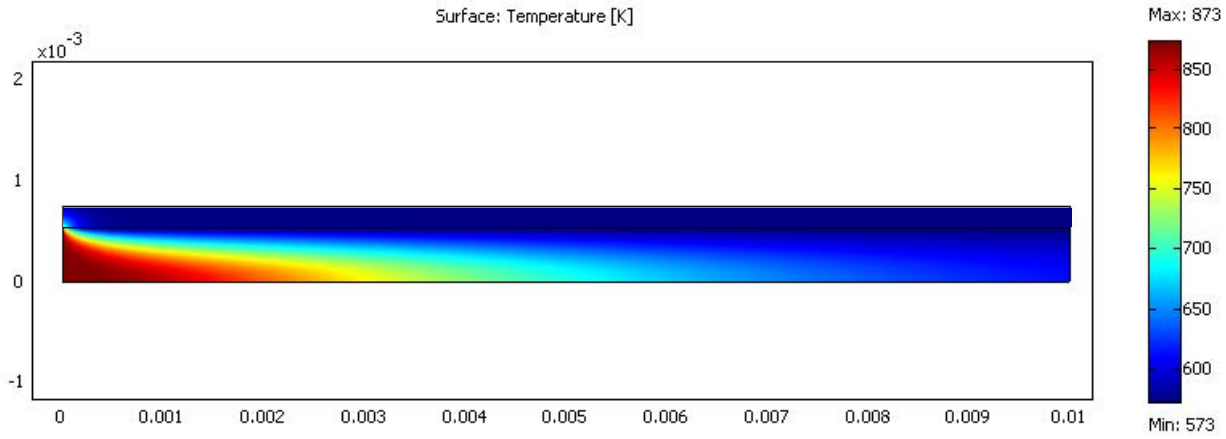

Fig 7.4-1 Temperature profile of a non reacting gas flowing in the cordierite channel exposed to a lower temperature environment.

An adiabatic channel in the real world would have maintained fairly constant the gas temperature, without heat sources or high heat losses through the low conductive wall. On the contrary, the temperature profile at the wall drops very fast, close to the entry section already. As a matter of fact, although the conductivity is small, the gas flows really slowly, and there's plenty of time for the heat to leave through the wall. Besides, being the heat source located at the surface, in the actual reactor there wouldn't be any resistance due to the transport from the bulk to the wall (which goes with a conductivity of 1/100 times less than that of the cordierite).

This simple calculation showed there can be a big heat loss chance. The monolith temperature is likely to tend towards that of the oven. The deep hot spots that could be expected with a non–conducting material are smoothed and the heat flows from the surface both to the gas and to the oven. With the profiles shown in this paragraph, an assumption of no radial temperature profile in the monolith can be taken, due to the extremely fast temperature transit through the solid phase. This is good because it is still true that a single channel is representative of the entire monolith.

One more issue we still have to address ourselves. Is the temperature profile to be considered flat or relatively low heat conduction in comparison with the fast release of the reaction enthalpy might cause some heat to accumulate in the most reactive areas? A way more detailed calculation is required to answer to it, bringing us to wonder if it's worth the effort. If a flat profile does extremely simplify the modeling indeed, it's also true that a fairly good prediction is linked to a rigorous heat model, being the kinetics very sensitive to the temperature.

7.4.2 Heat production in a thin layer near the surface

In the previous paragraph the evidence of no big radial gradients has been produced. A more strict representation of what happens in the outer channel, though, might act in support of either one of the two thermal hypotheses.

The geometry keeps the same, except that a thin layer is carved out of the gas phase, as a separate control volume (Fig 7.4-2).

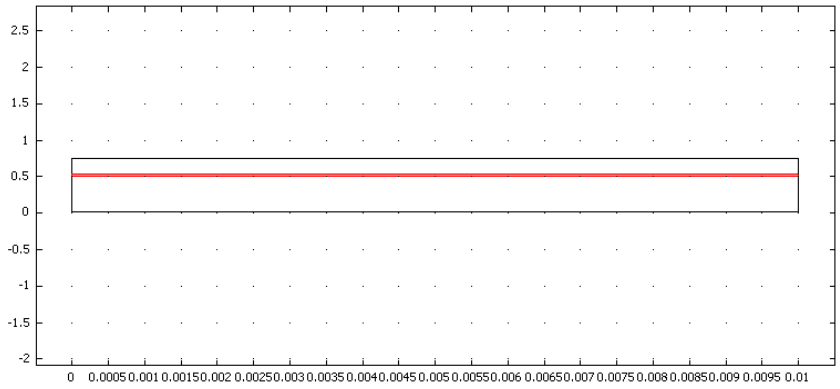

Fig 7.4-2 Thin layer of gas in which the heat source is located.

The boundary conditions are also different: the inlet temperature of the gas (873 K) is equal to the external temperature to which the wall of the channel is exposed. This mimes the preheating of the gas by the oven, where the monolith is placed.

The heat source is uniform in the layer volume, and globally reproduces the heat of reaction of 1%v CH_4 combustion (Tad=1115 K). Being the layer $3.5 \cdot 10^{-5}$ m thick, the heat source is $q=2.5 \cdot 10^{8}$ W $\cdot m^{-3}$. Indeed, a simulation with an adiabatic boundary condition on the wall gives an outlet gas temperature of about Tad (Fig 7.4-3).

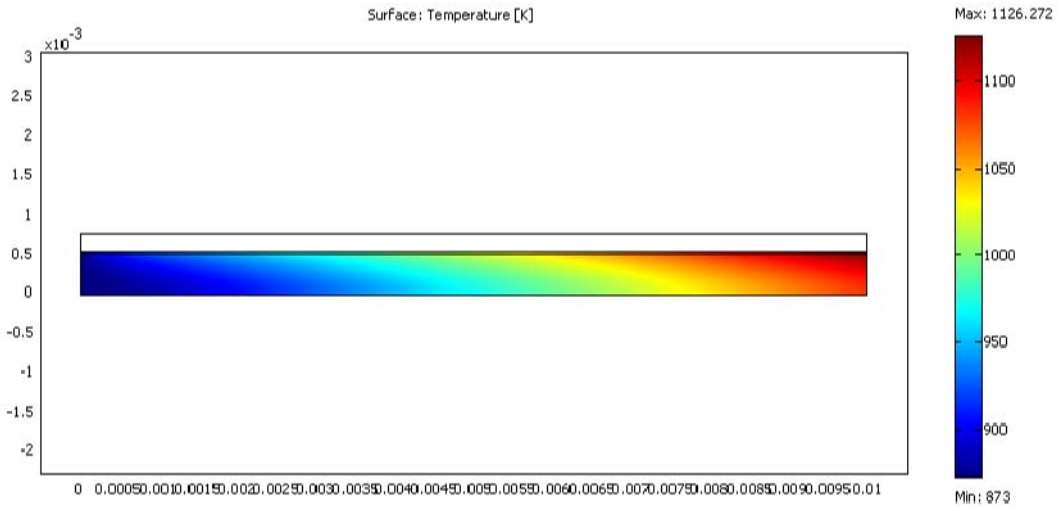

Fig 7.4-3 Simulation of the channel as adiabatic, with an heat source equivalent to the combustion of 1%v of CH_4 located in the layer.

Adopting the same q, the external boundary condition at the wall was modified in "heat flux", with an infinite temperature of 873 K and an heat transport coefficient of h=100 $W \cdot m^{-2} \cdot K^{-1}$, near that of 1 mm of rock wool at high temperatures (the actual extent of insulation surrounding the monolith). Results of both the gas and the solid phases are reported in Fig 7.4-4.

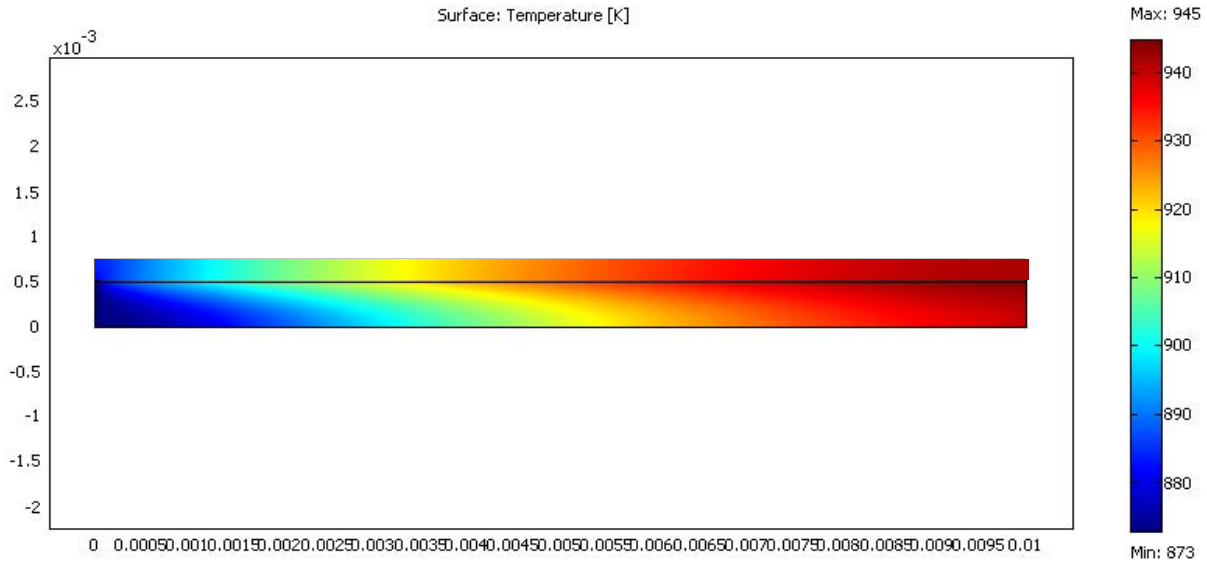

Fig 7.4-4 Channel temperature with heat losses towards the oven, through a rock wool insulation.

It turns out that the outlet temperature of the edge channel is somewhat in the middle between the isothermal and the adiabatic temperature. There is some extent of conduction through the solid, but the main heat flux is due to the fluid convection, as can be seen in Fig 7.4-5, where a zoom in on the gas layer shows a relative big extent of heat flux towards the bulk and a very small vertical component towards the solid.

In conclusion, if an half-way adiabatic channel is at the edge of the oven, we could expect that, already from the second row of channels, a full adiabatic condition applies (in fact, the channel described above is surely running in an asymmetric way, colder towards the outside wall and hotter in the inside).

We hold this issue as a clear enough proof that the adiabatic hypothesis is more suitable to the ceramic monolith.

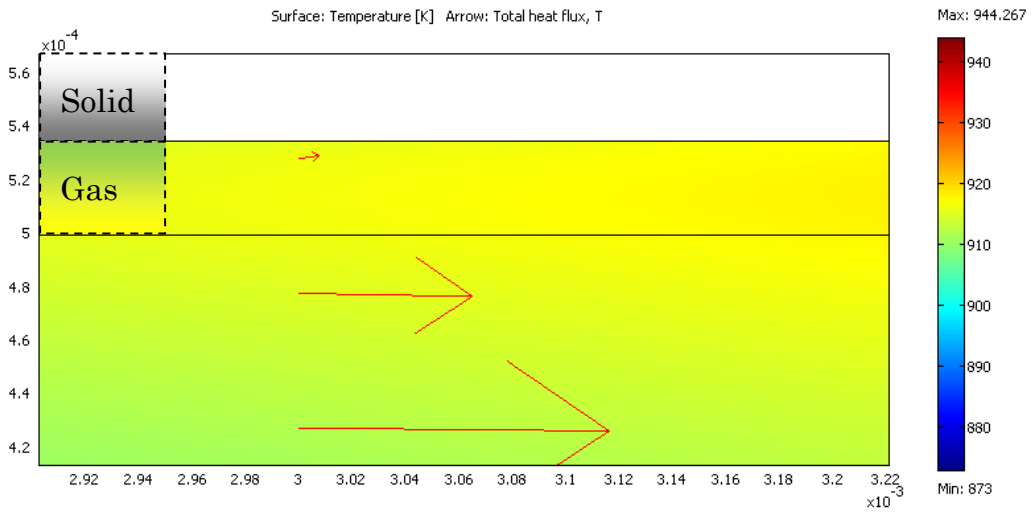

Fig 7.4-5 Total heat flux in the gas phase.

The non increasing temperature from the inlet thermocouple to the outlet might be explained by assuming a strong radiation hitting the frontal TC, affecting the reliability of the measurement. Though, further investigation in this subject aren't going to be done, being satisfactorily asserted the physics of the system, and reckoning that only the outlet thermocouple measurement is trustworthy.

7.5 Conclusions

Since I prefer to think at the monolith as adiabatic, I tried many hypotheses to match this idea with the experimental evidence.

A first hypothesis is that the fluid dynamics is different for the various channels, because a parabolic laminar profile exists in the quartz tube. The inner channel would have a residence time so low that the conversion in it is non-existent, while in the outer channels the reaction goes to completion. Nonetheless, some more detailed fluid dynamics calculations state the opposite: the monolith is a good enough obstacle to the laminar velocity profile developed in the quartz tube, so all the channel work with the same fluid dynamics. To this aim, a 3D simulation of one channel is used to derive the permeability of the monolith, and this parameter is then used in a 2D axial symmetric simulation of the quartz tube.

Another check is required on the conductivity at the wall: if exposed to a low temperature environment, the wall shows conductive, but if a heat source is located into a thin layer near the surface, the heat goes preferably inward the channel, in the bulk of the gas, instead than outward, passing through the channel. This is the best proof for the adiabatic party.

The explanation that explains both the adiabatic thermal model and the experimental evidence is that the TCin is hit by a strong radiation coming from the monolith, and its measurement is altered, so that it doesn't measure the T_G, but the T_S of the front face of the monolith.

Chapter 8

3D CFD modeling of the square channel

8.1 Ad hoc imago

As became clearer and clearer though this thesis, the CFD modeling with detailed surface chemistry is the top among all the models we can solve. A rather simple geometry and small volumes are required, to reduce the number of cells to a number we are able to solve as well as the computational time. The CFD allows considering the homogeneous kinetics, but this makes the solver very slow, because the kinetics must be solved for every cell, and the number of variables in the gas phase increases. In this problem we have a predominantly heterogeneous kinetics, so we keep neglecting the homogeneous ones: thus the chemistry is solved only for the cells close to the catalytic wall, and the intermediates of the reactions are present only as surface species, in a limited number of cells, while in the gas phase only the stable species are described.

8.2 Geometry

The square channel is simulated as an octant, as shown in Fig 7.3-1. Also the solid substrate is simulated, to account for some solid conduction through the ceramic material. The software adopted is FLUENT [13].

The mesh is uniform in the rectangular sections, with a step of 50μm, while that in the triangular faces is represented in Fig 8.2-1.

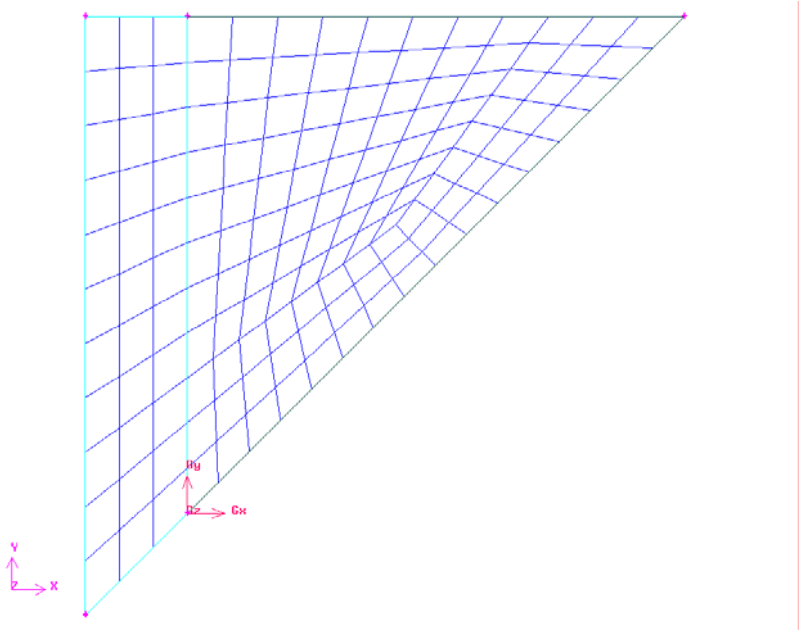

Fig 8.2-1 Mesh of the cross section.

It results in 29,000 hexahedral cells, with 2200 quadrilateral cells at the wall.

8.2.1 Boundary conditions

For the mass balance, the inlet composition is the feed composition, and the wall implements the surface chemistry mentioned in Chapter 2 [37] (the very same reaction mechanism used in all the 1D models). As for the 1D models, the presence of a washcoat largely increases the active surface area. To account for it, without any other indication, the surface to volume ratio, S_V, was corrected by a factor of 2. Furthermore, the S_V is then multiplied by the correction factor for ZrO_2.

For the momentum balance, the velocity profile is flat at the entrance, also in agreement with previous evidence (Chapter 7), and at the internal wall the non slip condition applies.

For the heat balance, the inlet has the feed temperature, at the internal wall there is the heat of reaction, but the wall is coupled with the surface zone, which means some heat conduction is allowed. The outer wall has an insulation boundary condition, being a symmetry plane between two identical channels.

8.3 Results

CFD calculations are very useful for visualizing a variable in the cross section of a channel, instead of the more abstract mean. Also, it gives insight in the reaction mechanism, because it correlates the zones with low velocity to where the conversion starts or to the hot spots. Moreover, it makes you understand easily the statements about the transport phenomena, because a profile in the cross section is soon evident. All these reasons motivate the choice of a representation of the contours in different cross sections along the reactor, to see how the composition or the temperature evolves.

As usual, I won't stop dwelling on O_2 as the most interesting among the species (Fig 8.3-1). The sections shown are chosen with a step of 1 mm, except for the first one: instead of reporting the entrance, less informative, I picked a section 0.1 mm after the inlet. The feed flows from right to left, in the direction pointed out by the arrow. To offer a better view, the octant was enclosed in a scheme of the channel, which includes the solid substrate.

Just the 0.1 mm section, the first contour in sight, gives a good deal of information on the reaction. In the bulk we find the feed oxygen concentration, still. Near the surface, though, the molar fraction is half that in the bulk, and it becomes one order of magnitude lower after 1 mm and almost zero after 2 mm (this quantitative discussion will be supported by the analysis of the mean profiles, in Fig 8.3-9). A non-trivial remark is due on the cross section composition pattern: mostly in the early section, but also in the last ones, the mass transport resistance produces strong gradients. The diffusion limits the O_2 supply to the surface, mainly because the reaction consumes it very fast. As a consequence, the O_2 in the bulk, being carried forward by convection, keeps to a non-zero value up to the end of the channel. Even if the O_2 composition was under-stoichiometry in the feed, we even recover it in the products!

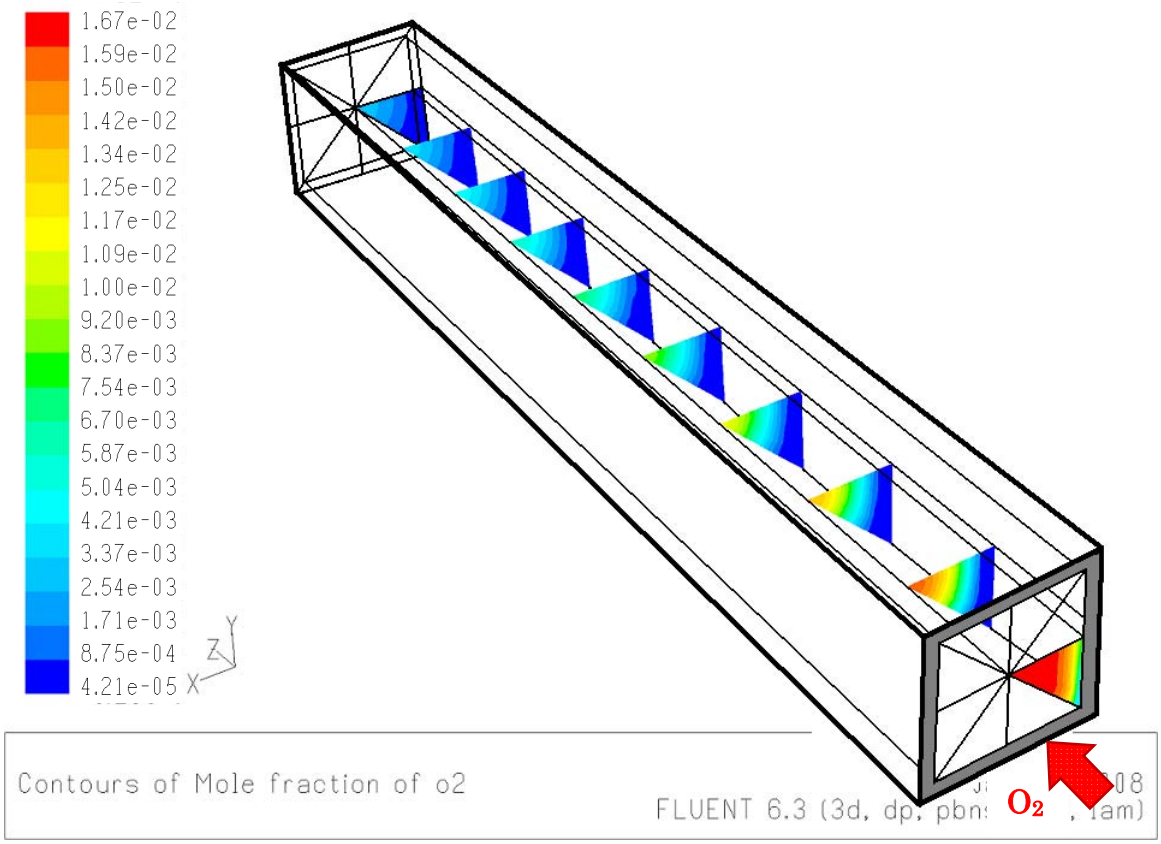

Fig 8.3-1 Contours of mole fractions of O_2 in different cross sections.

Dropping the channel scheme in the following figures, let's have a swift glance at the other species contours.

In Fig 8.3-2 we see the mole fraction of CH_4, which behaves more or less like the O_2. The main differences are at the front view, where at the surface the composition drop is much lower than for O_2, and in the rear sections, where the residual mole fraction is everywhere higher than zero, since this reactant is fed in excess, with respect to the stoichiometry. Nonetheless, also in this case we find an evident gradient inside the cross section, sign of some transport limitation.

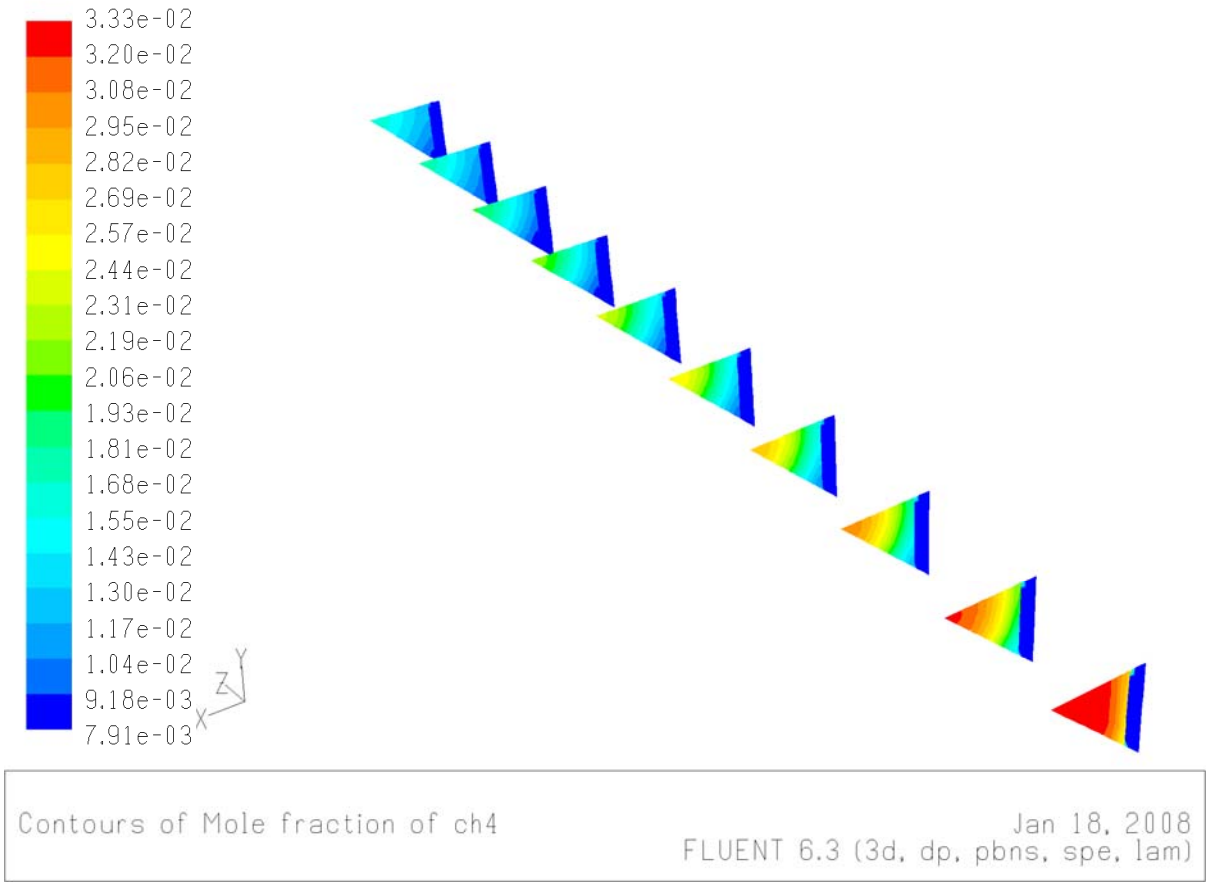

Fig 8.3-2 Contours of mole fractions of CH_4 in different cross sections.

In Fig 8.3-3, H_2O contours are reported. This product has an interesting behavior. In the front section its mole fraction is zero in the bulk and something near the surface, particularly in the proximity of the corner. In the central sections the concentration at the corner starts getting lower, which means the water becomes a reactant (see also Fig 8.3-8).

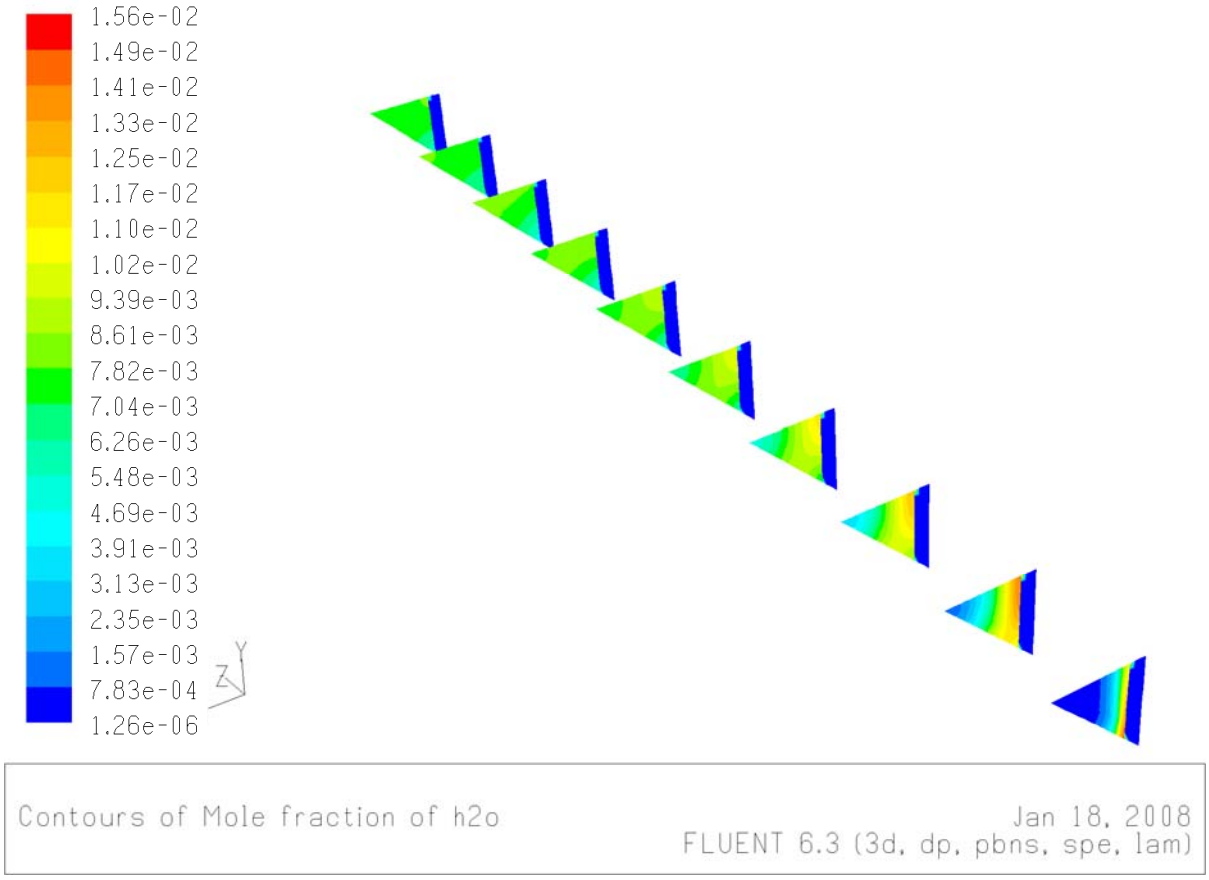

Fig 8.3-3 Contours of mole fractions of H_2O in different cross sections.

Instead, in Fig 8.3-4 you can see CO_2 contours. If the first view is qualitatively identical to water's, in the rest of the channel the profiles look different. CO_2 doesn't turn into a reactant, so the gradients are always directed from the surface to the bulk. Remarkably, unlike what happened in the 1D models, this species is being produced all along the reactor, and not only in the first few millimeters. This is s direct consequence of the O_2 behavior: as said previously, CO_2 appears to be produced only in the presence of O_2, which is now available up to the exit.

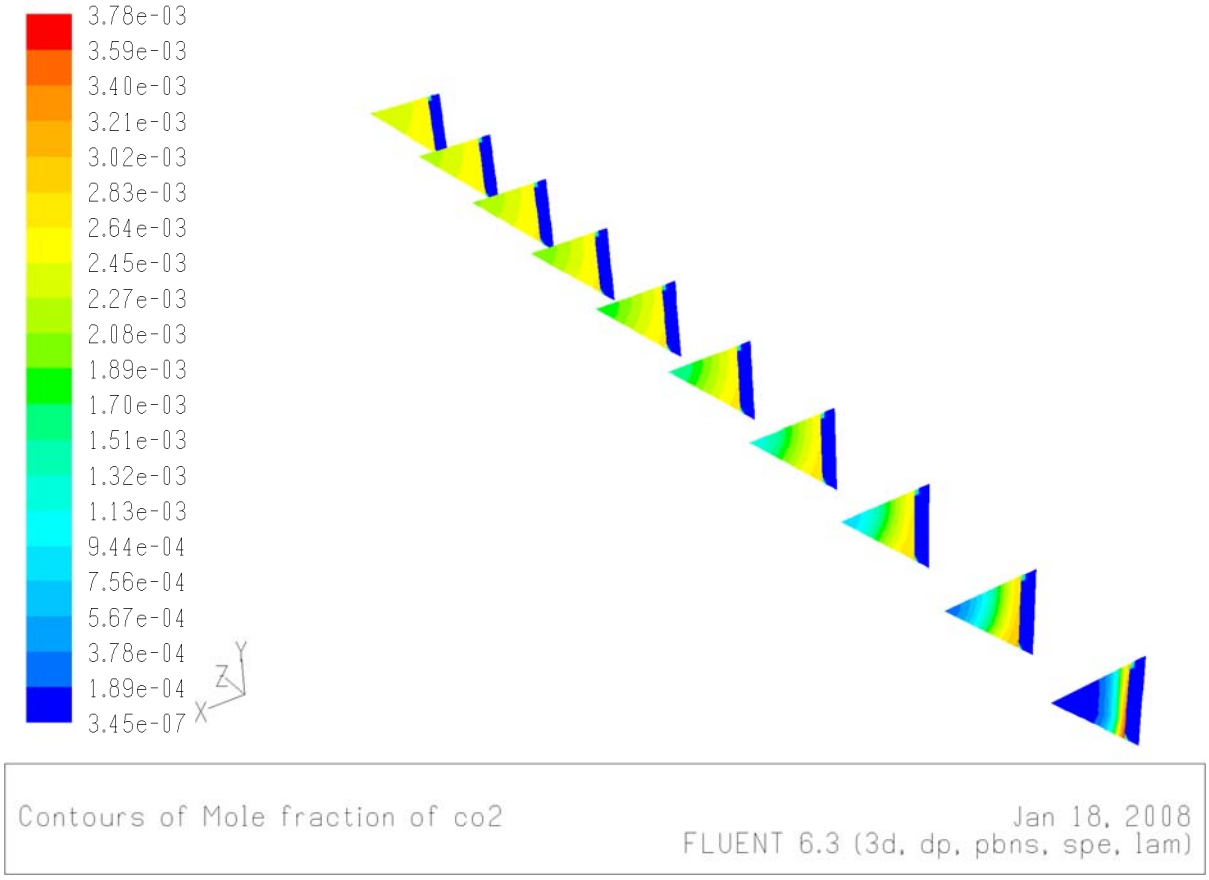

Fig 8.3-4 Contours of mole fractions of CO_2 in different cross sections.

Mole fractions of CO (Fig 8.3-5) and H_2 (Fig 8.3-6) have similar behavior. They are not present in the feed, thus their initial bulk composition is zero. Through the channel they are continuously produced at the surface and then diffuse into the bulk. The only difference is that H_2 appears only faintly at the entrance, and is produced mainly downstream only afterward.

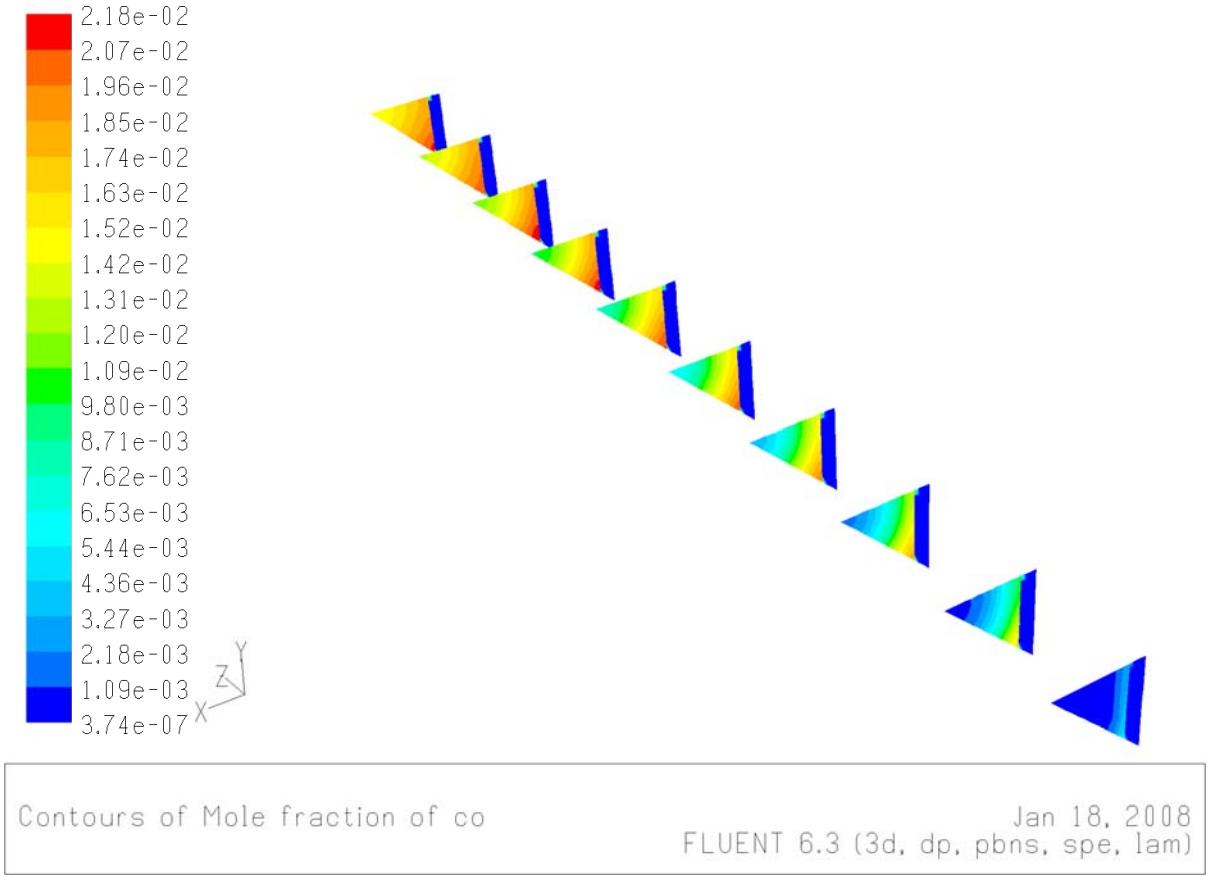

Fig 8.3-5 Contours of mole fractions of CO in different cross sections.

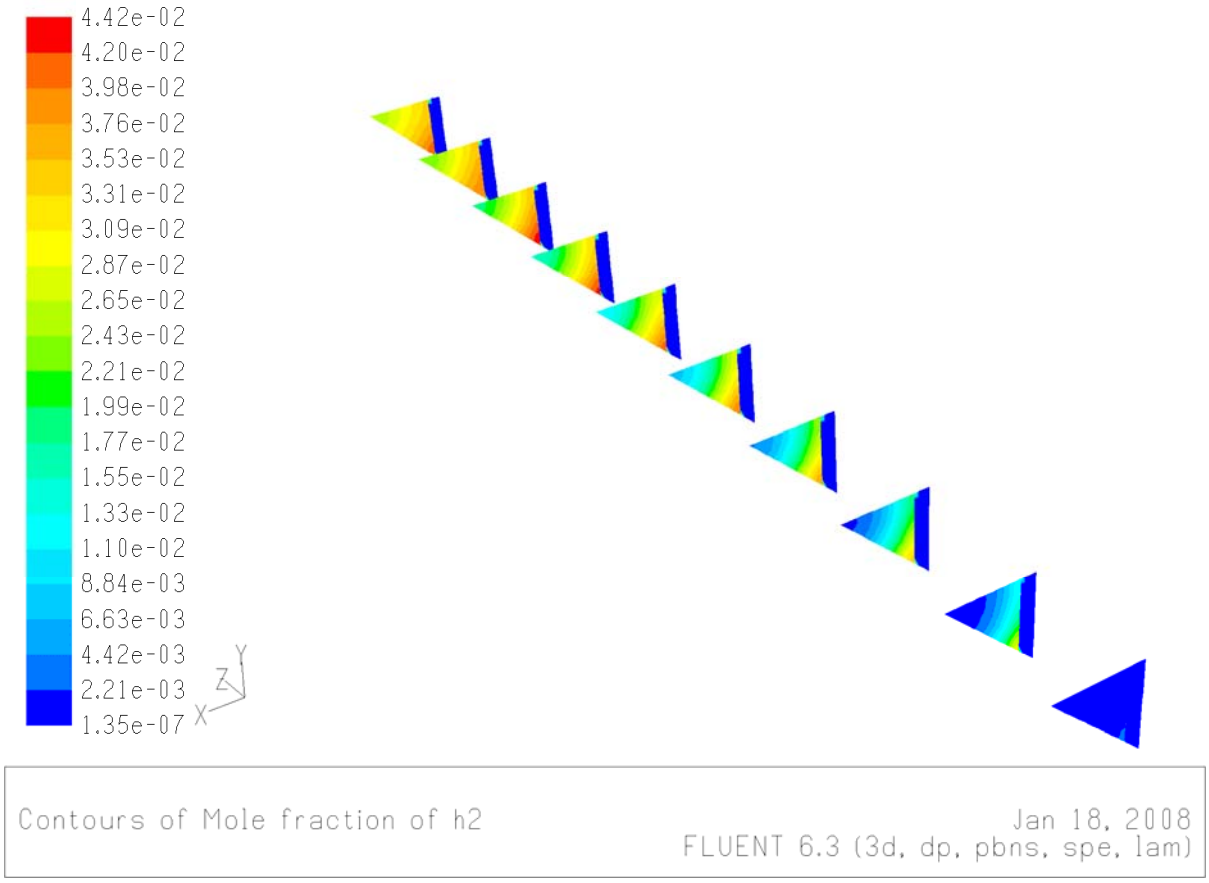

Fig 8.3-6 Contours of mole fractions of H_2 in different cross sections.

Recollecting the thermal behavior of this reacting system, in which the total oxidation is exothermic and the reforming endothermic, a look at the temperature pattern inside the reactor might turn out interesting (Fig 8.3-7). At the entrance the gas is cold, but the solid is already 100°C hotter than the feed. This happens because the conduction through the solid allows some heat moving towards the front section. Clearly the heat of reaction develops at the surface, where at the beginning the exothermic reactions predominate. From what we saw up to now, we expect the surface temperature to decrease in the second half of the reactor. Surprisingly, it does not, nor does the gas temperature! This model doesn't predict a different physical situation, just another species distribution, which has repercussions on the reaction mechanism, whose heat of reaction is generated in a different way. In particular, the presence of a maximum in the solid and then in the gas temperature was due to a switch from the exothermic reactions to those endothermic. The 3D model tells us that the contribution of the oxidation reactions continue till the end, balancing the heat absorbed by the endothermic reforming and ecxeeding it, with a resulting positive heat production all through the channel.

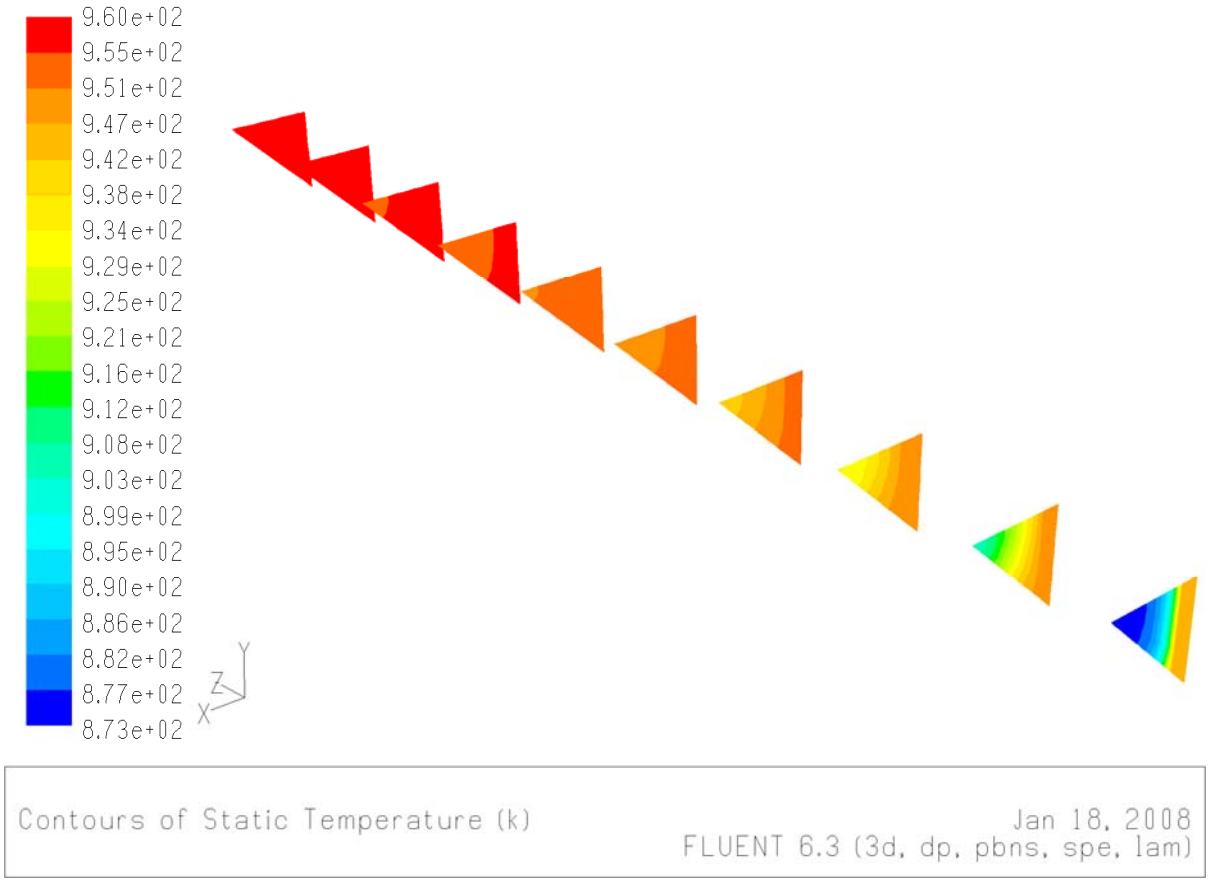

Fig 8.3-7 Contours of temperature in different cross sections.

Although the contour representation is very helpful for a qualitative understanding of the phenomena occurring in the whole channel, a plot of some mean quantities may give more quantitative information. The bulk mole fractions are obtained by a mass-averaged mean of the mass fractions in the cross section (Eq. 8.3-1), then turned into a molar basis.

$$\bar{Y}_i^{bulk} = \frac{\sum_{j=1}^{cells} Y_{i,j}\,\rho_j \left|\vec{v}_j \cdot \vec{A}_j\right|}{\sum_{j=1}^{cells} \rho_j \left|\vec{v}_j \cdot \vec{A}_j\right|} \qquad 8.3\text{-}1$$

Since the mesh is uniform on the internal wall, the BL composition at each z position is a mean of the mole fraction of a species in a line at x=0 (adjacent to the solid surface, as shown in Fig 8.3-8).

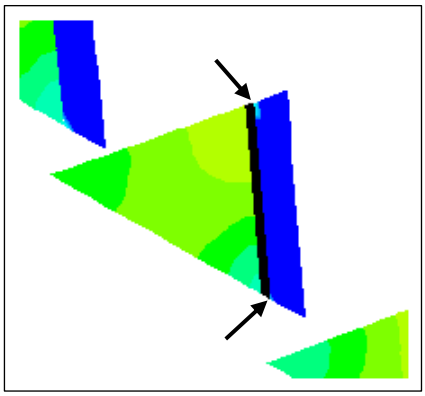

Fig 8.3-8 Line where the BL mean composition is calculated (pointed out by the two arrows). This particular is extracted from the H_2O contours.

In particular, in Fig 8.3-9 both bulk and BL compositions are presented, compared to the corresponding species profiles produced by the Nu-Sh-Cond model. Astonishingly, the species profiles are very different in the two models! For the bulk composition, CH_4 is quite the same, while we find a lot more O_2 left; we have more partial oxidation species (CO and H_2) and less oxidation ones (CO_2 and H_2O). For the BL composition, the O_2 profiles are coincident, while there is less CH_4; about the products, the trend is the same as for the bulk.

Clearly, what we find in the bulk results from what happened on the surface and also depends on the transport phenomena. Here we assume the kinetics matters are the same for both models, since I implemented the same surface kinetic mechanism and gave the same surface catalytic area. It's all but easy to give an interpretation to this behavior. Some help might come from the analysis of the apparent rate of productions of the species, e.g. the reactivity ratios.

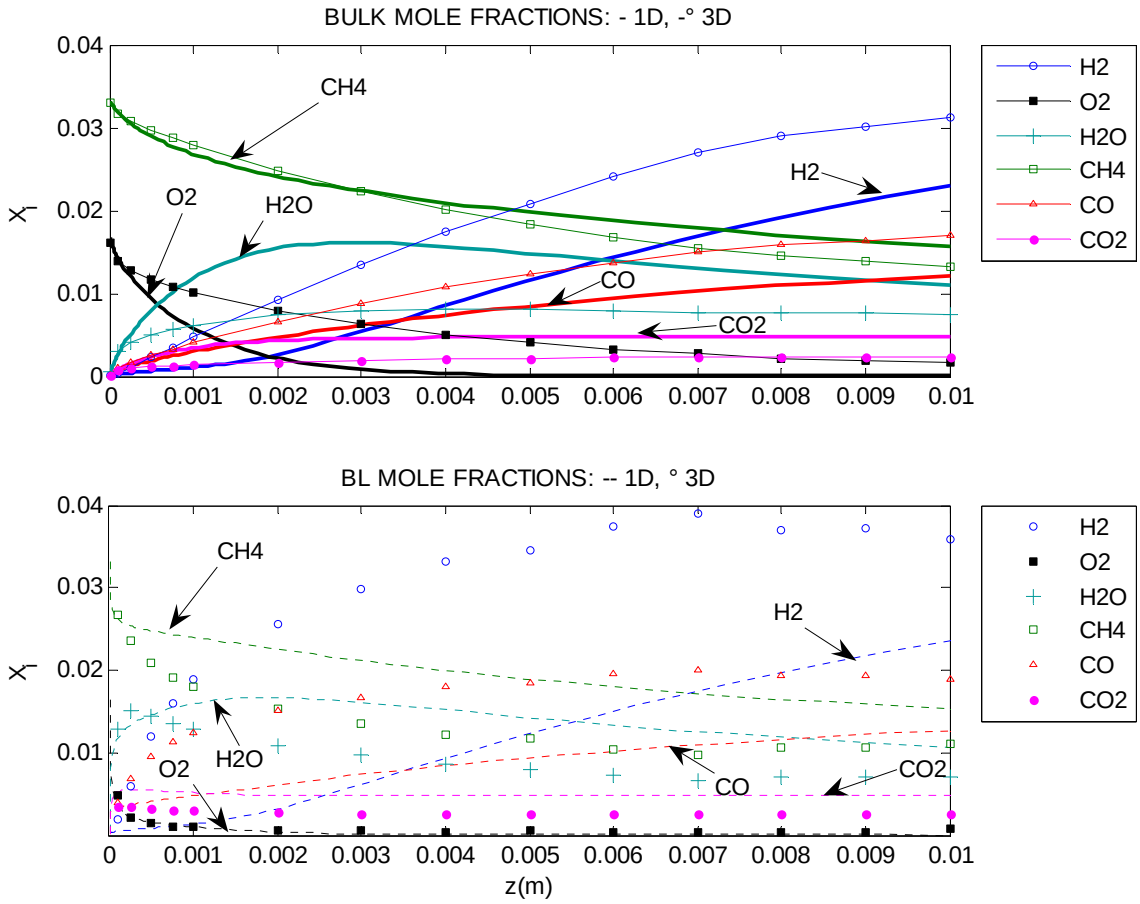

Fig 8.3-9 Comparison among CFD calculations and the Nu-Sh-Cond model.

In Fig 8.3-10 the stoichiometric coefficients calculated from the CFD are shown, together with those coming from the Nu-Sh-Cond model (already in Fig 5.8-4, but reported here in the small figure). The main difference between the two figures is that in the small one the kinetics keeps constant for at least 1 mm, and then moves towards another stoichiometry, reaching it after about 6 mm from the entrance; in the big one the kinetics is changing fast already from the entrance, and keeps moving up to 6-7 mm, where it stays almost constant (data are quite scattered at the end, because the chosen resolution is low). Getting to the details of every species, we notice that H_2 goes quite safely from 0 to 2, as before; CO from 0.5 to almost 1, not very different; CO_2 from 0.5 to somewhat above zero: the bit that lacks in the CO we find in the CO_2, which keeps above zero, differently from before; H_2O starts in both at about +2, but in the CFD it reaches a value only little below zero: it becomes a reactant, but the reforming is not occurring with great strength; as a consequence, O_2, which also here starts at about –1.5, exits the channel with a stoichiometric coefficient of –0.5: as suspected looking the temperature contours, O_2 is reacting with energy everywhere.

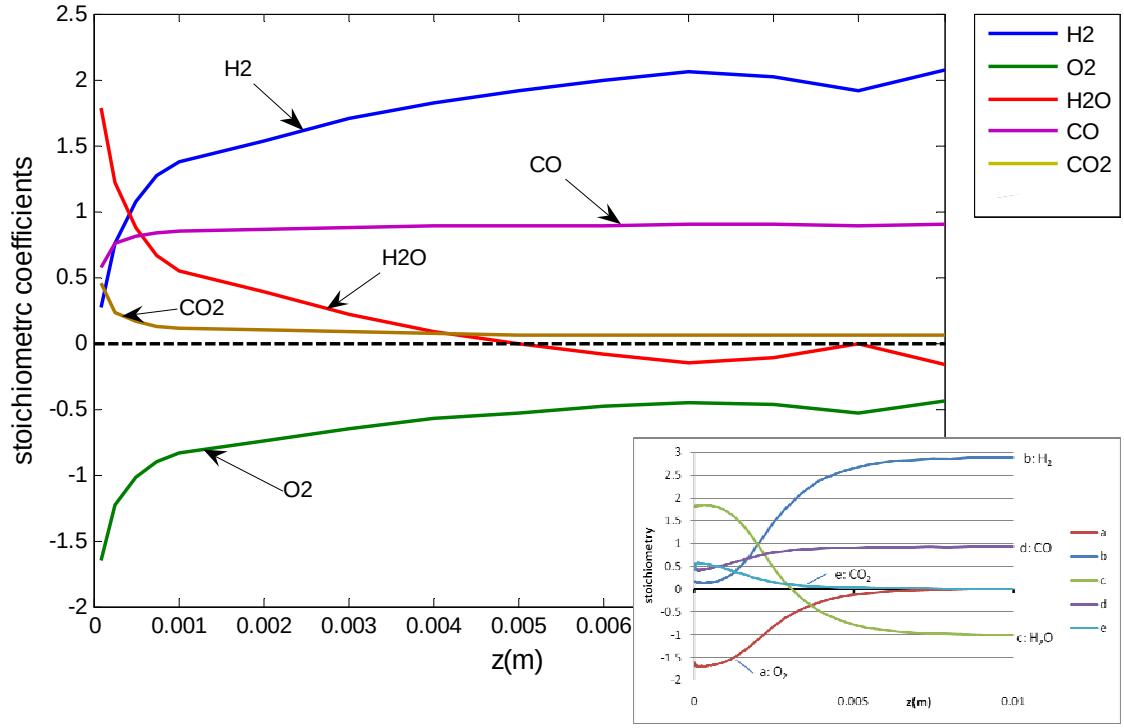

Fig 8.3-10 Comparison among stoichiometric coefficients from the CFD and from the Nu-Sh-Cond model (in the small figure).

Initial slopes of the species are the same, which confirms the kinetics is the same, as well. The fact that in the 1D model the stoichiometry keeps on the oxidation kinetics longer than in the CFD model explains why in the latter the CO_2 is lower and the O_2 is higher, even though their stoichiometric coefficients are non-zero all along the reactor.

The distribution of species in the channel is related also on the transport phenomena, and taking a look at them we might find an explanation on the differences between the two models.

8.4 Mass transfer coefficients

Mean Sh numbers in FLUENT were calculated according to the definition given in Chapter 3:

$$\overline{\mathrm{Sh}} = \frac{-\left(\frac{dY}{d(r/d)}\right)_S}{Y_b - Y_s} \qquad 3.4\text{-}3$$

where the derivative was calculated in the first cell beside the wall, and the characteristic length of the system, d, is the side of the square section, which also corresponds to the hydraulic diameter of the channel.

In Fig 8.4-1 the literature correlation [36] adopted for the Nu-Sh-Cond model is compared to those deduced from FLUENT for each species. In the proximity of the

entrance we deduce from the CFD a higher Sh than from the literature correlation. Afterwards, the calculated Sh numbers become lower than the S&L correlation prediction. Also, Sh depends on the species, being higher for H_2 and lower for CO_2. H_2O curve is not shown, because for it both the numerator and the denumerator become negative at some point, leading to an indefinite mean Sh.

In comparison with the correlation derived for heat transfer with constant heat flux at the wall, which corresponds to a first order kinetics, the mass transfer coefficients in presence of fast reactions are higher (see the beginning of the channel), while where the kinetics slows down they become lower (second part of the reactor). The direct consequence is that the kinetics is as fast as in the 1D model, at the beginning, but it lasts shorter, and then slows down. Looking again at the stoichiometric coefficients (Fig 8.3-10), we note that the TO in the 1D model continue up to 3 mm before the O_2 stoichiometric coefficient reaches –1, consuming a lot of O_2 and producing CO_2 and H_2O, while here that happens after half mm (that also explains why in the CFD we find less TO species). As a consequence, there is more O_2 left in the gas phase that slowly diffuses towards the surface. Note that without transport resistance, e.g. in the PFR, the O_2 disappears after 0.5 mm; with the literature Sh, the O_2 consumes after about 4 mm; with the real fluidynamics, it's still present at the exit, and the corresponding TO zone covers the entire channel.

There is a strong dependence of the mass transfer coefficients on the kinetics, because it determines the mass flux of each species at the wall, which in general is different from unity and also is different from one species to another, and that's why Sh is not unique for all the species: because their production/consumption rates at the wall are different.

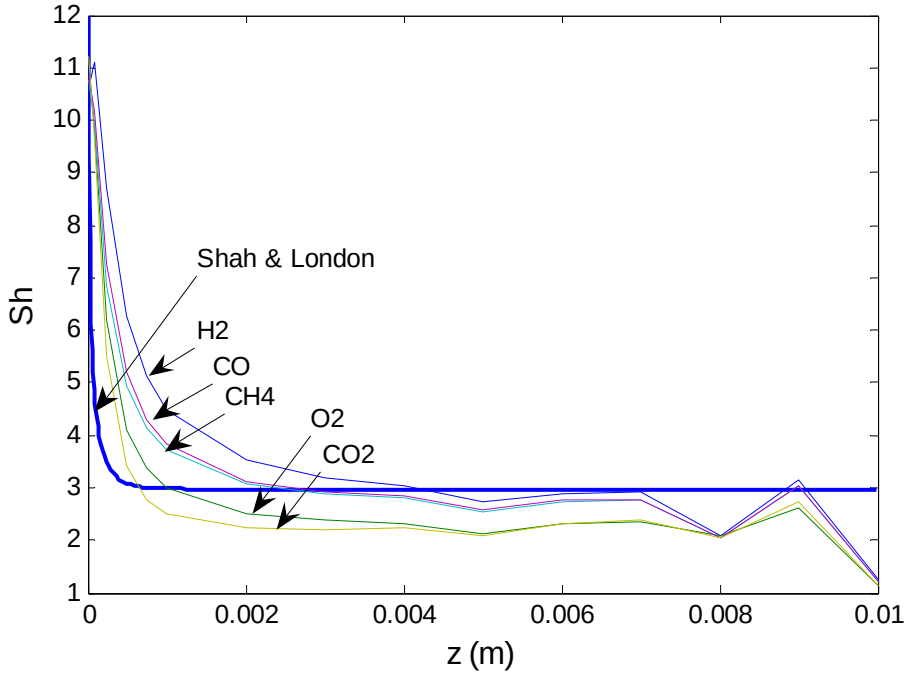

Fig 8.4-1 Sherwood number from Shah&London correlations and from FLUENT calculations.

Most probably, if we put these Sh numbers inside the Nu-Sh-Cond model, it would gain results similar to the FLUENT's. Besides, this might constitute a validation of the Nu-Sh-Cond model, being not available a data set comparable with that of the foam monolith. I'll put off this test for a future investigation.

8.5 Conclusions

The CFD modeling of the square channel turned out to be not a useless repetition of the conclusions from the 1D models, but, on the contrary, led to original observations.

For the first time we can have a deep look inside the channel: we acknowledge that the reaction starts at the corner, where the residence time is higher. In general, the composition close to the surface is different from that in the bulk. The variation of composition is continuous through the cross section, thus the whole 3D representation is clearly very important when homogeneous reactions occur.

Surprisingly, composition and temperature profiles are quite different from those of the Nu-Sh-Cond model. The physics of the process has not changed, but a different species distribution in the channel makes the oxidation reactions prevail all along the reactor. The O_2 in the outlet has a pretty high value, in comparison with equilibrium, and both temperature profiles keep increasing up to the end.

The stoichiometry is rather different, as well. It changes rapidly already at the beginning, causing a lower O_2 consumption. As a matter of facts, even though the CH_4 conversion at the outlet is the same, we find more partial oxidation species and less total oxidation ones.

The calculation of the mass transport coefficients from the real profiles showed that Sh is very dependent on the kinetics, and in particular there is a different Sh number for each species, since the production rate is different for every species and for each axial position. This conclusion is consistent with the results found in Chapter 3. This is also the most evident cause for the discrepancies of the results, from the 1D to the 3D model.

Chapter 9

General conclusions

This thesis is aimed to show the importance of coupling a detailed surface kinetics and a proper description of the transport phenomena. Several reactor models implementing a detailed surface mechanism were presented. The common practice is to implement directly the kinetics into the model, which might be a time-consuming process when the model applies to a different reacting system. Although the kinetics adopted all over this work is the same, the POM on Rh catalyst, the models virtually apply to any other reacting system, with minor adjustments. This is feasible just owing to a kinetics interpreter, linkable with the main program. For this purpose, Cantera was chosen: its routines can be called by the main programming languages and, not less important, it's been validating by several users.

Before starting with the analysis of the 1D models, time is suitable for some considerations about the traditional approach to the transport limited processes. Using CFD, it was shown that the Chilton–Colburn analogy can be seriously misleading where locally fast heterogeneous kinetics occurs. In general, in the entry region the Sherwood number calculated with the CFD is higher than that coming from the correlations obtained for the heat transfer problems. The asymptotic values, far from the entry region influence, are often coincident, but for kinetics higher than first order, also the asymptotic values mismatch. Sherwood correlations should be formulated as a function of the reaction order, since it modifies the concentration gradients on the surface, and thus also the effectiveness of the transport phenomena.

The mathematical formalization of the 1D models was presented separately from the results, to make the comparison among the different physical hypotheses easier. Complexity of the models increases, together with that of the solution techniques. As will be clear analyzing the results, it is never useless to solve a simpler model, consciously of its limitations, because it is much faster and it might provide already a good source of information. Besides, from the comparison with a more complex one the effects of the physical feature added might result clearer. The process of solving more and more complex models is the safer way towards most complicated ones: it guides in the right choices and it represents a sort of validation of the results.

The first case study is the application to a honeycomb monolith with square section channels, for which experimental data are available from the KTH-Royal Institute of Technology, Stockholm (SE). A preliminary analysis of the thermodynamic equilibrium is useful because it needn't any hypothesis over the kinetics: from the comparison, it results that only at the highest temperature the experimental conversion is getting close to it, without reaching it for the given contact time. The most idealized 1D reactor model, the PFR, predicts correctly the light off temperature of the catalyst, but over-estimates the conversion. The stoichiometry calculated on the species profiles, free from the interference of the transport phenomena, gives more insight in the chemistry adopted. It shows two different zones of the reactor: in the first part, where the oxygen is still present, the total oxidation kinetics prevails; farther on, the reforming reaction predominates. These clear conclusions must be read

carefully, because not all the physical phenomena are included in the model: more sophisticated models will show that there is an overlapping of the two chemical regimes, and that the real temperature profiles inside the reactor are very different from that obtained using this rough model.

Adding the heat transport coefficient and solid conductivity a considerable improvement on the temperature description is achieved. The conversion increases with the inlet temperature with the same scheme as in the experimental data, while this didn't happen in the PFR. Yet, this model lacks in the description of the mass transport coefficients, and this reflects in the results, because the light off temperature is too low: the reaction happens too soon as the reactants enter the channel and the great deal of heat produced is conducted by the solid towards the entrance, allowing the system reacting at temperatures lower than in the real world. Also here, a critical analysis of the results is necessary, not to produce false conclusions about the kinetics, for example.

The model complete with mass transfer coefficients is very tricky to solve, because of the presence of both algebraic and differential equations. The technique adopted is to turn the steady-state balances into transient, adding the accumulation term, and thus transforming all the equations in differential. The solution is still slow to achieve, but extremely stable to perturbations. The results show good agreement for both the light off temperature and the conversion, proving as the closest model to describe the experimental data, so far. There is a substantial difference between this lumped model and the PFR, visible through the apparent stoichiometry: basically, in the lumped model species appears to react more slowly, because there is an important resistance to the diffusion towards the surface that the simplest model didn't account for. The transfer phenomena strongly affect the conversion, particularly in the first part of the reactor, where the kinetics is really fast. In the second part the composition slowly approaches equilibrium: therefore, whatever reactor model with the right kinetics would lead to a conversion close to the experimental. The availability of only the exit composition is a serious limitation in the models validation. The following example, though, will help enforcing the statement about the importance of the inclusion of transport phenomena, allowing a much detailed validation of the calculated profiles.

The second case study is the modeling of spatially resolved measurements of temperature and concentration obtained in a foam monolith, carried out at the University of Minnesota, Minneapolis (USA). We critically analyzed the chemistry and transport limitations adopting two models, both sharing a detailed surface chemistry but differing by the account of gas-surface transport processes.

The simulation neglecting transport limitations correctly predicts the outlet concentrations, apparently because of the approach to equilibrium, but large disagreement are observed along the catalyst, particularly in the initial region. That proved the existence of regions where strong diffusive limitations prevail. We developed a pseudo-1D model, which differentiates the species and temperature in the bulk of the gas and at the surface and describe heat (including radiation) and mass transport through correlations with ad hoc parameters based on dedicate experiments.

With this model we correctly predicted the profiles along the reactor, for all species. Some deviations for CO_2 appear to be due to lacks in the chemistry. The solid temperature is well reproduced, as well, while the gas temperature is somewhere

higher than the experimental, possibly due to an overestimated heat transport coefficient. An analysis of the transport limitations has shown that the O_2 and H_2O display large concentration gradients between gas and surface because of their involvement in the total oxidation which is a very fast reaction. The analysis has thus shown that production and consumption rates at the catalytic surface are frequently high enough to enter a diffusive regime. Accordingly, we highlight the need to accompany the implementation of detailed surface chemistry with some account for the transport processes, both of mass and heat. Where the CFD applies, and this was not the case of the foam monolith, it surely is the most refined model we could choose. For this reason, we conclude the work going back to the square channel geometry, to find confirmations of the foundamental statements exposed in the previous part.

Before dealing with the CFD, a deeper understanding of the real reactor thermal behavior is necessary, because the use of the right temperature profile inside the reactor, and mostly on the surface, is crucial for the chemistry. The only two thermal hypotheses that allow one single channel representing the whole monolith are the isothermal and the adiabatic. In the reality, the channel will match none of the two, finding more likely in the middle, but we try to understand which one closer approximates the real conditions. The more intuitive adiabatic assumption crashes into some experimental evidence of the total oxidation, where there is no rise in the temperature from the inlet TC to the outlet TC. A first check was made on the fluidynamic of the quartz tube, right in front of the monolith: the velocity profile results flat, so all the channels have the same inlet flow rate. The more convincing proof in favor of the adiabaticity is the analysis of the direction of the heat fluxes when the heat source is located on the surface: the heat goes preferably inward the channel, in the bulk of the gas, instead than outward, passing through the channel. Therefore, the adiabatic hypothesis is retained, and the contrasting experimental evidence is explained by an incorrect measurement of the TCin, due to the hitting of radiation coming from the front face of the monolith.

The CFD model brought interesting results, also in comparison with the complete lumped model. It confirms the intuitions about the internal species distribution: the variation of a species is continuous from the bulk to the surface, with particular high gradients at the corners, where the reaction is faster due to lower gas velocity and higher temperature. The mean composition profiles are very different from those of the Nu-Sh-Cond model, and this reflects in a different temperature profile: now the temperatures keep increasing all along the reactor, meaning that the oxidation reaction is distributed through the entire channel, instead of limited in the first part. The stoichiometry is different as well: if at the beginning they coincide, then the CFD changes rapidly to a mixed TO-PO kinetics. Total oxidation, which is as fast as before at the entrance, then slows down. We look with suspicion at the transport phenomena, since the kinetics and the active surface area of the catalyst are the same as in the 1D model. Indeed, the Sh numbers calculated with FLUENT, if compared with the literature correlation used for the 1D model, are higher at the entrance, but then decrease and become lower. In particular, they're different for each species because they react with different reaction orders; that confirms that the Sh is also a function of the reaction order. As a result, the oxygen available at the surface is lower and lower, and that's why we find so much of it along the reactor, and why the TO zone is long not 0.5 mm like in the PFR, nor 4 mm like in the Nu-Sh-Cond, but even the entire

reactor! A direct consequence of this on the species distribution is that we find more partial oxidation species and less total oxidation ones.

At this time, it should be clear enough that the pure chemical description of a reactor is not sufficient. Using a unique mechanism, we saw how the predicted internal profiles vary adopting different reactor models. In particular, sometimes the reaction mechanism might be of secondary importance, in comparison with the description of the transport phenomena, when the process is highly transport limited (as for O_2). Yet, some other species, like CH_4, requires a good description of the chemistry, as well, because its composition is less transport limited, and an influence of the kinetics on the conversion is guaranteed. The importance of specific mass transport coefficients is been clear in the last few years, since dedicated experiments have been carried out, to replace the correlations coming from the heat transport theory. Although, it would be important to account also for the reactivity of the actual system involved in the experiment, to properly adapt correlations, usually realized with CO. As a matter of fact, the difference of a species composition between the surface and the bulk depends both on its diffusivity and on its production rate. The fluidynamic approach is higher precision, and, where applicable, highly recommended.

Appendix A – Mechanisms

A. 1. CHEMKIN format Deutschmann – Pt mechanism

```
!------------------------------------------------------------------------!
!************************************************************************
!****                                                                   *
!****     C2H6 PARTIAL OXIDATION SURFACE MECHANISM  ON PT               *
!****                                                                   *
!****     Version       March 2000                                      *
!****                                                                   *
!****     D. Zerkle, Los Alamos National Laboratory, USA                *
!****     O. Deutschmann, M. Wolf, Heidelberg University, Germany       *
!****                                                                   *
!****     Ref.: D.K. Zerkle, M.D. Allendorf, M. Wolf, O. Deutschmann.   *
!****           Understanding Homogeneous and Heterogeneous             *
!****           Contributions to the Platinum-Catalyzed Partial         *
!****           Oxidation of Ethane in a Short Contact Time Reactor.    *
!****           J. Catal. 196(2000) 18-39.                              *
!****                                                                   *
!****                                                                   *
!****     Kinetic data:                                                 *
!****      k = A * T**b * exp (-Ea/RT)         A          b       Ea    *
!****                                       (cm,mol,s)    -      J/mol  *
!****                                                                   *
!****                                                                   *
!****     (SURFACE CHEMKIN format)                                      *
!****                                                                   *
!************************************************************************
SITE/PT_SURFACE/    SDEN/2.72E-9/
   PT(S) C2H6(S)/2/ C2H4(S) C2H2(S) H(S) O(S) CH3(S)
   OH(S) H2O(S) C(S) CHCH2(S) CHCH3(S) CO2(S) CO(S) CH2CH3(S)
   CCH3(S) CCH2(S) CCH(S) CH2(S)s CH(S)
END
THERMO ALL
  300.0   1000.0   3000.0
PT(S)                  PT  1               S    300.0    3000.0  1000.0       1
 0.00000000E+00 0.00000000E+00 0.00000000E+00 0.00000000E+00 0.00000000E+00    2
 0.00000000E+00 0.00000000E+00 0.00000000E+00 0.00000000E+00 0.00000000E+00    3
 0.00000000E+00 0.00000000E+00 0.00000000E+00 0.00000000E+00                   4
! Dummy thermo data (EM):
C2H6(S)               0C   2H   6PT  2     I    300.00   3000.00 1000.00      1
 0.30016165E+01 0.54084505E-02-0.40538058E-06-0.53422466E-09 0.11451887E-12    2
-0.32752722E+04-0.10965984E+02 0.12919217E+01 0.72675603E-02 0.98179476E-06    3
```

```
-0.20471294E-08 0.90832717E-13-0.25745610E+04-0.11983037E+01                   4
C2H4(S)               0C   2H   4PT  1     I    300.00   3000.00 1000.00      1
 0.30016165E+01 0.54084505E-02-0.40538058E-06-0.53422466E-09 0.11451887E-12    2
-0.32752722E+04-0.10965984E+02 0.12919217E+01 0.72675603E-02 0.98179476E-06    3
-0.20471294E-08 0.90832717E-13-0.25745610E+04-0.11983037E+01                   4
C2H2(S)               0C   2H   2PT  1     I    300.00   3000.00 1000.00      1
 0.30016165E+01 0.54084505E-02-0.40538058E-06-0.53422466E-09 0.11451887E-12    2
-0.32752722E+04-0.10965984E+02 0.12919217E+01 0.72675603E-02 0.98179476E-06    3
-0.20471294E-08 0.90832717E-13-0.25745610E+04-0.11983037E+01                   4
CHCH2(S)              0C   2H   3PT  1     I    300.00   3000.00 1000.00      1
 0.30016165E+01 0.54084505E-02-0.40538058E-06-0.53422466E-09 0.11451887E-12    2
-0.32752722E+04-0.10965984E+02 0.12919217E+01 0.72675603E-02 0.98179476E-06    3
-0.20471294E-08 0.90832717E-13-0.25745610E+04-0.11983037E+01                   4
CHCH3(S)              0C   2H   4PT  1     I    300.00   3000.00 1000.00      1
 0.30016165E+01 0.54084505E-02-0.40538058E-06-0.53422466E-09 0.11451887E-12    2
-0.32752722E+04-0.10965984E+02 0.12919217E+01 0.72675603E-02 0.98179476E-06    3
-0.20471294E-08 0.90832717E-13-0.25745610E+04-0.11983037E+01                   4
CH2CH3(S)             0C   2H   5PT  1     I    300.00   3000.00 1000.00      1
 0.30016165E+01 0.54084505E-02-0.40538058E-06-0.53422466E-09 0.11451887E-12    2
-0.32752722E+04-0.10965984E+02 0.12919217E+01 0.72675603E-02 0.98179476E-06    3
-0.20471294E-08 0.90832717E-13-0.25745610E+04-0.11983037E+01                   4
CCH3(S)               0C   2H   3PT  1     I    300.00   3000.00 1000.00      1
 0.30016165E+01 0.54084505E-02-0.40538058E-06-0.53422466E-09 0.11451887E-12    2
-0.32752722E+04-0.10965984E+02 0.12919217E+01 0.72675603E-02 0.98179476E-06    3
-0.20471294E-08 0.90832717E-13-0.25745610E+04-0.11983037E+01                   4
CCH2(S)               0C   2H   2PT  1     I    300.00   3000.00 1000.00      1
 0.30016165E+01 0.54084505E-02-0.40538058E-06-0.53422466E-09 0.11451887E-12    2
-0.32752722E+04-0.10965984E+02 0.12919217E+01 0.72675603E-02 0.98179476E-06    3
-0.20471294E-08 0.90832717E-13-0.25745610E+04-0.11983037E+01                   4
CCH(S)                0C   2H   1PT  1     I    300.00   3000.00 1000.00      1
 0.30016165E+01 0.54084505E-02-0.40538058E-06-0.53422466E-09 0.11451887E-12    2
-0.32752722E+04-0.10965984E+02 0.12919217E+01 0.72675603E-02 0.98179476E-06    3
-0.20471294E-08 0.90832717E-13-0.25745610E+04-0.11983037E+01                   4
! end EM dummy data
H(S)              92491H   1PT  1          I    300.00   3000.00 1000.00      1
 0.10696996E+01 0.15432230E-02-0.15500922E-06-0.16573165E-09 0.38359347E-13    2
-0.50546128E+04-0.71555238E+01-0.13029877E+01 0.54173199E-02 0.31277972E-06    3
-0.32328533E-08 0.11362820E-11-0.42277075E+04 0.58743238E+01                   4
O(S)              92491O   1PT  1          I    300.00   3000.00 1000.00      1
 0.19454180E+01 0.91761647E-03-0.11226719E-06-0.99099624E-10 0.24307699E-13    2
-0.14005187E+05-0.11531663E+02-0.94986904E+00 0.74042305E-02-0.10451424E-05    3
-0.61120420E-08 0.33787992E-11-0.13209912E+05 0.36137905E+01                   4
CH3(S)                0C   1H   3PT  1     I    300.00   3000.00 1000.00      1
 0.30016165E+01 0.54084505E-02-0.40538058E-06-0.53422466E-09 0.11451887E-12    2
-0.32752722E+04-0.10965984E+02 0.12919217E+01 0.72675603E-02 0.98179476E-06    3
-0.20471294E-08 0.90832717E-13-0.25745610E+04-0.11983037E+01                   4
CH2(S)s               0C   1H   2PT  1     I    300.00   3000.00 1000.00      1
```

```
 0.74076122E+00 0.48032533E-02-0.32825633E-06-0.47779786E-09 0.10073452E-12    2
 0.10443752E+05 0.40842086E+00-0.14876404E+00 0.51396289E-02 0.11211075E-05    3
-0.82755452E-09-0.44572345E-12 0.10878700E+05 0.57451882E+01                   4
OH(S)              92491O   1H   1PT  1     I    300.00   3000.00 1000.00      1
 0.18249973E+01 0.32501565E-02-0.31197541E-06-0.34603206E-09 0.79171472E-13    2
-0.26685492E+05-0.12280891E+02-0.20340881E+01 0.93662683E-02 0.66275214E-06    3
-0.52074887E-08 0.17088735E-11-0.25319949E+05 0.89863186E+01                   4
H2O(S)             92491O   1H   2PT  1     I    300.00   3000.00 1000.00      1
 0.25803051E+01 0.49570827E-02-0.46894056E-06-0.52633137E-09 0.11998322E-12    2
-0.38302234E+05-0.17406322E+02-0.27651553E+01 0.13315115E-01 0.10127695E-05    3
-0.71820083E-08 0.22813776E-11-0.36398055E+05 0.12098145E+02                   4
C(S)                   0C   1PT  1          I    300.00   3000.00 1000.00      1
 0.15792824E+01 0.36528701E-03-0.50657672E-07-0.34884855E-10 0.88089699E-14    2
 0.99535752E+04-0.30240495E+01 0.58924019E+00 0.25012842E-02-0.34229498E-06    3
-0.18994346E-08 0.10190406E-11 0.10236923E+05 0.21937017E+01                   4
CO2(S)            081292C   1O   2PT  1     I   300.00   3000.00  1000.00      1
 0.46900000E+00 0.62660000E-02 0.00000000E-00 0.00000000E-00 0.00000000E-00    2
-0.50458700E+05-0.45550000E+01 0.46900000E+00 0.62662000E-02 0.00000000E-00    3
 0.00000000E-00 0.00000000E-00-0.50458700E+05-0.45550000E+01                   4
CO(S)                  0C   1O   1PT  1     I    300.00   3000.00 1000.00      1
 0.47083778E+01 0.96037297E-03-0.11805279E-06-0.76883826E-10 0.18232000E-13    2
-0.32311723E+05-0.16719593E+02 0.48907466E+01 0.68134235E-04 0.19768814E-06    3
 0.12388669E-08-0.90339249E-12-0.32297836E+05-0.17453161E+02                   4
CH(S)                  0C   1H   1PT  1     I    300.00   3000.00 1000.00      1
-0.48242472E-02 0.30446239E-02-0.16066099E-06-0.29041700E-09 0.57999924E-13    2
 0.22595219E+05 0.56677818E+01 0.84157485E+00 0.13095380E-02 0.28464575E-06    3
 0.63862904E-09-0.42766658E-12 0.22332801E+05 0.11452305E+01                   4
END
!
!!*****************************************************************************!
!!*********         C2H6/O2 Surface Reaction on Pt                    **********!
!!*****************************************************************************!
REACTION  MWOFF JOULES/MOLE
!
C2H6 + 2PT(S)        => C2H6(S)                0.015      0.0       0.0
   STICK
C2H4 + PT(S)         => C2H4(S)                0.015      0.0       0.0
   STICK
C2H2 + PT(S)         => C2H2(S)                0.05       0.0       0.0
   STICK
H2 + 2PT(S)          => 2H(S)                  0.046      0.0       0.0
   STICK
   FORD/PT(S) 1.0/
O2 + 2PT(S)          => 2O(S)                  21.0      -1.0       0.0
   STICK
! O2 + 2PT(S) => 2O(S)                      1.80E+21   -0.5   0.0
!   DUPLICATE
```

```
! O2 + 2PT(S) => 2O(S)                          0.023    0.00       0.00
!   DUPLICATE         STICK
CH4 + 2PT(S)         => CH3(S) + H(S)           9.E-4      0.0      72000.0
   STICK
CH4 + O(S) + PT(S)   => CH3(S) + OH(S)          1.84E+7   0.7      42000.0
   COV/O(S) 0.0 0.0 8000./                     !1.36E-10 1/s
CH4 + OH(S) + PT(S)  => CH3(S) + H2O(S)         1.0        0.0      10000.0
   STICK
CH4 + C(S)           => CHCH3(S)                7.E-9      0.0      23000.0
   STICK
   COV/C(S) 0.0 0.0 4750./
H2O + PT(S)          => H2O(S)                  0.75       0.0       0.0
   STICK
CO2 + PT(S)          => CO2(S)                  0.005      0.0       0.0
   STICK
CO + PT(S)           => CO(S)                   0.84       0.0       0.0
   STICK
C2H5 + PT(S)         => CH2CH3(S)               1.0        0.0       0.0
   STICK
CH3 + PT(S)          => CH3(S)                  1.0        0.0       0.0
   STICK
H + PT(S)            => H(S)                    1.0        0.0       0.0
   STICK
O + PT(S)            => O(S)                    1.0        0.0       0.0
   STICK
OH + PT(S)           => OH(S)                   1.0        0.0       0.0
   STICK
C2H6(S)              => 2PT(S) + C2H6           1.0E13     0.0      20900.0
C2H4(S)              => PT(S) + C2H4            1.0E13     0.0      50200.0
C2H2(S)              => PT(S) + C2H2            1.0E12     0.0      58600.0
2H(S)                => 2PT(S) + H2             1.0E13     0.0      67400.0
   COV/H(S) 0.0 0.0 -10000./
2O(S)                => 2PT(S) + O2             1.0E13     0.0     227400.0
   COV/O(S) 0.0 0.0 -188000./
! 2O(S) => O2 + 2PT(S)                 3.70E+21   0.00   213200.0
!   COV/O(S) 0.0    0.0   -60000.0/
CH3(S) + H(S)        => CH4 + 2PT(S)            4.1E11     0.0      50000.0
   COV/H(S) 0.0 0.0 -5000./
CH3(S) + OH(S)       => CH4 + O(S) + PT(S)      1.0E13     0.0      85900.0
   COV/H(S) 0.0 0.0 -5000./
CHCH3(S)             => CH4 + C(S)              1.0E10     0.0      25500.0
   COV/C(S) 0.0 0.0 -47500./
CH3(S) + H2O(S)      => CH4 + OH(S) + PT(S)     1.0E13     0.0      23000.0
H2O(S)               => H2O + PT(S)             4.5E12     0.0      41800.0
CO2(S)               => CO2 + PT(S)             1.0E13     0.0      27100.0
CO(S)                => CO + PT(S)              2.0E16     0.0     146000.0
   COV/CO(S) 0.0 0.0 -33000./
```

```
CH2CH3(S)            => PT(S) + C2H5           1.0E13     0.0     173000.0
CH3(S)               => PT(S) + CH3            1.0E13     0.0     163000.0
H(S)                 => H + PT(S)              6.0E13     0.0     254400.0
   COV/H(S) 0.0 0.0 -5000./
O(S)                 => O + PT(S)              1.0E13     0.0     358800.0
   COV/O(S) 0.0 0.0 -94000./
OH(S)                => OH + PT(S)             5.0E13     0.0     251100.0
   COV/O(S) 0.0 0.0 -167000./
H(S) + O(S)          => OH(S) + PT(S)          3.5E12     0.0      11200.0
OH(S) + PT(S)        => H(S) + O(S)            2.0E11     0.0      77300.0
   COV/O(S) 0.0 0.0 -73200./
H(S) + OH(S)         => H2O(S) + PT(S)         5.5E12     0.0      66200.0
H2O(S) + PT(S)       => H(S) + OH(S)           3.1E10     0.0     101400.0
   COV/O(S) 0.0 0.0 167000./
2OH(S)               => H2O(S) + O(S)          2.0E12     0.0      74000.0
H2O(S) + O(S)        => 2OH(S)                 2.7E11     0.0      43100.0
   COV/O(S) 0.0 0.0 241000./
C(S) + O(S)          => CO(S) + PT(S)          1.0E11     0.0         0.0
CO(S) + PT(S)        => C(S) + O(S)            1.0E11     0.0     236500.0
   COV/CO(S) 0.0 0.0 -33000./
CO(S) + O(S)         => CO2(S) + PT(S)         1.0E11     0.0     117600.0
   COV/CO(S) 0.0 0.0 -33000./
CO2(S) + PT(S)       => CO(S) + O(S)           1.0E11     0.0     173300.0
   COV/CO(S) 0.0 0.0 -94000./
CO(S) + OH(S)        => CO2(S) + H(S)          5.4E10     0.0      38700.0
   COV/CO(S) 0.0 0.0 -33000./
CO2(S) + H(S)        => CO(S) + OH(S)           5.4E10     0.0      28300.0
CH3(S) + PT(S)       => CH2(S)s + H(S)          3.4E13     0.0      70300.0
CH2(S)s + H(S)       => CH3(S) + PT(S)          8.4E13     0.0        0.0
   COV/H(S) 0.0 0.0 -5000.0/
CH2(S)s + PT(S)       => CH(S) + H(S)           2.0E14     0.0      58900.0
   COV/C(S) 0.0 0.0 50000.0/
CH(S) + H(S)          => CH2(S)s + PT(S)        8.4E13     0.0        0.0
   COV/H(S) 0.0 0.0 -5000.0/
CH(S) + PT(S)          => C(S) + H(S)           8.4E13     0.0        0.0
   COV/H(S) 0.0 0.0 -5000.0/
C(S) + H(S)            => CH(S) + PT(S)         3.4E13     0.0     138000.0
C2H6(S) + O(S)         => CH2CH3(S) +OH(S)+PT(S) 1.0E13     0.0      25100.0
CH2CH3(S) + OH(S)+PT(S)=> C2H6(S) + O(S)        1.0E13     0.0      77400.0
C(S) + H2              => CH2(S)s               0.04       0.0      29700.0
   STICK
   COV/C(S) 0.0 0.0 4600./
CH2(S)s              => C(S) + H2              7.69E13    0.0      25100.0
   COV/C(S) 0.0 0.0 50000./
C2H6(S)              => CH2CH3(S) + H(S)       1.0E13     0.0      57700.0
CH2CH3(S) + H(S)     => C2H6(S)                1.0E13     0.0      41800.0
C2H6(S)              => 2CH3(S)                7.0E12     0.0      89000.0
```

```
     2CH3(S)                => C2H6(S)                2.7E12     0.0      14500.0
     CH2CH3(S) + PT(S)      => CHCH3(S) + H(S)        2.7E12     0.0      54400.0
     CHCH3(S) + H(S)        => CH2CH3(S) + PT(S)      2.7E12     0.0      29300.0
     C2H4(S)                => CHCH3(S)               1.0E13     0.0      83300.0
     CHCH3(S)               => C2H4(S)                1.0E13     0.0      75300.0
     C2H4(S) + PT(S)        => CHCH2(S) + H(S)        1.0E13     0.0     112700.0
     CHCH2(S) + H(S)        => C2H4(S) + PT(S)        1.0E13     0.0      33500.0
     CHCH3(S) + PT(S)       => CCH3(S) + H(S)         5.4E13     0.0      99100.0
     CCH3(S) + H(S)         => CHCH3(S) + PT(S)       1.0E13     0.0      75300.0
     CHCH3(S) + PT(S)       => CHCH2(S) + H(S)        1.0E13     0.0     128500.0
     CHCH2(S) + H(S)        => CHCH3(S) + PT(S)       1.0E13     0.0      57300.0
     CCH3(S) + PT(S)        => CH3(S) + C(S)          1.0E13     0.0      46900.0
        COV/C(S) 0.0 0.0 50000./
     CH3(S) + C(S)          => CCH3(S) + PT(S)        1.0E13     0.0      46000.0
     CCH3(S)                => CHCH2(S)               1.0E13     0.0     176000.0
     CHCH2(S)               => CCH3(S)                1.0E13     0.0     128600.0
     CHCH2(S) + PT(S)       => CCH2(S) + H(S)         1.0E13     0.0     121300.0
     C2H2(S) + H(S)         => CHCH2(S) + PT(S)       1.0E13     0.0      51700.0
     C2H2(S)                => CCH2(S)                1.0E13     0.0      61500.0
     CCH2(S)                => C2H2(S)                1.0E13     0.0       4200.0
     C2H2(S) + PT(S)        => CCH(S)  + H(S)         1.0E13     0.0     133500.0
     CCH(S) + H(S)          => C2H2(S) + PT(S)        1.0E13     0.0      66900.0
     CCH(S) + PT(S)         => CH(S) + C(S)           1.0E13     0.0     125100.0
     CH(S) + C(S)           => CCH(S) + PT(S)         1.0E13     0.0     121300.0
     END
```

A. 2. Cantera format Deutschmann – Pt mechanism

```
#
# see http://reaflow.iwr.uni-heidelberg.de/~Olaf.Deutschmann/ for
# more about this mechanism
#
#-----------------------------------------------------------------------!
#***********************************************************************
#****                                                                  *
#****     CH4-O2 SURFACE MECHANISM  ON PT                              *
#****                                                                  *
#****     Version 1.2   November  1995                                 *
#****                                                                  *
#****     O. Deutschmann, IWR, Heidelberg University, Germany          *
#****                                                                  *
#****     Kinetic data:                                                *
#****      k = A * T**b * exp (-Ea/RT)         A          b       Ea   *
#****                                       (cm,mol,s)    -      J/mol *
#****                                                                  *
#****                                                                  *
#***********************************************************************
#
#  Ref:- 1.) Deutschman et al., 26th Symp. (Intl.) on Combustion,1996
#            pp. 1747-1754
#-----------------------------------------------------------------------
#
#  Converted to Cantera format
#  by ck2cti on Thu Aug 21 07:58:45 2003
#
#-----------------------------------------------------------------------

units(length = "cm", time = "s", quantity = "mol", act_energy = "J/mol")
```

```
#
# Define a gas mixture with species imported from GRI-Mech.
# Reactions will be imported from GRI-Mech 3.0, as long as they
# don't involve species not declared here. Transport properties
# will be computed using a mixture-averaged model.
#
ideal_gas(name = "gas",
         elements = "O H C N Ar",
         species = """gri30: H2      H       O       O2      OH
                            H2O     HO2     H2O2
         C       CH      CH2     CH2(S)  CH3     CH4     CO      CO2
         HCO     CH2O    CH2OH   CH3O    CH3OH   C2H     C2H2    C2H3
         C2H4    C2H5    C2H6    HCCO    CH2CO   HCCOH AR N2""",
          transport = 'Mix',
          reactions = 'gri30: all',
          options = ['skip_undeclared_elements',
                     'skip_undeclared_species'],
          initial_state = state(temperature = 300.0, pressure = OneAtm,
                                mole_fractions = 'CH4:0.095, O2:0.21, AR:0.79')
          )


ideal_interface(name = "Pt_surf",
                elements = " Pt  H  O  C ",
                species = """ PT(S) H(S)
 H2O(S)  OH(S)  CO(S)  CO2(S)  CH3(S)
                CH2(S)s  CH(S)  C(S)  O(S) """,
                phases = "gas",
                site_density = 2.7063e-9,
                reactions = "all",
                initial_state = state(temperature = 900.0,
                                      coverages = 'O(S):0.0, PT(S):0.5, H(S):0.5')
                )

#-------------------------------------------------------------------------------
#  Species data
#
# Note that reactions 12-14 are reversible, and therefore require thermo
# data
#-------------------------------------------------------------------------------

species(name = "PT(S)",
    atoms = " Pt:1 ",
    thermo = (
       NASA( [  300.00,  1000.00], [  0.000000000E+00,   0.000000000E+00,
                0.000000000E+00,   0.000000000E+00,   0.000000000E+00,
                0.000000000E+00,   0.000000000E+00] ),
       NASA( [ 1000.00,  3000.00], [  0.000000000E+00,   0.000000000E+00,
                0.000000000E+00,   0.000000000E+00,   0.000000000E+00,
                0.000000000E+00,   0.000000000E+00] )
             )
       )

species(name = "H(S)",
    atoms = " H:1  Pt:1 ",
    thermo = (
       NASA( [  300.00,  1000.00], [ -1.302987700E+00,   5.417319900E-03,
                3.127797200E-07,  -3.232853300E-09,   1.136282000E-12,
               -4.227707500E+03,   5.874323800E+00] ),
       NASA( [ 1000.00,  3000.00], [  1.069699600E+00,   1.543223000E-03,
               -1.550092200E-07,  -1.657316500E-10,   3.835934700E-14,
               -5.054612800E+03,  -7.155523800E+00] )
             )
       )

species(name = "H2O(S)",
    atoms = " O:1  H:2  Pt:1 ",
    thermo = (
       NASA( [  300.00,  1000.00], [ -2.765155300E+00,   1.331511500E-02,
                1.012769500E-06,  -7.182008300E-09,   2.281377600E-12,
               -3.639805500E+04,   1.209814500E+01] ),
       NASA( [ 1000.00,  3000.00], [  2.580305100E+00,   4.957082700E-03,
               -4.689405600E-07,  -5.263313700E-10,   1.199832200E-13,
               -3.830223400E+04,  -1.740632200E+01] )
             )
       )

species(name = "OH(S)",
```

```
    atoms = " O:1  H:1  Pt:1 ",
    thermo = (
       NASA( [  300.00,  1000.00], [ -2.034088100E+00,   9.366268300E-03,
                6.627521400E-07,  -5.207488700E-09,   1.708873500E-12,
               -2.531994900E+04,   8.986318600E+00] ),
       NASA( [ 1000.00,  3000.00], [  1.824997300E+00,   3.250156500E-03,
               -3.119754100E-07,  -3.460320600E-10,   7.917147200E-14,
               -2.668549200E+04,  -1.228089100E+01] )
             )
       )

species(name = "CO(S)",
    atoms = " C:1  O:1  Pt:1 ",
    thermo = (
       NASA( [  300.00,  1000.00], [  4.890746600E+00,   6.813423500E-05,
                1.976881400E-07,   1.238866900E-09,  -9.033924900E-13,
               -3.229783600E+04,  -1.745316100E+01] ),
       NASA( [ 1000.00,  3000.00], [  4.708377800E+00,   9.603729700E-04,
               -1.180527900E-07,  -7.688382600E-11,   1.823200000E-14,
               -3.231172300E+04,  -1.671959300E+01] )
             )
       )

species(name = "CO2(S)",
    atoms = " C:1  O:2  Pt:1 ",
    thermo = (
       NASA( [  300.00,  1000.00], [  4.690000000E-01,   6.266200000E-03,
                0.000000000E+00,   0.000000000E+00,   0.000000000E+00,
               -5.045870000E+04,  -4.555000000E+00] ),
       NASA( [ 1000.00,  3000.00], [  4.690000000E-01,   6.266000000E-03,
                0.000000000E+00,   0.000000000E+00,   0.000000000E+00,
               -5.045870000E+04,  -4.555000000E+00] )
             )
       )

species(name = "CH3(S)",
    atoms = " C:1  H:3  Pt:1 ",
    thermo = (
       NASA( [  300.00,  1000.00], [  1.291921700E+00,   7.267560300E-03,
                9.817947600E-07,  -2.047129400E-09,   9.083271700E-14,
               -2.574561000E+03,  -1.198303700E+00] ),
       NASA( [ 1000.00,  3000.00], [  3.001616500E+00,   5.408450500E-03,
               -4.053805800E-07,  -5.342246600E-10,   1.145188700E-13,
               -3.275272200E+03,  -1.096598400E+01] )
             )
       )

species(name = "CH2(S)s",
    atoms = " C:1  H:2  Pt:1 ",
    thermo = (
       NASA( [  300.00,  1000.00], [ -1.487640400E-01,   5.139628900E-03,
                1.121107500E-06,  -8.275545200E-10,  -4.457234500E-13,
                1.087870000E+04,   5.745188200E+00] ),
       NASA( [ 1000.00,  3000.00], [  7.407612200E-01,   4.803253300E-03,
               -3.282563300E-07,  -4.777978600E-10,   1.007345200E-13,
                1.044375200E+04,   4.084208600E-01] )
             )
       )

species(name = "CH(S)",
    atoms = " C:1  H:1  Pt:1 ",
    thermo = (
       NASA( [  300.00,  1000.00], [  8.415748500E-01,   1.309538000E-03,
                2.846457500E-07,   6.386290400E-10,  -4.276665800E-13,
                2.233280100E+04,   1.145230500E+00] ),
       NASA( [ 1000.00,  3000.00], [ -4.824247200E-03,   3.044623900E-03,
               -1.606609900E-07,  -2.904170000E-10,   5.799992400E-14,
                2.259521900E+04,   5.667781800E+00] )
             )
       )

species(name = "C(S)",
    atoms = " C:1  Pt:1 ",
    thermo = (
       NASA( [  300.00,  1000.00], [  5.892401900E-01,   2.501284200E-03,
               -3.422949800E-07,  -1.899434600E-09,   1.019040600E-12,
                1.023692300E+04,   2.193701700E+00] ),
       NASA( [ 1000.00,  3000.00], [  1.579282400E+00,   3.652870100E-04,
```

```
               -5.065767200E-08,  -3.488485500E-11,   8.808969900E-15,
                9.953575200E+03,  -3.024049500E+00] )
             )
       )

species(name = "O(S)",
    atoms = " O:1  Pt:1 ",
    thermo = (
       NASA( [  300.00,  1000.00], [ -9.498690400E-01,   7.404230500E-03,
               -1.045142400E-06,  -6.112042000E-09,   3.378799200E-12,
               -1.320991200E+04,   3.613790500E+00] ),
       NASA( [ 1000.00,  3000.00], [  1.945418000E+00,   9.176164700E-04,
               -1.122671900E-07,  -9.909962400E-11,   2.430769900E-14,
               -1.400518700E+04,  -1.153166300E+01] )
             )
       )



#-------------------------------------------------------------------------------
#  Reaction data
#-------------------------------------------------------------------------------

#  Reaction 1
surface_reaction("H2 + 2 PT(S) => 2 H(S)", [4.45790E+10, 0.5, 0],
                 order = "PT(S):1")

#  Reaction 2
surface_reaction( "2 H(S) => H2 + 2 PT(S)",
                Arrhenius(3.70000E+21, 0, 67400,
                           coverage = ['H(S)', 0.0, 0.0, -6000.0]))

#  Reaction 3
surface_reaction( "H + PT(S) => H(S)",   stick(1.00000E+00, 0, 0))

#  Reaction 4
surface_reaction( "O2 + 2 PT(S) => 2 O(S)",   Arrhenius(1.80000E+21, -0.5, 0),
                  options = 'duplicate')

#  Reaction 5
surface_reaction( "O2 + 2 PT(S) => 2 O(S)",   stick(2.30000E-02, 0, 0),
                  options = 'duplicate')

#  Reaction 6
surface_reaction( "2 O(S) => O2 + 2 PT(S)",
                Arrhenius(3.70000E+21, 0, 213200,
                           coverage = ['O(S)', 0.0, 0.0, -60000.0]) )

#  Reaction 7
surface_reaction( "O + PT(S) => O(S)",   stick(1.00000E+00, 0, 0))

#  Reaction 8
surface_reaction( "H2O + PT(S) => H2O(S)",   stick(7.50000E-01, 0, 0))

#  Reaction 9
surface_reaction( "H2O(S) => H2O + PT(S)",   [1.00000E+13, 0, 40300])

#  Reaction 10
surface_reaction( "OH + PT(S) => OH(S)",   stick(1.00000E+00, 0, 0))

#  Reaction 11
surface_reaction( "OH(S) => OH + PT(S)",   [1.00000E+13, 0, 192800])

#  Reaction 12
surface_reaction( "H(S) + O(S) <=> OH(S) + PT(S)",   [3.70000E+21, 0, 11500])

#  Reaction 13
surface_reaction( "H(S) + OH(S) <=> H2O(S) + PT(S)",   [3.70000E+21, 0, 17400])

#  Reaction 14
surface_reaction( "OH(S) + OH(S) <=> H2O(S) + O(S)",   [3.70000E+21, 0, 48200])

#  Reaction 15
surface_reaction( "CO + PT(S) => CO(S)",   [1.61800E+20, 0.5, 0],
                  order = "PT(S):2")

#  Reaction 16
surface_reaction( "CO(S) => CO + PT(S)",   [1.00000E+13, 0, 125500])
```

```
#  Reaction 17
surface_reaction( "CO2(S) => CO2 + PT(S)",   [1.00000E+13, 0, 20500])

#  Reaction 18
surface_reaction( "CO(S) + O(S) => CO2(S) + PT(S)",   [3.70000E+21, 0, 105000])

#  Reaction 19
surface_reaction( "CH4 + 2 PT(S) => CH3(S) + H(S)",   [4.63340E+20, 0.5, 0],
                order = "PT(S):2.3")

#  Reaction 20
surface_reaction( "CH3(S) + PT(S) => CH2(S)s + H(S)",
                  [3.70000E+21, 0, 20000])

#  Reaction 21
surface_reaction( "CH2(S)s + PT(S) => CH(S) + H(S)",   [3.70000E+21, 0, 20000])

#  Reaction 22
surface_reaction( "CH(S) + PT(S) => C(S) + H(S)",   [3.70000E+21, 0, 20000])

#  Reaction 23
surface_reaction( "C(S) + O(S) => CO(S) + PT(S)",   [3.70000E+21, 0, 62800])

#  Reaction 24
surface_reaction( "CO(S) + PT(S) => C(S) + O(S)",   [1.00000E+18, 0, 184000])
```

A. 3. CHEMKIN format Deutschmann – Rh mechanism

```
!------------------------------------------------------------------------!
!SURFACE MECHANISM OF THE PARTIAL OXIDATION OF CH4 ON RHODIUM
!************************************************************************
!****                                                                  *
!****     CPO OF CH4 ON Rh - SURFACE MECHANISM                         *
!****                                                                  *
!****     Version 1.0   February 13, 2001                              *
!****                                                                  *
!****     O. Deutschmann, R. Schwiedernoch, L. Maier,                  *
!****        Heidelberg University, Germany                            *
!****     S. Tummala, L. D. Schmidt, University of Minnesota, USA      *
!****                                                                  *
!****                                                                  *
!****     NOTE: That is a first version that needs further             *
!****           improvements, e.g. methanization, reforming etc.!!!    *
!****                                                                  *
!****                                                                  *
!****     Ref:  O. Deutschmann, R. Schwiedernoch, L.I. Maier,          *
!****           D. Chatterjee. Natural Gas Conversion in Monolithic    *
!****           Catalysts: Interaction of Chemical Reactions and       *
!****           Transport Phenomena.  Natural Gas Conversion VI,       *
!****           Studies in Surface Science and Catalysis 136,          *
!****           E. Iglesia, J.J. Spivey, T.H. Fleisch (eds.),          *
!****           p. 215-258, Elsevier, 2001                             *
!****                                                                  *
!****     Kinetic data:                                                *
```

```
!****      k = A * T**b * exp (-Ea/RT)         A          b       Ea   *
!****                                        (cm,mol,s)    -     kJ/mol *
!****                                                                   *
!****                                                                   *
!****     (SURFACE CHEMKIN format, tested formally with Vers.II only!) *
!****                                                                   *
!************************************************************************
SITE/RH_SURFACE/    SDEN/2.72E-9/
Rh(s)   H2O(s)  H(s)  OH(s)   CO(s)   C(s)
CH3(s)  CH2(s)  CH(s)   CH4(s)  O(s)    CO2(s)
END
!
THERMO ALL
  300.0   1000.0   3000.0
! all data are dummy data (they are not needed - all rxns irrev.)
O(s)                    O   1Rh  1          I    300.00   3000.00 1000.00      1
 0.00000000E+00 0.00000000E+00 0.00000000E+00 0.00000000E+00 0.00000000E+00    2
 0.00000000E+00 0.00000000E+00 0.00000000E+00 0.00000000E+00 0.00000000E+00    3
 0.00000000E+00 0.00000000E+00 0.00000000E+00 0.00000000E+00                   4
O2(s)                   O   2Rh  1          I    300.00   3000.00 1000.00      1
 0.00000000E+00 0.00000000E+00 0.00000000E+00 0.00000000E+00 0.00000000E+00    2
 0.00000000E+00 0.00000000E+00 0.00000000E+00 0.00000000E+00 0.00000000E+00    3
 0.00000000E+00 0.00000000E+00 0.00000000E+00 0.00000000E+00                   4
H(s)                    H   1Rh  1          I    300.00   3000.00 1000.00      1
 0.00000000E+00 0.00000000E+00 0.00000000E+00 0.00000000E+00 0.00000000E+00    2
 0.00000000E+00 0.00000000E+00 0.00000000E+00 0.00000000E+00 0.00000000E+00    3
 0.00000000E+00 0.00000000E+00 0.00000000E+00 0.00000000E+00                   4
H2(s)                   H   2Rh  1          I    300.00   3000.00 1000.00      1
 0.00000000E+00 0.00000000E+00 0.00000000E+00 0.00000000E+00 0.00000000E+00    2
 0.00000000E+00 0.00000000E+00 0.00000000E+00 0.00000000E+00 0.00000000E+00    3
 0.00000000E+00 0.00000000E+00 0.00000000E+00 0.00000000E+00                   4
H2O(s)                  O   1H   2Rh  1     I    300.00   3000.00 1000.00      1
 0.00000000E+00 0.00000000E+00 0.00000000E+00 0.00000000E+00 0.00000000E+00    2
 0.00000000E+00 0.00000000E+00 0.00000000E+00 0.00000000E+00 0.00000000E+00    3
 0.00000000E+00 0.00000000E+00 0.00000000E+00 0.00000000E+00                   4
OH(s)                   O   1H   1Rh  1     I    300.00   3000.00 1000.00      1
 0.00000000E+00 0.00000000E+00 0.00000000E+00 0.00000000E+00 0.00000000E+00    2
 0.00000000E+00 0.00000000E+00 0.00000000E+00 0.00000000E+00 0.00000000E+00    3
 0.00000000E+00 0.00000000E+00 0.00000000E+00 0.00000000E+00                   4
Rh(s)                   Rh  1              S    300.00   3000.00 1000.00      1
 0.00000000E+00 0.00000000E+00 0.00000000E+00 0.00000000E+00 0.00000000E+00    2
 0.00000000E+00 0.00000000E+00 0.00000000E+00 0.00000000E+00 0.00000000E+00    3
 0.00000000E+00 0.00000000E+00 0.00000000E+00 0.00000000E+00                   4
CO(s)                   C   1O   1Rh  1     I    300.00   3000.00 1000.00      1
 0.00000000E+00 0.00000000E+00 0.00000000E+00 0.00000000E+00 0.00000000E+00    2
 0.00000000E+00 0.00000000E+00 0.00000000E+00 0.00000000E+00 0.00000000E+00    3
 0.00000000E+00 0.00000000E+00 0.00000000E+00 0.00000000E+00                   4
```

```
CO2(s)                  C   1O   2Rh  1     I    300.00   3000.00 1000.00      1
 0.00000000E+00 0.00000000E+00 0.00000000E+00 0.00000000E+00 0.00000000E+00    2
 0.00000000E+00 0.00000000E+00 0.00000000E+00 0.00000000E+00 0.00000000E+00    3
 0.00000000E+00 0.00000000E+00 0.00000000E+00 0.00000000E+00                   4
C(s)                    C   1Rh  1          I    300.00   3000.00 1000.00      1
 0.00000000E+00 0.00000000E+00 0.00000000E+00 0.00000000E+00 0.00000000E+00    2
 0.00000000E+00 0.00000000E+00 0.00000000E+00 0.00000000E+00 0.00000000E+00    3
 0.00000000E+00 0.00000000E+00 0.00000000E+00 0.00000000E+00                   4
CH(s)                   C   1H   1Rh  1     I    300.00   3000.00 1000.00      1
 0.00000000E+00 0.00000000E+00 0.00000000E+00 0.00000000E+00 0.00000000E+00    2
 0.00000000E+00 0.00000000E+00 0.00000000E+00 0.00000000E+00 0.00000000E+00    3
 0.00000000E+00 0.00000000E+00 0.00000000E+00 0.00000000E+00                   4
CH2(s)                  C   1H   2Rh  1     I    300.00   3000.00 1000.00      1
 0.00000000E+00 0.00000000E+00 0.00000000E+00 0.00000000E+00 0.00000000E+00    2
 0.00000000E+00 0.00000000E+00 0.00000000E+00 0.00000000E+00 0.00000000E+00    3
 0.00000000E+00 0.00000000E+00 0.00000000E+00 0.00000000E+00                   4
CH3(s)                  C   1H   3Rh  1     I    300.00   3000.00 1000.00      1
 0.00000000E+00 0.00000000E+00 0.00000000E+00 0.00000000E+00 0.00000000E+00    2
 0.00000000E+00 0.00000000E+00 0.00000000E+00 0.00000000E+00 0.00000000E+00    3
 0.00000000E+00 0.00000000E+00 0.00000000E+00 0.00000000E+00                   4
CH4(s)                  C   1H   4Rh  1     I    300.00   3000.00 1000.00      1
 0.00000000E+00 0.00000000E+00 0.00000000E+00 0.00000000E+00 0.00000000E+00    2
 0.00000000E+00 0.00000000E+00 0.00000000E+00 0.00000000E+00 0.00000000E+00    3
 0.00000000E+00 0.00000000E+00 0.00000000E+00 0.00000000E+00                   4
END
!
 REACTIONS      JOULES/MOLE
!*********************************************************************
!**** 1.  ADSORPTION
!*********************************************************************
H2      +Rh(s)   +Rh(s)  =>H(s)    +H(s)      0.010E-00  0.0       0.0
                                          STICK
O2      +Rh(s)   +Rh(s)  =>O(s)    +O(s)      0.010E-00  0.0       0.0
                                          STICK
CH4     +Rh(s)           =>CH4(s)            8.000E-03  0.0       0.0
                                          STICK
H2O     +Rh(s)  =>H2O(s)                     1.000E-01  0.0       0.0
                                          STICK
CO2     +Rh(s)  =>CO2(s)                     1.000E-05  0.0       0.0
                                          STICK
CO      +Rh(s)  =>CO(s)                      5.000E-01  0.0       0.0
                                          STICK
!*********************************************************************
!**** 2. DESORPTION
!*********************************************************************
H(s)    +H(s)   =>Rh(s)   +Rh(s)   +H2        3.000E+21  0.0      77800
O(s)    +O(s)   =>Rh(s)   +Rh(s)   +O2        1.300E+22  0.0     355200
```

```
H2O(s)          =>H2O     +Rh(s)              3.000E+13  0.0      45000
CO(s)           =>CO      +Rh(s)              3.500E+13  0.0     133400
CO2(s)          =>CO2     +Rh(s)              1.000E+13  0.0      21700
CH4(s)          =>CH4     +Rh(s)              1.000E+13  0.0      25100
!************************************************************************
!**** 3.  SURFACE REACTIONS
!************************************************************************
H(s)    +O(s)   =>OH(s)   +Rh(s)              5.000E+22  0.0      83700
OH(s)   +Rh(s)  =>H(s)    +O(s)               3.000E+20  0.0      37700
H(s)    +OH(s)  =>H2O(s)  +Rh(s)              3.000E+20  0.0      33500
H2O(s)  +Rh(s)  =>H(s)    +OH(s)              5.000E+22  0.0     106400
OH(s)   +OH(s)  =>H2O(s)  +O(s)               3.000E+21  0.0     100800
H2O(s)  +O(s)   =>OH(s)   +OH(s)              3.000E+21  0.0     224200
C(s)    +O(s)   =>CO(s)   +Rh(s)              3.000E+22  0.0      97900
CO(s)   +Rh(s)  =>C(s)    +O(s)               2.500E+21  0.0     169000
CO(s)   +O(s)   =>CO2(s)  +Rh(s)              1.400E+20  0.0     121600
CO2(s)  +Rh(s)  =>CO(s)   +O(s)               3.000E+21  0.0     115300
!************************************************************************
CH4(s)  +Rh(s)  =>CH3(s)  +H(s)               3.700E+21  0.0      61000
CH3(s)  +H(s)   =>CH4(s)  +Rh(s)              3.700E+21  0.0      51000
CH3(s)  +Rh(s)  =>CH2(s)  +H(s)               3.700E+24  0.0     103000
CH2(s)  +H(s)   =>CH3(s)  +Rh(s)              3.700E+21  0.0      44000
CH2(s)  +Rh(s)  =>CH(s)   +H(s)               3.700E+24  0.0     100000
CH(s)   +H(s)   =>CH2(s)  +Rh(s)              3.700E+21  0.0      68000
CH(s)   +Rh(s)  =>C(s)    +H(s)               3.700E+21  0.0      21000
C(s)    +H(s)   =>CH(s)   +Rh(s)              3.700E+21  0.0     172800
!************************************************************************
CH4(s)  +O(s)   =>CH3(s)  +OH(s)              1.700E+24  0.0      80300
CH3(s)  +OH(s)  =>CH4(s)  +O(s)               3.700E+21  0.0      24300
CH3(s)  +O(s)   =>CH2(s)  +OH(s)              3.700E+24  0.0     120300
CH2(s)  +OH(s)  =>CH3(s)  +O(s)               3.700E+21  0.0      15100
CH2(s)  +O(s)   =>CH(s)   +OH(s)              3.700E+24  0.0     158400
CH(s)   +OH(s)  =>CH2(s)  +O(s)               3.700E+21  0.0      36800
CH(s)   +O(s)   =>C(s)    +OH(s)              3.700E+21  0.0      30100
C(s)    +OH(s)  =>CH(s)   +O(s)               3.700E+21  0.0     145500
!************************************************************************
END
```

A. 4. Cantera format Deutschmann – Rh mechanism

```
#-----------------------------------------------------------------------!
#************************************************************************
#****                                                                  *
#****     CH4-O2 SURFACE MECHANISM  ON RH                              *
#****                                                                  *
#****     Swiedernoch 2003                                             *
#****                                                                  *
#****     O. Deutschmann, IWR, Heidelberg University, Germany          *
#****                                                                  *
#****     Kinetic data:                                                *
#****      k = A * T**b * exp (-Ea/RT)         A          b       Ea   *
#****                                       (cm,mol,s)    -      J/mol *
#****                                                                  *
```

```
#****                                                                  *
#************************************************************************

units(length = "cm", time = "s", quantity = "mol", act_energy = "J/mol")


#
# Define a gas mixture with species imported from GRI-Mech.
# Reactions will be imported from GRI-Mech 3.0, as long as they
# don't involve species not declared here. Transport properties
# will be computed using a mixture-averaged model.
#
ideal_gas(name = "gas",
         elements = "O H C N Ar",
         species = """gri30: H2  O2  H2O  CH4  CO  CO2  AR """,
          transport = 'Mix',
          reactions = 'gri30: all',
          options = ['skip_undeclared_elements',
                     'skip_undeclared_species'],
          initial_state = state(temperature = 300.0, pressure = OneAtm,
                                mole_fractions = 'CH4:0.3, O2:0.1, AR:0.6')
          )


ideal_interface(name = "Rh_surf",
                elements = " Rh  H  O  C ",
                species = """ Rh(s) H(s)
                H2O(s)  OH(s)  CO(s)  CO2(s)  CH4(s) CH3(s)
                CH2(s)  CH(s)  C(s)  O(s) """,
                phases = "gas",
                site_density = 2.72e-9,
                reactions = "all",
                initial_state = state(temperature = 900.0,
                                      coverages = 'O(s):0.0, Rh(s):1.0, H(s):0.0')
                )

#-------------------------------------------------------------------------------
#  Species data
#-------------------------------------------------------------------------------

species(name = "Rh(s)",
    atoms = " Rh:1 ",
    thermo = (
       NASA( [  300.00,  1000.00], [  0.000000000E+00,   0.000000000E+00,
                0.000000000E+00,   0.000000000E+00,   0.000000000E+00,
                0.000000000E+00,   0.000000000E+00] ),
       NASA( [ 1000.00,  3000.00], [  0.000000000E+00,   0.000000000E+00,
                0.000000000E+00,   0.000000000E+00,   0.000000000E+00,
                0.000000000E+00,   0.000000000E+00] )
             )
       )

species(name = "H(s)",
    atoms = " H:1  Rh:1 ",
    thermo = (
       NASA( [  300.00,  1000.00], [ -1.302987700E+00,   5.417319900E-03,
                3.127797200E-07,  -3.232853300E-09,   1.136282000E-12,
               -4.227707500E+03,   5.874323800E+00] ),
       NASA( [ 1000.00,  3000.00], [  1.069699600E+00,   1.543223000E-03,
               -1.550092200E-07,  -1.657316500E-10,   3.835934700E-14,
               -5.054612800E+03,  -7.155523800E+00] )
             )
       )

species(name = "H2O(s)",
    atoms = " O:1  H:2  Rh:1 ",
    thermo = (
       NASA( [  300.00,  1000.00], [ -2.765155300E+00,   1.331511500E-02,
                1.012769500E-06,  -7.182008300E-09,   2.281377600E-12,
               -3.639805500E+04,   1.209814500E+01] ),
       NASA( [ 1000.00,  3000.00], [  2.580305100E+00,   4.957082700E-03,
               -4.689405600E-07,  -5.263313700E-10,   1.199832200E-13,
               -3.830223400E+04,  -1.740632200E+01] )
             )
       )

species(name = "OH(s)",
    atoms = " O:1  H:1  Rh:1 ",
```

```
    thermo = (
       NASA( [  300.00,  1000.00], [ -2.034088100E+00,   9.366268300E-03,
                6.627521400E-07,  -5.207488700E-09,   1.708873500E-12,
               -2.531994900E+04,   8.986318600E+00] ),
       NASA( [ 1000.00,  3000.00], [  1.824997300E+00,   3.250156500E-03,
               -3.119754100E-07,  -3.460320600E-10,   7.917147200E-14,
               -2.668549200E+04,  -1.228089100E+01] )
             )
       )

species(name = "CO(s)",
    atoms = " C:1  O:1  Rh:1 ",
    thermo = (
       NASA( [  300.00,  1000.00], [  4.890746600E+00,   6.813423500E-05,
                1.976881400E-07,   1.238866900E-09,  -9.033924900E-13,
               -3.229783600E+04,  -1.745316100E+01] ),
       NASA( [ 1000.00,  3000.00], [  4.708377800E+00,   9.603729700E-04,
               -1.180527900E-07,  -7.688382600E-11,   1.823200000E-14,
               -3.231172300E+04,  -1.671959300E+01] )
             )
       )

species(name = "CO2(s)",
    atoms = " C:1  O:2  Rh:1 ",
    thermo = (
       NASA( [  300.00,  1000.00], [  4.690000000E-01,   6.266200000E-03,
                0.000000000E+00,   0.000000000E+00,   0.000000000E+00,
               -5.045870000E+04,  -4.555000000E+00] ),
       NASA( [ 1000.00,  3000.00], [  4.690000000E-01,   6.266000000E-03,
                0.000000000E+00,   0.000000000E+00,   0.000000000E+00,
               -5.045870000E+04,  -4.555000000E+00] )
             )
       )

species(name = "CH4(s)",
    atoms = " C:1  H:4  Rh:1 ",
    thermo = (
       NASA( [  300.00,  1000.00], [  0.000000000E+00,   0.000000000E+00,
                0.000000000E+00,   0.000000000E+00,   0.000000000E+00,
                0.000000000E+00,   0.000000000E+00] ),
       NASA( [ 1000.00,  3000.00], [  0.000000000E+00,   0.000000000E+00,
                0.000000000E+00,   0.000000000E+00,   0.000000000E+00,
                0.000000000E+00,   0.000000000E+00] )
             )
       )

species(name = "CH3(s)",
    atoms = " C:1  H:3  Rh:1 ",
    thermo = (
       NASA( [  300.00,  1000.00], [  1.291921700E+00,   7.267560300E-03,
                9.817947600E-07,  -2.047129400E-09,   9.083271700E-14,
               -2.574561000E+03,  -1.198303700E+00] ),
       NASA( [ 1000.00,  3000.00], [  3.001616500E+00,   5.408450500E-03,
               -4.053805800E-07,  -5.342246600E-10,   1.145188700E-13,
               -3.275272200E+03,  -1.096598400E+01] )
             )
       )

species(name = "CH2(s)",
    atoms = " C:1  H:2  Rh:1 ",
    thermo = (
       NASA( [  300.00,  1000.00], [ -1.487640400E-01,   5.139628900E-03,
                1.121107500E-06,  -8.275545200E-10,  -4.457234500E-13,
                1.087870000E+04,   5.745188200E+00] ),
       NASA( [ 1000.00,  3000.00], [  7.407612200E-01,   4.803253300E-03,
               -3.282563300E-07,  -4.777978600E-10,   1.007345200E-13,
                1.044375200E+04,   4.084208600E-01] )
             )
       )

species(name = "CH(s)",
    atoms = " C:1  H:1  Rh:1 ",
    thermo = (
       NASA( [  300.00,  1000.00], [  8.415748500E-01,   1.309538000E-03,
                2.846457500E-07,   6.386290400E-10,  -4.276665800E-13,
                2.233280100E+04,   1.145230500E+00] ),
       NASA( [ 1000.00,  3000.00], [ -4.824247200E-03,   3.044623900E-03,
               -1.606609900E-07,  -2.904170000E-10,   5.799992400E-14,
```

```
               2.259521900E+04,   5.667781800E+00] )
            )
       )

species(name = "C(s)",
    atoms = " C:1  Rh:1 ",
    thermo = (
       NASA( [  300.00,  1000.00], [  5.892401900E-01,   2.501284200E-03,
              -3.422949800E-07,  -1.899434600E-09,   1.019040600E-12,
               1.023692300E+04,   2.193701700E+00] ),
       NASA( [ 1000.00,  3000.00], [  1.579282400E+00,   3.652870100E-04,
              -5.065767200E-08,  -3.488485500E-11,   8.808969900E-15,
               9.953575200E+03,  -3.024049500E+00] )
            )
       )

species(name = "O(s)",
    atoms = " O:1  Rh:1 ",
    thermo = (
       NASA( [  300.00,  1000.00], [ -9.498690400E-01,   7.404230500E-03,
              -1.045142400E-06,  -6.112042000E-09,   3.378799200E-12,
              -1.320991200E+04,   3.613790500E+00] ),
       NASA( [ 1000.00,  3000.00], [  1.945418000E+00,   9.176164700E-04,
              -1.122671900E-07,  -9.909962400E-11,   2.430769900E-14,
              -1.400518700E+04,  -1.153166300E+01] )
            )
       )



#-------------------------------------------------------------------------------
#  Reaction data
#-------------------------------------------------------------------------------

#!*********************************************************************
#!**** 1.  ADSORPTION
#!*********************************************************************

#  Reaction 1
surface_reaction( "H2      + Rh(s) + Rh(s)  => H(s)    + H(s)",
                  stick(0.010E+00, 0, 0))

#  Reaction 2
surface_reaction( "O2      + Rh(s) + Rh(s)   =>O(s)    + O(s)",
                  stick(0.010E+00, 0, 0))

#  Reaction 3
surface_reaction( "CH4     + Rh(s)           =>CH4(s)",
                  stick(0.008E+00, 0, 0))

#  Reaction 4
surface_reaction( "H2O     + Rh(s)  =>H2O(s)",
                  stick(1.000E-01, 0, 0))

#  Reaction 5
surface_reaction( "CO2     + Rh(s)  =>CO2(s)",
                  stick(1.000E-05, 0, 0))

#  Reaction 6
surface_reaction( "CO      + Rh(s)  =>CO(s)",
                  stick(5.000E-01, 0, 0))

#!*********************************************************************
#!**** 2. DESORPTION
#!*********************************************************************

#  Reaction 7
surface_reaction( "H(s)    + H(s)   =>Rh(s)   + Rh(s)   + H2",   [3.000E+21, 0.0, 77800])

#  Reaction 8
#surface_reaction( "O(s)    + O(s)   =>Rh(s)   + Rh(s)   + O2",
#                Arrhenius(1.300E+22, 0.0, 355200,
#                          coverage = ['O(s)', 0.0, 0.0, -280000]))
#  Reaction 8
surface_reaction( "O(s)    + O(s)   =>Rh(s)   + Rh(s)   + O2", [1.300E+22, 0.0, 355200])

#  Reaction 9
surface_reaction( "H2O(s)          =>H2O     + Rh(s)",   [3.000E+13, 0.0, 45000])
```

```
#  Reaction 10
#surface_reaction( "CO(s)           =>CO      + Rh(s)",
#                Arrhenius(3.500E+13, 0.0, 133400,
#                          coverage = ['O(s)', 0.0, 0.0, -15000]))
#  Reaction 10
surface_reaction( "CO(s)           =>CO      + Rh(s)",   [3.500E+13, 0.0, 133400])

#  Reaction 11
surface_reaction( "CO2(s)          =>CO2     + Rh(s)",   [1.000E+13, 0.0, 21700])

#  Reaction 12
surface_reaction( "CH4(s)          =>CH4     + Rh(s)",   [1.000E+13, 0.0, 25100])

#!**********************************************************************
#!**** 3.  SURFACE REACTIONS
#!**********************************************************************

#  Reaction 13
surface_reaction( "H(s)    + O(s)   =>OH(s)   + Rh(s)",   [5.000E+22, 0.0, 83700])

#  Reaction 14
surface_reaction( "OH(s)   + Rh(s)  =>H(s)    + O(s)",   [3.000E+20, 0.0, 37700])

#  Reaction 15
surface_reaction( "H(s)    + OH(s)  =>H2O(s)  + Rh(s)",   [3.000E+20, 0.0, 33500])

#  Reaction 16
surface_reaction( "H2O(s)  + Rh(s)  =>H(s)    + OH(s)",   [5.000E+22, 0.0, 104700])

#  Reaction 17
surface_reaction( "OH(s)   + OH(s)  =>H2O(s)  + O(s)",   [3.000E+21, 0.0, 100800])

#  Reaction 18
surface_reaction( "H2O(s)  + O(s)   =>OH(s)   + OH(s)",   [3.000E+21, 0.0, 171800])

#  Reaction 19
surface_reaction( "C(s)    + O(s)   =>CO(s)   + Rh(s)",   [3.000E+22, 0.0, 97900])

#  Reaction 20
surface_reaction( "CO(s)   + Rh(s)  =>C(s)    + O(s)",   [2.500E+21, 0.0, 169000])

#  Reaction 21
surface_reaction( "CO(s)   + O(s)   =>CO2(s)  + Rh(s)",   [1.400E+20, 0.0, 121600])

#  Reaction 22
surface_reaction( "CO2(s)  + Rh(s)  =>CO(s)   + O(s)",   [3.000E+21, 0.0, 115300])

#!**********************************************************************

#  Reaction 23
surface_reaction( "CH4(s)  + Rh(s)  =>CH3(s)  + H(s)",   [3.700E+21, 0.0, 61000])

#  Reaction 24
surface_reaction( "CH3(s)  + H(s)   =>CH4(s)  + Rh(s)",   [3.700E+21, 0.0, 51000])

#  Reaction 25
surface_reaction( "CH3(s)  + Rh(s)  =>CH2(s)  + H(s)",   [3.700E+24, 0.0, 103000])

#  Reaction 26
surface_reaction( "CH2(s)  + H(s)   =>CH3(s)  + Rh(s)",   [3.700E+21, 0.0, 44000])

#  Reaction 27
surface_reaction( "CH2(s)  + Rh(s)  =>CH(s)   + H(s)",   [3.700E+24, 0.0, 100000])

#  Reaction 28
surface_reaction( "CH(s)   + H(s)   =>CH2(s)  + Rh(s)",   [3.700E+21, 0.0, 68000])

#  Reaction 29
surface_reaction( "CH(s)   + Rh(s)  =>C(s)    + H(s)",   [3.700E+21, 0.0, 21000])

#  Reaction 30
surface_reaction( "C(s)    + H(s)   =>CH(s)   + Rh(s)",   [3.700E+21, 0.0, 172800])

#!**********************************************************************

#  Reaction 31
surface_reaction( "CH4(s)  + O(s)   =>CH3(s)  + OH(s)",   [1.700E+24, 0.0, 80300])
```

```
#  Reaction 32
surface_reaction( "CH3(s)  + OH(s)  =>CH4(s)  + O(s)",   [3.700E+21, 0.0, 24300])

#  Reaction 33
surface_reaction( "CH3(s)  + O(s)   =>CH2(s)  + OH(s)",   [3.700E+24, 0.0, 120300])

#  Reaction 34
surface_reaction( "CH2(s)  + OH(s)  =>CH3(s)  + O(s)",   [3.700E+21, 0.0, 15100])

#  Reaction 35
surface_reaction( "CH2(s)  + O(s)   =>CH(s)   + OH(s)",   [3.700E+24, 0.0, 158400])

#  Reaction 36
surface_reaction( "CH(s)   + OH(s)  =>CH2(s)  + O(s)",   [3.700E+21, 0.0, 36800])

#  Reaction 37
surface_reaction( "CH(s)   + O(s)   =>C(s)    + OH(s)",   [3.700E+21, 0.0, 30100])

#  Reaction 38
surface_reaction( "C(s)    + OH(s)  =>CH(s)   + O(s)",   [3.700E+21, 0.0, 145500])
```

Appendix B – Codes

B. 1. Equilibrium

```
% GRImech used for thermodynamic properties
clear all
gas = GRI30;

T=573:10:1143; %K, select Tmin,DT,Tmax
for k=1:length(T)
InletConcentration='CH4:0.0333, O2:0.0167, N2:0.95';
set(gas,'T',T(k),'P',oneatm,'X',InletConcentration);
equilibrate(gas,'HP');
X(k,:)=molefractions(gas);
Tad(k)=temperature(gas);
riga=num2str(k+2);
end
disp('Writing results in EXCEL')
xlswrite('equilRis.xls',T'-273.15,1,'A3')
xlswrite('equilRis.xls',Tad'-273.15,1,'B3')
xlswrite('equilRis.xls',X.*100,1,'C3')

nsp = nSpecies(gas);
titles={'T' 'Tad'};
titles(3:nsp+2)=speciesnames(gas);
subtitles={'°C' '°C' '%'};
xlswrite('equilRis.xls',titles,1,'A1')
xlswrite('equilRis.xls',subtitles,1,'A2')
```

B. 2. PFR

```
function PFRmonolithRh
%PFR model. Validated with PLUG CK3.6 without MotzWise Correction
%All the temperatures are expressed in kilo-Kelvin, to reduce stiffness

close all
clear all

%%%% Cantera initialization %%%%

gas = importPhase('rhmechN2.cti','gas');
surf = importInterface('rhmechN2.cti','Rh_surf', gas);
%species in rhmechN2.cti:  H2  O2  H2O  CH4  CO  CO2  N2

%%%% Geometry definition %%%%

l=1.07e-3;          %m, cell side
ncell=89;           %cells number
ds=0.22e-3;         %m, strutt. thickness
L=1.0e-2;           %m, length catalyst monolith
CrossA=ncell*l^2;   %m2, cross section of all the monolith
epsV=l^2/(ds+l)^2; %m3/m3, void fraction (void/total volume)
Sv=4/l*24/18;       %1/m, surface to (void) volume ratio

%%% Set the thermal behavior of the reactor %%%%%

% Either one of the following keywords:
% 'ADIA': adiabatic
% 'ISOT': isothermal
% 'PROF': given axial T profile, not available jet
TB = 'ADIA';

%%%%%% Set the initial conditions %%%%%%%
%Set lab conditions
Tlab=0.29315;       %kK
Vdot=2.5667e-3/60; %m3/s, flow rate at T=20°C=Tlab

%Inlet concentration and temperature
InletConcentration='CH4:0.0333, O2:0.0167, N2:0.95';

% Choose if interested in a T-loop with outlet results
% or in spatial profiles
```

```
% in the latest case, set Tlow=Thigh
Tlow=0.3; %kC
Thigh=0.85; %kC
dT=0.05; %kC
Tn=Tlow:dT:Thigh;

%%%% model start - stop user input %%%%
T=Tlab;
set(gas,'T',T*1000,'P',oneatm,'X',InletConcentration);
rho=density(gas);  %kg/m3
v=Vdot / CrossA;   %m/s, interstitial velocity
G = rho * v;       %g/cm2/s, at the Tlab

%%%%%%%%%% Integrating PFR Balances %%%%%%%%%%%%
nsp = nSpecies(gas);

for n=1:length(Tn)

    T0=Tn(n)+0.273 %kK, inlet temperature
    set(gas,'T',T0*1000,'P',oneatm,'X',InletConcentration);
    Y0=massFractions(gas);
    options=odeset('AbsTol',1e-12,'RelTol',1e-8);
    V0=[Y0; T0];
    [zpfr,V]=ode45(@MHBalancesPFR,[0 L],V0,options,gas,surf,G,Sv,TB);


    if length(Tn)==1
        for k=1:length(zpfr)
            Yz(k,:)=V(k,1:nsp);  %mass frac
            Tz(k)=V(k,end);  %kK
            Y=Yz(k,:);
            comp='';
            for i=1:nsp-1
                comp=strcat(comp,speciesName(gas,i), ':',num2str(Y(i)),',');
            end
            comp=strcat(comp,speciesName(gas,nsp), ':',num2str(Y(end)));
            set(gas,'Y',comp{1:end});
            Xz(k,:)=moleFractions(gas);
        end
    else
        Ypfr(n,:)=V(end,1:nsp);  %mass frac
        Tpfr(n)=V(end,end);  %kK

        Y=Ypfr(n,:);
        comp='';
        for i=1:nsp-1
            comp=strcat(comp,speciesName(gas,i), ':',num2str(Y(i)),',');
        end
        comp=strcat(comp,speciesName(gas,nsp), ':',num2str(Y(end)));
        set(gas,'Y',comp{1:end});
        Xpfr(n,:)=moleFractions(gas);
    end
end

%%%%%%%%%% Post Processing Results %%%%%%%%%%%%
ifplot=1;
ifexcel=1;

if ifplot
    if length(Tn)==1
        leg=[];
        for i=1:nsp-1
            leg=[leg speciesName(gas,i)];
        end

        figure(1)
        plot(Tn.*1000,Xz(:,1:end-1),'linewidth',1.5),hold on
        xlabel('z (m)','Fontsize',12)
        ylabel('mol frac','Fontsize',12)
        title('Composition Profiles','Fontsize',14)
        eval([ 'print -dmeta' ' C.emf'])
        legend(leg,-1)

        figure(2)
        plot(Tn.*1000,Tz.*1000-273,'linewidth',1.5),hold on
        xlabel('z (m)','Fontsize',12)
        ylabel('T (°C)','Fontsize',12)
        title('Temperature Profile','Fontsize',14)
```

```
        eval([ 'print -dmeta' ' T.emf'])
    else
        leg=[];
        for i=1:nsp-1
            leg=[leg speciesName(gas,i)];
        end

        figure(1)
        plot(Tn.*1000,Xpfr(:,1:end-1),'linewidth',1.5),hold on
        xlabel('Tin (°C)','Fontsize',12)
        ylabel('mol frac','Fontsize',12)
        title('Composition Profiles','Fontsize',14)
        eval([ 'print -dmeta' ' C.emf'])
        legend(leg,-1)

        figure(2)
        plot(Tn.*1000,Tpfr.*1000-273,'linewidth',1.5),hold on
        xlabel('Tin (°C)','Fontsize',12)
        ylabel('Tout (°C)','Fontsize',12)
        title('Temperature Profile','Fontsize',14)
        eval([ 'print -dmeta' ' T.emf'])

    end
end %ifplot

if ifexcel
    if length(Tn)==1
    titles={'z' 'T'};
    titles(3:nsp+2)=speciesnames(gas);
    subtitles={'m' '°C' '%'};

    xlswrite('PFRRes.xls',zpfr,1,'A3')
    xlswrite('PFRRes.xls',Tz'.*1000-273,1,'B3')
    xlswrite('PFRRes.xls',Xz.*100,1,'C3')
    xlswrite('PFRRes.xls',titles,1,'A1')
    xlswrite('PFRRes.xls',subtitles,1,'A2')
    else
    titles={'T' 'Tad'};
    titles(3:nsp+2)=speciesnames(gas);
    subtitles={'°C' '°C' '%'};

    xlswrite('PFRRes.xls',Tn'.*1000,1,'A3')
    xlswrite('PFRRes.xls',Tpfr'.*1000-273,1,'B3')
    xlswrite('PFRRes.xls',Xpfr.*100,1,'C3')
    xlswrite('PFRRes.xls',titles,1,'A1')
    xlswrite('PFRRes.xls',subtitles,1,'A2')
    end
end %ifexcel

%-------------------------------------------------------------------------

function dVdz=MHBalancesPFR(z,V,gas,surf,G,Sv,TB)

nsp = nSpecies(gas);
Y=V(1:nsp); %mass frac
T=V(end);   %kK

comp='';
for i=1:nsp-1
    comp=strcat(comp,speciesName(gas,i), ':',num2str(Y(i)),',');
end
comp=strcat(comp,speciesName(gas,nsp), ':',num2str(Y(end)));
set(gas,'T',T*1000,'P',oneatm,'Y',comp{1:end});
setTemperature(surf, T*1000);
advanceCoverages(surf,1);
sdot=netProdRates(surf); %kmol/m2/s
W=molarMasses(gas); %kg/kmol
cp=cp_mass(gas);   %J/kgK
Hf=enthalpies_RT(gas).*gasconstant.*T*1000; %J/kmol

% Species Balances
dYdz=Sv*(sdot(1:nsp).*W)./G; %1/m
% Entalpy balance
switch TB
    case 'ADIA'
dTdz=-(Sv*dot(sdot(1:nsp),Hf/1000))/(G*cp); %kK/m
    case 'ISOT'
dTdz=0;
```

```
%     case 'PROF'
%         dTdz=
end

dVdz=[dYdz; dTdz];
```

B. 3. NuCond

```
function NuCondRh
%PFR adiabatic model with axial conduction through the solid,
%and heat transfer coefficient

close all
clear all

%%%% Cantera initialization %%%%
gas = importPhase('rhmechN2.cti','gas');
surf = importInterface('rhmechN2.cti','Rh_surf', gas);
% species in rhmechN2.cti:  H2  O2  H2O  CH4  CO  CO2  N2

%%%% Geometry definition %%%%

l=1.07e-3;          %m, cell side
ncell=89;           %cells number
ds=0.22e-3;         %m, strutt. thickness
L=1.0e-2;           %m, length catalyst monolith
CrossA=ncell*l^2;   %m2, cross section of all the monolith
epsV=l^2/(ds+l)^2; %m3/m3, void fraction (void/total volume)
Sv=4/l*24/18;       %1/m, surface to (void) volume ratio *24/18
                    %     because of the ZrO2

%%%%%% Set the initial conditions %%%%%%%
Tlab=0.29315;       %kK
Vdot=2.5667e-3/60; %m3/s, flow rate at T=20°C=Tlab

% Inlet concentration and temperature
InletConcentration='CH4:0.0333, O2:0.0167, N2:0.95';

% Select the host solution source
% (usually, the 'PFR' is a good enough starting solution,
% but an error like: "unable to solve the collocation equations -- a
% singular Jacobian encountered" may occur. If that is the case, just solve
% the closest T0 possible, and then switch to 'OLD', moving the T0 little
% by little)
% 'PFR'; initialize with a PFR model
% 'OLD'; initialize with an existing solution. matlab.mat
init='PFR';

%%%% model start - stop user input %%%%
T=Tlab;
set(gas,'T',T*1000,'P',oneatm,'X',InletConcentration);
rho=density(gas); %kg/m3
v=Vdot / CrossA; %m/s
G = rho * v; %g/cm2/s, at the Tlab

Ndot=oneatm*Vdot/gasconstant/(Tlab*1000);
WM=meanMolarMass(gas);
Mdot=Ndot*WM;

%%%%%%%%%% Integrate Balances %%%%%%%%%%%%

switch init
    case 'PFR'
        %Initialization with a PFR solution
        T0=0.7+0.273; %kK, inlet temperature
        set(gas,'T',T0*1000);
        H0=enthalpy_mass(gas) %J/kg
        Y0=massFractions(gas);
        nsp = nSpecies(gas);
        options=optimset('TolFun',1e-30);
        V0=[Y0; T0];
        [zpfr,V]=ode15s(@MHBalancesPFR,[0 L],V0,options,gas,surf,G,Sv);

        Ypfr=V(:,1:nsp);  %mass frac
        Tpfr=V(:,end);  %kK
        TSpfr=Tpfr+0.01;  %kK
        T1pfr=[0; diff(Tpfr)./diff(zpfr)]; %kK/m
        for k=1:length(zpfr)
```

```
            comp='';
            for i=1:nsp-1
                comp=strcat(comp,speciesName(gas,i), ':',num2str(Ypfr(k,i)),',');
            end
            comp=strcat(comp,speciesName(gas,nsp), ':',num2str(Ypfr(k,end)));
            set(gas,'Y',comp{1:end});
            Xpfr(k,:)=moleFractions(gas);
        end
        subplot(2,1,1),plot(zpfr,Xpfr(:,1:end-1)),hold on
        subplot(2,1,2),plot(zpfr,Tpfr),hold on
    case 'OLD'
        load matlab.mat
        T0=0.54+0.273; %kK, inlet temperature
        set(gas,'T',T0*1000);
        H0=enthalpy_mass(gas); %J/kg

        zpfr=z';
        Ypfr=Y';
        Tpfr=T';
        T1pfr=[0; diff(Tpfr)./diff(zpfr)]; %kK/m
        TSpfr=TS';
end

%BVP modeling
solinit = bvpinit(zpfr,@BVinit,[],Tpfr,TSpfr,T1pfr,Ypfr,zpfr,nsp);
sol = bvp4c(@MHBalances,@BC,solinit,[],gas,surf,epsV,G,H0,l,Sv,Y0,T0)
save
z=sol.x;
V=sol.y; %[nsp+2,nz]
Y=V(1:nsp,:);  %mass frac
T=V(end-2,:);  %kK
TS=V(end-1,:);  %kK
X=[];
for k=1:length(z)
comp='';
for i=1:nsp-1
    comp=strcat(comp,speciesName(gas,i), ':',num2str(Y(i,k)),',');
end
comp=strcat(comp,speciesName(gas,nsp), ':',num2str(Y(end,k)));
set(gas,'Y',comp{1:end});
X(:,k)=moleFractions(gas);
end
settemperature(gas,T(end).*1000);
H1=enthalpy_mass(gas) %J/kg
Q1=-5.67e-8*0.8*((T(1)*1000)^4-(TS(1)*1000)^4)/Mdot*CrossA %J/kg
Q2=(+5.67e-8*0.8*((T(end)*1000)^4-(TS(end)*1000)^4))/Mdot*CrossA %J/kg
errH=(H0-H1)/H0*100
err2=(H0/epsV-H1/epsV-Q1/(1-epsV)-Q2/(1-epsV))/(H0/epsV)*100
subplot(2,1,1),plot(z,X(1:end-1,:),'--')
subplot(2,1,2),plot(z,T,'--',z,TS,'--r')
save

file=['NuConsRes' num2str(T0*1000-273) '.xls'];
    titles={'z' 'T' 'TS'};
    titles(4:nsp+3)=speciesnames(gas);
    subtitles={'m' '°C' '°C' '%'};

    xlswrite(file,z',1,'A3')
    xlswrite(file,T'.*1000-273,1,'B3')
    xlswrite(file,TS'.*1000-273,1,'C3')
    xlswrite(file,X'.*100,1,'D3')
    xlswrite(file,titles,1,'A1')
    xlswrite(file,subtitles,1,'A2')

%-------------------------------------------------------------------------

function dVdz=MHBalancesPFR(z,V,gas,surf,G,Sv)

nsp = nSpecies(gas);
Y=V(1:nsp);   %mass frac
T=V(end);   %kK

comp='';
for i=1:nsp-1
    comp=strcat(comp,speciesName(gas,i), ':',num2str(Y(i)),',');
end
comp=strcat(comp,speciesName(gas,nsp), ':',num2str(Y(end)));
set(gas,'T',T*1000,'P',oneatm,'Y',comp{1:end});
```

```
setTemperature(surf, T*1000);
advanceCoverages(surf,1);
sdot=netProdRates(surf); %kmol/m2/s
W=molarMasses(gas); %kg/kmol
cp=cp_mass(gas);   %J/kgK
Hf=enthalpies_RT(gas).*gasconstant.*T*1000; %J/kmol

% Species Balances
dYdz=Sv*(sdot(1:nsp).*W)./G; %1/m
% Entalpy balance
dTdz=-(Sv*dot(sdot(1:nsp),Hf/1000))/(G*cp); %kK/m

dVdz=[dYdz; dTdz];

%#########################################################################
function dVdz=MHBalances(z,V,gas,surf,epsV,G,H0,l,Sv,Y0,T0)

nsp = nSpecies(gas);
Y=V(1:nsp);   %mass frac
T=V(end-2);   %kK
TS=V(end-1);   %kK
T1S=V(end);    %kK/m

comp='';
for i=1:nsp-1
    comp=strcat(comp,speciesName(gas,i), ':',num2str(Y(i)),',');
end
comp=strcat(comp,speciesName(gas,nsp), ':',num2str(Y(end)));
set(gas,'T',T*1000,'P',oneatm,'Y',comp{1:end});
setTemperature(surf, T*1000);
advanceCoverages(surf,1);
sdot=netProdRates(surf); %kmol/m2/s
W=molarMasses(gas); %kg/kmol
cp=cp_mass(gas);   %J/kgK
Hf=enthalpies_RT(gas).*gasconstant.*T*1000; %J/kmol

% Species Balances
dYdz=Sv*(sdot(1:nsp).*W)./G; %1/m

% Determining transport coefficient from bulk to surface
ni=viscosity(gas); %kg/m/s
D=mixDiffCoeffs(gas);  %Mixture-averaged diffusion coefficients (m2/s).
rho=density(gas); %kg/m3
la= thermalConductivity(gas); %W/m/K
cp=cp_mass(gas);              %J/kgK
%Dimensionless numbers definition
Re=G*l/ni; %referred to the void volume
Pr=ni*cp/la;
Pe=Re*Pr;

zstar=max([(z/l)/Pe,1e-8]);
%Shah & London:
Nu=2.977+(8.827*(zstar.*1e3).^(-0.545)).*exp(zstar.*(-48.2));
Kt=Nu*la/l; %J/s/K/m^2

% Entalpy balances
dTdz = - Kt*Sv*(T-TS)/(G*cp); %kK/m
laS=1.132e-6*(TS*1000)^2-3.228e-3*(TS*1000)+4.793; %J/(s*m*K), cordierite
dlaSdTS=1000*(2*1.132e-6*(TS*1000)-3.228e-3); %J/(s*m*K2), cordierite
dTSdz=T1S; %kK/m
d2TSdz2=-1/laS*dlaSdTS*T1S^2+(- Kt*Sv*(T-TS)+Sv*dot(sdot(1:nsp),Hf/1000))/(laS*epsV/(1-epsV));
%kK/m2

dVdz=[dYdz; dTdz; dTSdz; d2TSdz2];

%#########################################################################
function Vinit = BVinit(z,Tpfr,TSpfr,T1pfr,Ypfr,zpfr,nsp)

for i=1:nsp
Vinit(i)=interp1(zpfr,Ypfr(:,i),z); %Yi
end
Vinit(nsp+1)=interp1(zpfr,Tpfr,z); %TG
Vinit(nsp+2)=interp1(zpfr,TSpfr,z); %TS
Vinit(nsp+3)=interp1(zpfr,T1pfr,z); %dTS

%#########################################################################
function res = BC(Va,Vb,gas,surf,epsV,G,H0,l,Sv,Y0,T0)
```

```
nsp = nSpecies(gas);
%V=[Y(nsp) TG TS dTS]
Y=Vb(1:nsp);   %mass frac
T=Vb(end-2);   %kK
TS=Vb(end-1);   %kK
laSin=1.132e-6*(TS(1)*1000)^2-3.228e-3*(TS(1)*1000)+4.793; %J/(s*m*K), cordierite
laSout=1.132e-6*(TS(end)*1000)^2-3.228e-3*(TS(end)*1000)+4.793; %J/(s*m*K), cordierite

res = [];
for i=1:nsp
    res=[res;
        Va(i)-Y0(i)];
end
      res=[res;
          Va(nsp+1)-T0;
          Va(nsp+3)-(-5.67e-8*0.8*((Va(nsp+1)*1000)^4-(Va(nsp+2)*1000)^4)/1000)/laSin;
          Vb(nsp+3)-(+5.67e-8*0.8*((Vb(nsp+1)*1000)^4-(Vb(nsp+2)*1000)^4)/1000)/laSout];
%Note: if no radiation occurs at the rear and front edges, put the last 2
%entries of the BCs matrix as follows:
%           Va(nsp+3)-0;
%           Vb(nsp+3)-0];
```

B. 4. NuSh

```
function NuSh
close all
clear all
clc

%Cantera initialization
gas = importPhase('rhmechN2.cti','gas');
surf = importInterface('rhmechN2.cti','Rh_surf', gas);
species=' H2     O2   H2O     CH4     CO      CO2     N2'

%Geometry definition
l=1.07e-3;  %m %cell side
ncell=89;   %cell number
ds=0.22e-3; %m %strutt. thickness
L=1.0e-2;%1.0e-2;      %m, length cat. monolith
CrossA=ncell*l^2; %m2
epsV=l^2/(ds+l)^2;  %m3/m3
Sv=4/l*24/18;  %1/m, surface to (void) volume ratio, for Zr2O3

%%%%%% Set the initial conditions %%%%%%%
%Set lab
Tlab=0.293; %kK All the temperatures are expressed in kilo-Kelvin,
Vdot=2.5667e-3/60; %m3/s, at T=20°C=Tlab

%Inlet concentration and temperature
InletConcentration='CH4:0.0333, O2:0.0167, N2:0.95';
Tinlet=0.273+0.2; %kK

%Processing inlet flow
T=Tlab;
set(gas,'T',T*1000,'P',oneatm,'X',InletConcentration);
rho=density(gas); %kg/m3
v=Vdot / CrossA; %m/s
G = rho * v; %g/cm2/s, at the Tlab

TG0=Tinlet; %kK, inlet temperature

% %%%%%%%%%% Integrate DAE Balances %%%%%%%%%%%%
%
 YG0=massFractions(gas);

 nsp = nSpecies(gas);
 Var0=[YG0' TG0 YG0' TG0];

 %Mass matrix
 M=zeros(length(Var0));
 for i=1:nsp+1
     M(i,i)=1;
 end

VectAbstol=ones(2*nsp+2,1).*1e-7;
VectAbstol(nsp+1)=1e-6;
VectAbstol(2*nsp+2)=1e-6;
```

```
options=odeset('Mass',M,'MStateDependence','none',...
    'AbsTol',VectAbstol,'RelTol',1e-3,'MaxOrder',1,'BDF','on','InitialStep',1e-12);
[z,Var]=ode15s(@DAEBalances,[0 L],Var0,options,gas,surf,G,l,Sv);

YG=Var(:,1:nsp); %mass frac
TG=Var(:,nsp+1);   %kK
YS=Var(:,nsp+2:2*nsp+1); %mass frac
TS=Var(:,end);   %kK

        for k=1:length(z)
            Y=YG(k,:);
            comp='';
            for i=1:nsp-1
                comp=strcat(comp,speciesName(gas,i), ':',num2str(Y(i)),',');
            end
            comp=strcat(comp,speciesName(gas,nsp), ':',num2str(Y(end)));
            set(gas,'Y',comp{1:end});
            XG(k,:)=moleFractions(gas);
        end

        for k=1:length(z)
            Y=YS(k,:);
            comp='';
            for i=1:nsp-1
                comp=strcat(comp,speciesName(gas,i), ':',num2str(Y(i)),',');
            end
            comp=strcat(comp,speciesName(gas,nsp), ':',num2str(Y(end)));
            set(gas,'Y',comp{1:end});
            XS(k,:)=moleFractions(gas);
        end
Vold=Var;
save
plot(z,TG,z,TS)
pause
plot(z,YG)
pause
close all

%##########################################################################

function Vout=DAEBalances(z,V,gas,surf,G,l,Sv)
z
nsp = nSpecies(gas);
%Defining local variables
YG=V(1:nsp); %mass frac
TG=V(nsp+1);   %kK
YS=V(nsp+2:2*nsp+1); %mass frac
TS=V(end);   %kK

%Bulk definition in Cantera
Y=YG;
T=TG;
comp='';
for i=1:nsp-1
    comp=strcat(comp,speciesName(gas,i), ':',num2str(Y(i)),',');
end
comp=strcat(comp,speciesName(gas,nsp), ':',num2str(Y(end)));
set(gas,'T',T*1000,'P',oneatm,'Y',comp{1:end});
rho=density(gas);              %kg/m3
WT=molarMasses(gas); %kg/kmol
D=mixDiffCoeffs(gas);  %Mixture-averaged diffusion coefficients (m2/s).
la= thermalConductivity(gas); %W/m/K
cp=cp_mass(gas);               %J/kgK
ni=viscosity(gas); %kg/m/s
%Adim. Numbers Definition
Re=G*l/ni; %referred to the void volume
Pr=ni*cp/la;
zstar=max([(z/l)/(Re*Pr),1e-5]);
Nu=2.977+(8.827*(zstar.*1e3).^(-0.545)).*exp(zstar.*(-48.2));
Kt=Nu*la/l; %J/s/K/m^2
Kc=ones(1,nsp).*Nu.*D'./l; %m/s

for i=1:nsp
    dYGdz(i) =(-Kc(i)*Sv*rho*(YG(i)-YS(i)))/G; %1/m
end
dTGdz = (-Kt*Sv*(TG-TS))/(G*cp); %kK/m

%BL definition in Cantera
```

```
Y=YS;
T=TS;
comp='';
for i=1:nsp-1
    comp=strcat(comp,speciesName(gas,i), ':',num2str(Y(i)),',');
end
comp=strcat(comp,speciesName(gas,nsp), ':',num2str(Y(end)));
set(gas,'T',T*1000,'P',oneatm,'Y',comp{1:end});
rhoBL=density(gas);             %kg/m3
setTemperature(surf, T*1000);
advanceCoverages(surf,1);
% cov = coverages(surf)';
wdot = netProdRates(surf); %kmol/m2/s
Hf=enthalpies_RT(gas).*gasconstant.*T*1000; %J/kmol

for i=1:nsp
    fYS(i)=( Kc(i) * rhoBL * (YG(i)-YS(i)) + ...
        (wdot(i).*WT(i)));
end
fTS=(Kt*(TG-TS)-dot(wdot(1:nsp),Hf/1000)); %kK/m2

Vout = [dYGdz'; dTGdz; fTS; fYS'];
```

Acknowledgments

The author would like to thank Prof. Lanny D. Schmidt for one semester hospitality at the University of Minnesota and Prof. Sven Järås for one month at KTH – Royal Institute of Technology. Also, University of Padova is gratefully acknowledged for financial support of the whole scholarship.

References

[1] M. Bizzi, L. Basini, G. Saracco, V. Specchia, *Short contact time catalytic partial oxidation of methane: analysis of transport phenomena effects*, Chem. Eng. J., **90** (2002) 97-106.

[2] M. Bizzi, L. Basini, G. Saracco, V. Specchia, Modeling a transport phenomena limited reactivity in short contact time catalytic partial axidation reactors, Ind. Eng. Chem. Res., **42** (2003) 62-71.

[3] M. Bizzi, G. Saracco, R. Schwiedernoch, O. Deutschmann, *Modeling the partial oxidation of methane in a fixed bed with detailed chemistry*, AIChE J., **50** [6] (2004) 1289-99.

[4] H. W. Brauer, F. Fetting, *Stofftransport bei Wandreaktion im Einlaufgebiet eines Strömungsrohres*, Chemie Ing. Tech. 38 (1966) 30-35.

[5] G. Buzzi-Ferraris, BzzMath 5.0, http://www.chem.polimi.it/homes/gbuzzi/

[6] **Cantera**: D.G. Goodwin, *An open-source, extensible software suite for CVD process simulation*. In Proceedings of CVD XVI and EuroCVD Fourteen, M Allendorf, Maury, and F Teyssandier (Eds.), Electrochemical Society, (2003) 155-162.

[7] P. Canu, S. Vecchi, *CFD simulation of reactive flows: catalytic combustion in a monolith*, AIChE J. **48** [12] (2002) 2921-2935.

[8] **CHEMKIN**, ReactionDesign.

[9] N.J. Degenstein, PhD Thesis, University of Minnesota, 2007.

[10] O. Deutschmann, L. Schmidt, *Modeling the partial oxidation of methane in a short-contact-time reactor*, AIChE J., **44** [11] (1998) 2465-77.

[11] http://www.detchem.com/

[12] S. Eriksson, A. Schneider, F. Mantzaras, M. Wolf, S. Järås, *Experimental and numerical investigation of supported rhodium catalysts for partial oxidation of methane in exhaust gas diluted reaction mixtures*, Chem. Eng. Sci., **62** [15] (2007) 3991-4011.

[13] **FLUENT** 6.3, Ansys.

[14] J. G. Fourie, J. P. Du Plessis, *Effective and coupled thermal conductivities of isotropic open-cellular foams*, AIChE J., **50** [3] (2004) 547-556.

[15] L. Giani, G. Groppi, E. Tronconi, *Mass-transfer characterization of metallic foams as supports for structured catalysts*, Ind. Eng. Chem. Res., **44** (2005) 4993-5002.

[16] L. Giani, G. Groppi, E. Tronconi, *Heat transfer characterization of metallic foams*, Ind. Eng. Chem. Res., **44** (2005) 9078-9085.

[17] C.T. Goralski Jr., R.P. O'Connor, L.D. Schmidt, Modeling homogeneous and heterogeneous chemistry n the production of syngas from methane, Chem. Eng. Sci., **55** (2000) 1357-1370.

[18] U. Grigull, H. Tratz, *Thermischer Einlauf in ausgebildeter laminarer Rohrströmung*, Int. J. Heat Mass Transfer, **8** (1965) 669-678.

[19] GRI-Mech 3.0, http://www.me.berkeley.edu/gri-mech/

[20] D. P. H. Hasselman, K. Y. Donaldson, Jeng Liu, L. J. Gauckler, P. D. Ownby, *Thermal conductivity of a particulate-diamond-reinforced cordierite matrix composite*, J. Am. Ceram. Soc., **77** [7] (1994) 1757-60.

[21] D.A. Hickman, L.D. Schmidt, *Steps in CH_4 oxidation on Pt and Rh surfaces – High-temperature reactor simulations*, AIChE J., **39** (1993) 1164-1177.

[22] R. Horn, N.J. Degenstein, K.A. Williams, L.D. Schmidt, *Spatial and temporal profiles in millisecond partial oxidation processes*, Catal. Lett. **110** (2006) 169.

[23] R. Horn, K.A. Williams, N.J. Degenstein, L.D. Schmidt, *Syngas by catalytic partial oxidation of methane on rhodium: mechanistic conclusions from spatially resolved measurements and numerical simulations*, J. Catal. **242** (2006) 92-102.

[24] R. Horn, K. A. Williams, N. J. Degenstein, A. Bitsch-Larsen, D. Dalle Nogare, S. A. Tupy, L. D. Schmidt, *Methane catalytic partial oxidation on autothermal Rh and Pt foam catalyst: Oxidation and reforming zones, transport effects, and approach to thermodynamic equilibrium*, J. Catal., **249** [2] (2007) 380-393.

[25] R. Horn, K. A. Williams, N.J. Degenstein, A. Bitsch-Larsen, D. Dalle Nogare, S. A. Tupy, L. D. Schmidt, *Methane catalytic partial oxidation on autothermal Rh and Pt foam catalyst: Oxidation and reforming zones, transport effects, and approach to thermodynamic equilibrium*, J. Catal., **249** [2] (2007) 380-393.

[26] F.P. Incropera, D.P. DeWitt, *Fundamentals of Heat and Mass Transfer*, 5th Edition, Wiley.

[27] S.T. Kolaczkowski, Catal. Today, Modeling catalytic combustion in monolithic reactors – challenges faced, Catal. Today, **47** (1999) 209-218.

[28] D. Kunii, K. Suzuki, *Particle-to-fluid heat and mass transfer in packed beds of fine particles*, Chem. Eng. Sci., **10** [7] (1967) 845-852.

[29] O. Levenspiel, *Chemical Reaction Engineering,* 3rd Ed., 1999, John Wiley and Sons.

[30] M. Maestri, A. Beretta, G. Groppi, E. Tronconi, P. Forzatti, *Comparison among structured and packed-bed reactors for the catalytic partial oxidation of CH_4 at short contact times*, Cat. Today, **105** (2005) 709-717.

[31] **Matlab**, MathWorks.

[32] **Multiphysics**, COMSOL.

[33] P.A. Nelson, T.R. Galloway, *Particle-to-fluid heat and mass transfer in dense systems of fine particles*, Chem. Eng. Sci., **30** (1975) 1-6.

[34] L.D. Pfefferle, *Heterogeneous/homogeneous reactions and transport coupling for catalytic combustion systems: a review of model alternatives*, Cat. Today, **26** (1995) 255-265.

[35] A. Scarabello, *Two-stage route catalytic combustion of methane for gas turbine applications: experimental study of catalyst preparation and preformance*, MS thesis, Università di Padova, 2003/04.

[36] R.K. Shah, A. L. London, *Laminar flow forced convection in ducts*, Academic Press, New York, 1978.

[37] R. Schwiedernoch, S. Tischer, C. Correa, O. Deutschmann, *Experimental and numerical study on the transient behavior of partial oxidation of methane in a catalytic monolith*, Chem. Eng. Sci., **58** (2003) 633-642.

[38] E.E. Svensson, personal communication.

[39] N.V. Vernikovskaya, L.N. Bobrova, L.G. Pinaeva, V.A. Sadykov, I.A. Zolotarskii, V.A. Sobyanin, I. Buyakou, V. Kalinin, S. Zhdanok, *Transient behavior of the methane partial oxidation in a short contact time reactor: modeling on the base of catalyst detailed chemistry*, Chem. Eng. J., **134** (2007) 180-189.